NASA CONTRACTOR REPORT 177473

P-102

Astrometric Telescope Facility Isolation and Pointing Study

William Hibble
Terry Allen
Louis Jackson
James Medbery
Richard Self

Date for general release January 1990

CONTRACT NAS2-32815
January 1988

National Aeronautics and
Space Administration

NASA CONTRACTOR REPORT 177473

Astrometric Telescope Facility Isolation and Pointing Study

William Hibble
Terry Allen
Louis Jackson
James Medbery
Richard Self

Prepared for
Ames Research Center
under Contract NAS2-32815

January 1988

National Aeronautics and
Space Administration

Ames Research Center
Moffett Field, California 94035

SUMMARY

The Astrometric Telescope Facility (ATF) is scheduled to be a major user of the space station's Payload Pointing System (PPS) capabilities. However, because of the very stringent pointing requirements of ATF, some means of improving PPS pointing performance must be provided. This report presents the results of a study conducted to investigate the ATF pointing performance achievable through the addition of a magnetic pointing and isolation system between the PPS upper gimbal and the ATF and, separately, through the addition of a passive isolation system between the space station and the PPS base. The primary emphasis is placed on the magnetic system results. While the ATF will require active line-of-sight roll control, the roll stability requirements are not as stringent as the pointing requirements. Because of this less stringent stability specification and because the disturbance level into the roll control loop is comparable to the disturbance seen by the pointing loop, the study did not address roll performance.

In addition to defining pointing performance for the magnetic system a candidate magnetic pointing and isolation system configuration has been defined and includes: actuators, sensors, power and signal transfer devices, and associated support electronics. The candidate configuration, which allows full 360° roll motion, establishes realistic power, weight and size requirements for the magnetic system.

The pointing performance results from the study indicate that a magnetic pointing and isolation system can meet the ATF pointing requirements with a PPS base translational disturbance acceleration of up to 0.018g. Base rotational disturbances are determined to be insignificant in their effect on magnetic pointing performance.

In order to meet ATF pointing requirements by incorporating a passive isolator below the PPS base the isolation bandwidth must be very low: less than 0.1 Hz on all axes. Such an isolator would require an extremely large stroke - over 3 ft for the disturbance magnitude specified for this study!

The candidate magnetic pointing and isolation configuration defined for the study is based on an assumed 0.01 g peak translation acceleration disturbance. The system fits within the available annular region between the PPS and ATF, requires less than 800 watts peak operational power, and weighs less then 2000 lbs.

The magnetic system provides superior pointing performance, is based on current technology, and compared to the ATF payload, adds only modestly to system power and weight requirements. By contrast, a passive base isolation system having the required bandwidth and stroke is not practical using current technology.

SECTION 1.0

INTRODUCTION

SECTION 1.0
INTRODUCTION

One of the major scheduled users for the space station's (SS) Payload Pointing System (PPS) is the Astrometric Telescope Facility (ATF), an experiment which will be operated over a twenty-year period to investigate the presence of planetary systems around neighboring stars. The primary component of the ATF is a 21.5 meter telescope. Unfortunately, the current pointing specification for PPS pointing stability does not meet the needs of the ATF.

Space station disturbance accelerations and motions are expected to generate PPS pointing errors levels, even for a c.g. mounted payload, that are significantly above ATF specifications. In addition, the proposed PPS gimbal arrangement does not provide the level of payload roll motion control demanded by the ATF. To alleviate these problems some form of vernier pointing system added to the PPS or isolation system added between the SS and PPS will be required.

This report presents the results of a study conducted by the Honeywell Satellite System Division (HSSD) for NASA-Ames (ATF Isolation and Pointing Study) which had as its primary objective the determination of ATF pointing performance achievable by adding a magnetic pointing and isolation system (a vernier pointing system) between the PPS and the ATF.

The magnetic system provides a noncontacting interface between the PPS gimbal system and the ATF. Magnetic actuators similar to the one illustrated in Figure 1-1 are used to point the ATF inertially and to isolate the ATF from PPS translational motions. The stators of the actuators are connected to the PPS, the armatures are attached to the ATF.

The magnetic system pointing performance results are primarily parametric in nature, defining pointing performance as a function of the level of input disturbance from the space station and of allowable control bandwidths, for both pointing and isolation functions.

The secondary objectives of the ATF study include; i.) the comparison of the magnetic system performance with ATF pointing performance obtained by adding a passive isolation system to the base of the PPS and, ii.) the definition of a candidate magnetic pointing and isolation configuration which serves as a basis for establishing a magnetic system power, weight and size budget. These results are, of course, also reported.

The proposed magnetic system design is based on HSSD's activities over the past decade in developing similar magnetic pointing and isolation systems for space and ground test applications. These applications include, the Vernier Isolation Pointing Systems (VIPS) developed for NASA-LaRC, the Vibration Isolation and Pointing System (VIPS), and the Space Active Vibration Isolator (SAVI) currently being developed for the Air Force.

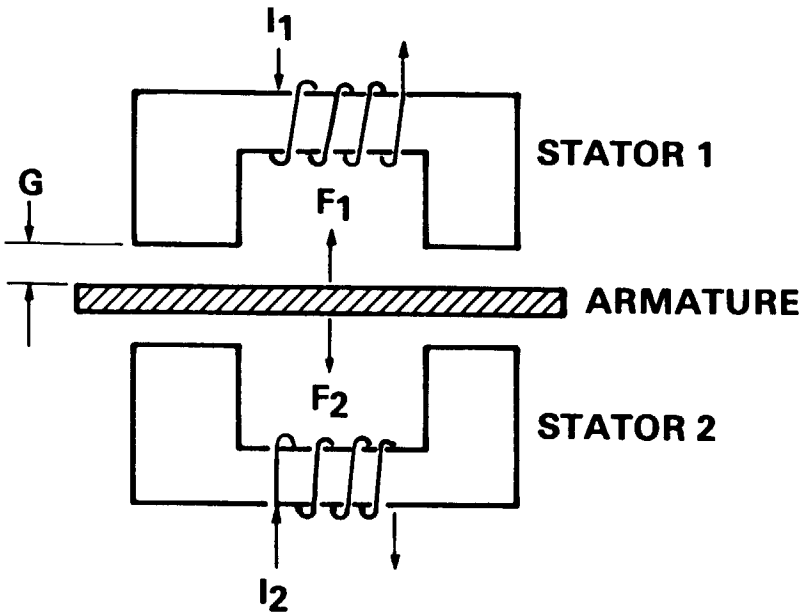

- Attractive Force F_1 and F_2
- F Insensitive to Armature Rotation and Cross Axes Translation
- Armature Isolated From Stator Disturbance Forces

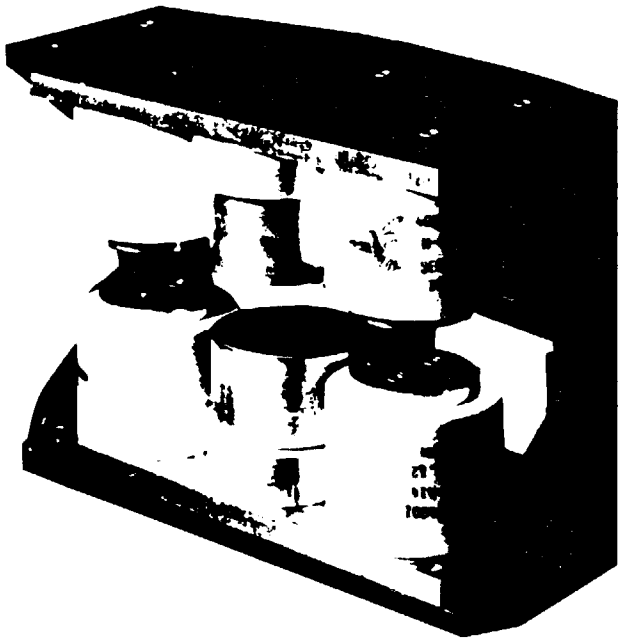

- $F \sim I^2$
- $F \sim G^{-2}$
- Moving Armature Is Passive

P1554-62-3

Figure 1-1
Magnetic Actuator

There are, obviously, other options for enhancing PPS performance than the two systems considered in this report. For example, the integrated "gimbal-translational isolation" system, GIMBAL-FLEX, developed by Martin Aerospace might be considered as an alternative to the proposed magnetic system. Similarly, an active base isolator might be offered as a substitute for the passive concept considered in the study. However, the two configurations considered for the ATF study are viewed as the best options for achieving required ATF performance without modifying the basic PPS design. The magnetic system provides a high level of pointing performance while integrating easily with the PPS and the ATF and, as the results of the study indicate, remaining within power, weight and size budgets established for an ATF vernier pointing system. On the other hand, a passive base isolation should provide the least expensive option if it produces the required improvement in pointing performance.

The outline of this final report follows closely the order of the ATF Isolation and Pointing Study final presentation given at NASA-Ames on 14 July 1987. Figures and tables in the report are primarily reproductions of charts from that presentation.

Performance results from the study are based on simple planar models of the ATF and PPS pointing systems. In the absence of a better definition for the SS structure and SS disturbance sources, such a simplified model is adequate for assessing approximate performance and performance sensitivity with respect to input disturbance levels.

SECTION 2.0

ATF POINTING AND SLEW REQUIREMENTS

SECTION 2.0
ATF POINTING AND SLEW REQUIREMENTS

2.1 POINTING STABILITY

ATF pointing stability requirements are determined by the sensitivity of the degradation in experiment performance to the level and frequency content of telescope pointing jitter. The frequency sensitivity is greatest at the experiment sensor grating (Ronchi ruling motion) frequency and at harmonics and subharmonics of this frequency. The grating frequency is variable but will be set so that the most important harmonics and subharmonics lie between 5 and 200 Hz. At these discrete frequencies the pointing jitters must be less than 0.01 arcsec. This specification has been interpreted as applying to the sum of all jitter components between 5 and 200 Hz.

It may be possible, once the SS disturbances are precisely characterized, to set the grating frequency so as to separate the disturbance and grating frequencies. This would allow the jitter limit to be increased. In the absence of such a characterization the most stringent requirement must be applied.

The limit on pointing jitter for frequencies below 5 Hz and above 200 Hz are much less severe, 1 arcsec and 0.1 arcsec respectively. Table 2-1 summarizes the ATF pointing stability requirements for the three frequency ranges noted.

For the ATF study, compliance with the stated pointing requirements was evaluated based on steady state system response to single frequency disturbances applied below and above 5 Hz. The disturbance frequencies were selected to produce the worst case pointing errors in the two frequency regions. Such a procedure is very conservative if the magnitude of the single frequency disturbance used in the study (in either frequency region) is comparable to the sum of actual disturbance components in the associated frequency region.

2.2 PAYLOAD SLEW REQUIREMENTS

Slew requirements for the ATF are based on the fact that the angular separation between ATF targets may be as large as 90 degrees and that, to minimize nonoperational time, the transition time from one target to another should be no more than five minutes. The ability of an ATF pointing system to satisfy these conditions will be determined by the torque limits of the pointing system and by any angular rate limit imposed on the ATF motion.

In assessing compliance for the ATF magnetic pointing study the torque limit was assumed to be dictated by the PPS and was set at 34 N.m (25 ft-lbs.) No rate limit was assumed.

TABLE 2-1

ATF POINTING STABILITY AND SLEW REQUIREMENTS

- Pointing Stability for Disturbances

  Below 5 Hz -- ≤1 arcsec

- Pointing Stability for Disturbances

  Above 5 Hz -- 0.01 arcsec

- Above 200 Hz -- <0.1 arcsec

- Slew Requirement -- 90 degrees in 5 minutes

2.3 PAYLOAD ROLL REQUIREMENTS

Payload line of sight roll control is required for the ATF during target observation. In order to maintain inertial stability of the experiment around the payload line of sight an ATF pointing system must accommodate as much as ±15 degrees relative rotation between the payload and pointing system around the payload line of sight axis. An ATF vernier pointing system added to the PPS must provide this roll control. The assumed (for this report) nominal 3 gimbal PPS configuration, illustrated in Figure 2-1, does not allow for payload roll control when the elevation gimbal is positioned as illustrated. If a vernier pointing system is not added to the PPS, and an operational scenario which avoids this gimbal position can not be defined, a roll ring around the telescope would need to be added inside the top gimbal or as a substitute for the top gimbal.

In addition to inertial payload roll control during observations the ATF experiment operation requires that the ATF pointer provide the ability to perform ±180-degree inertial roll slew maneuvers between observations. The relative roll motion requirement imposed on the magnetic pointing and isolation system is ±200 degrees, thus accommodating the combined effects of a roll slew and roll control during observation. A roll mechanism added to the PPS as a "top gimbal" would also have to meet such motion requirements.

While the candidate magnetic pointing and isolation system defined for this study meets ATF roll requirements the pointing stability study has not addressed the level of achievable roll control stability.

2.4 SIZE RESTRICTIONS

The magnetic pointing and isolation system must fit within an annular region between the PPS upper gimbal trunions and the ATF. This region has a 1.8 M inner diameter and a 2.5 M outer diameter.

2.5 REQUIREMENT COMPLIANCE

As the performance and candidate design study results presented in this report show a magnetic pointing and isolation system can meet the ATF pointing and slew requirements. This compliance is summarized in Table 2-2.

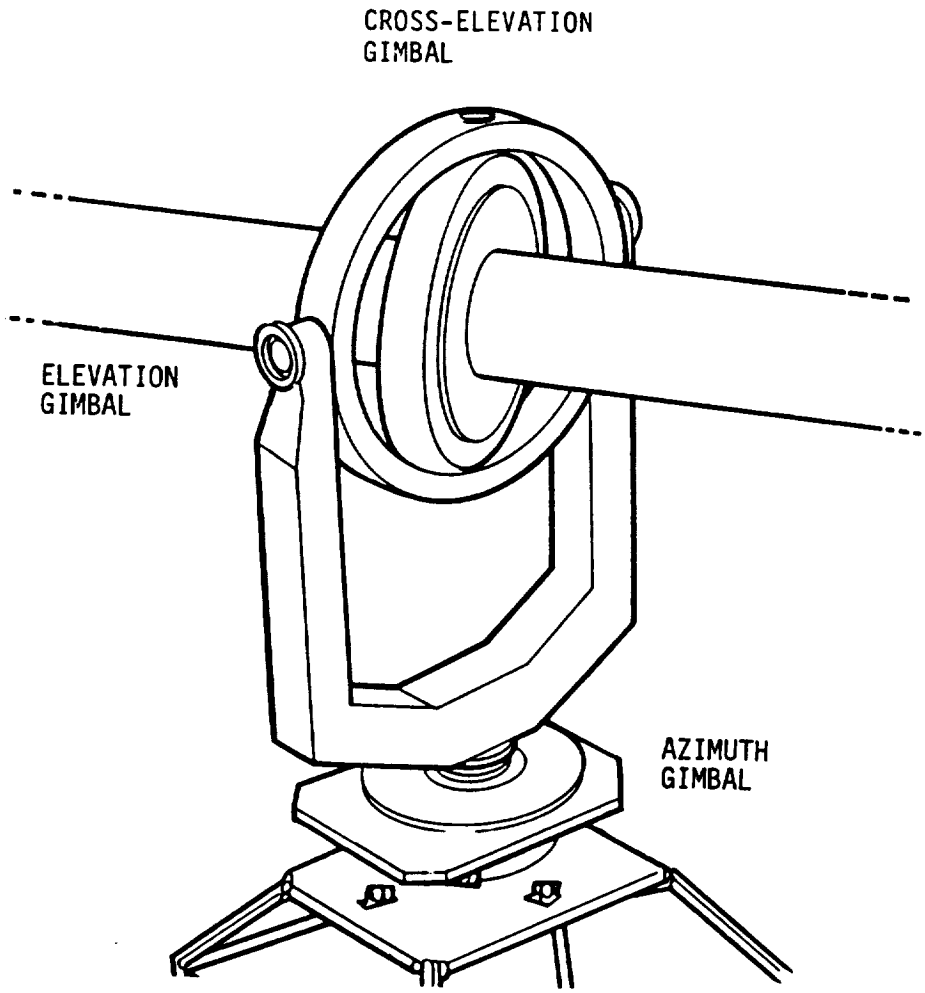

Figure 2-1
PPS Gimbal Configuration

TABLE 2-2

MAGNETIC POINTING AND ISOLATION
SYSTEM COMPLIANCE WITH ATF
REQUIREMENTS

1.	Pointing Stability -	Proposed control design meets pointing stability requirements for space station disturbance levels up to 0.018 g.
2.	Slew Requirements -	The ATF can be repositioned within 5 minutes for any slew maneuver of 90° or less using a peak torque of 34 N.m units and with less than a 0.5°/sec. peak rate.
3.	Roll Requirements -	The proposed magnetic configuration provides >±180° roll motion thus accommodating roll control and roll slews.
4.	Size Requirements -	The proposed design fits within the available annular region between the PPS and the ATF.

SECTION 3.0

SPACE STATION DISTURBANCE CHARACTERIZATION

SECTION 3.0
SPACE STATION DISTURBANCE CHARACTERIZATION

The major sources of ATF pointing errors are expected to be the space station motions and accelerations generated at the base of the PPS. The translational accelerations at the PPS control center (intersection of the gimbal axis in Figure 2-1), resulting from both translational and angular accelerations at the PPS base, produce a disturbance torque to the PPS control loop that is proportional to the offset between the control point and the payload center of gravity (c.g.). Similarly, the space station rotational motion is coupled into the PPS control loops by the gimbal bearing friction and by any fluid couplings or electrical cabling required for the payload.

By adding an isolator below the PPS the disturbance levels into the pointing loops are reduced. Alternatively, the magnetic pointing and isolation system, by adding a noncontacting interface between the PPS and the ATF, removes the effect of the rotational coupling to the payload, attenuates the translational disturbances transmitted through the PPS, and makes payload pointing control very insensitive to the gimbal to payload c.g. offset since the magnetic system provides the pointing control. In addition, the magnetic system isolates the payload from disturbances produced by the PPS itself.

In order to define how effective a magnetic pointing and isolation system or a base isolation system is in producing the desired pointing performance for ATF some estimate of the PPS base motions and accelerations must be provided. Ideally, models of the space station and space stations disturbance forces and torques would be used to generate this data. However, the space station is not defined well enough to allow this option. Thus, for the ATF pointing study disturbances at the PPS base are assumed to consist of discrete spectrums of sinusoidal rotations and translational accelerations. The discrete disturbance assumption is supported by the PPS disturbance specification included in the PPS development spec. generated by the Astro Space Division of General Electric, "Development Specification for the Payload Pointing System," Spec. No. SVS-11376, Jan., 1987. This disturbance specification, reproduced in Table 3-1, defines PPS base plate rotational deflection components in arcsec and linear acceleration components in ft./sec^2.

Under the assumption of a discrete disturbance spectrum meaningful study performance results are obtained by limiting the spectrum to two frequencies, one above 5 Hz and the other below 5 Hz, as described in the previous section. The two frequencies are selected to provide worst case pointing errors in these respective frequency ranges. Conservative results are obtained if the magnitude of the single frequency disturbance is comparable to the sum of the magnitude of the actual discrete spectrum components.

In this ATF study a nominal 0.01 g translation acceleration magnitude has been assumed for the linear disturbance levels, both below and above 5 Hz. The magnitude was suggested by NASA-Ames. Notice that 0.01 g or .32 ft/sec^2 (.098 m/sec^2)is greater than the sum of the components of linear disturbance in Table 3-1. For rotational disturbance a one arcmin rotational magnitude has been used in the study. Again, note that this is much larger than the sum of the rotational magnitudes in Table 3-1.

TABLE 3-1

ANTICIPATED DISTURBANCE INPUTS FROM SPACE STATION

LINEAR ACCELERATIONS AT BASE PLATE OF PPS

Freq (Hz)	Amplitude (ft/sec^2)
0.24	0.002
0.4	0.001
0.56	0.002
0.8	0.006
0.87	0.003
1.0	0.012
2.0	0.02
2.07	0.012

ROTATIONAL DEFLECTIONS AT BASE PLATE

Freq (Hz)	Amplitude (arc sec)
0.33	0.4
0.41	0.9
0.51	1.08
1.0	0.37
2.0	0.4
2.04	0.3
2.23	0.3
2.28	0.35

"Development Specification for the Payload Pointing System" Spec No. SVS-11376, Jan 1987, General Electric Co, Astro Space Div.

SECTION 4.0

MAGNETIC POINTING AND ISOLATION PERFORMANCE MODEL

SECTION 4.0
MAGNETIC POINTING AND ISOLATION PERFORMANCE MODEL

In order to define a model of the PPS-magnetic system some basic assumptions about the system's physical characteristics and operations are required. The following items summarize the assumptions made for the ATF study.

- Only the bottom two gimbal of the PPS configuration of Figure 2-1, (azimuth and elevation) are retained. The space required for the magnetic system does not provide room for the cross elevation yoke.
- The magnetic system stators are mounted to the elevation gimbal yoke. Exact placement is unimportant for preliminary performance evaluation.
- In order to accommodate the ±200-degree roll requirement the magnetic system armature is formed as a continuous ring attached to the ATF.
- The control point for the magnetic system is placed as close as possible to the ATF center of gravity.
- Inertial pointing control of the ATF is accomplished with the magnetic actuators. PPS gimbal control is used to orient the actuator stators so as to follow the angular motion of the armature ring.

Figure 4-1 illustrates a configuration based on these assumptions. The bottom view in the figure looks along the payload X axis normal to both the line of sight of the payload, (Z axis) and the elevation gimbal axis. It shows two actuators, oriented parallel to the payload axis, which can provide pointing control around the X axis and translational isolation along Z. Pointing control of the elevation yoke around the X axis (following payload motion on this axis), is achieved using the azimuth gimbal.

The pointing performance of the proposed magnetic pointing and isolation system was evaluated using a planar three degree of freedom (3 DOF) simulation based on the configuration in Figure 4-1. (The simulation was developed using the MATRIX-X design and analyses program from Integrated Systems Inc.) The 3 DOF's in the performance model include, i.) payload inertial angular motion around the payload X axis, θ_P, ii.) PPS elevation yoke angular motion around the X axis, θ_G, and iii.) translational motion of the payload normal to the pointing control axis, Zp. As Figure 4-1 makes clear, the elevation yoke rotation around the X axis is determined by the azimuth gimbal rotation and by the PPS base rotation normal to the two gimbal axes, θ_N. This latter parameter is viewed as a disturbance input to the model.

The selected planar model was chosen because it allows all potential disturbance sources, including θ_N, to be evaluated, without the complexity and cost of an 8 DOF model.

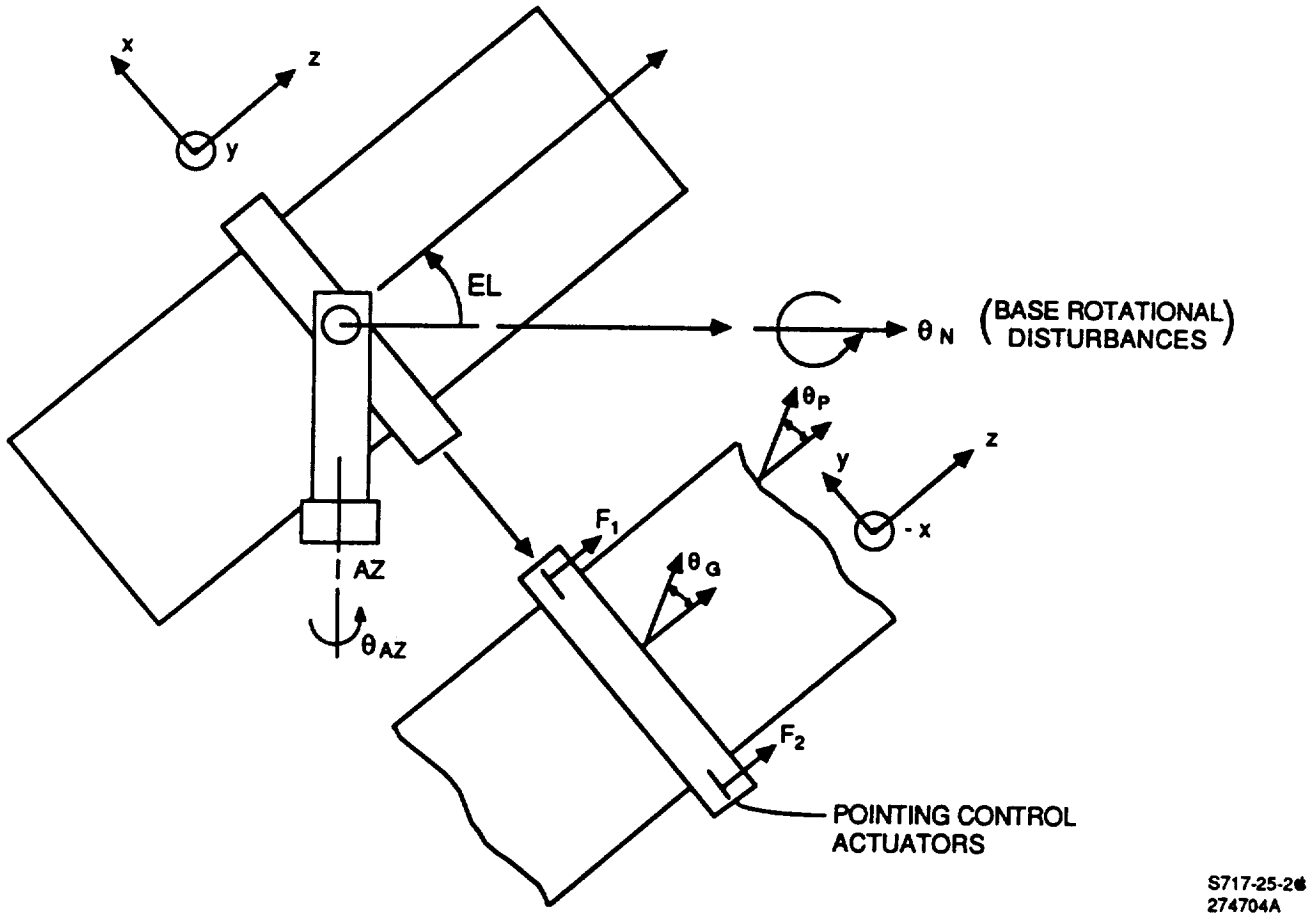

Figure 4-1
ATF Magnetic Pointing and Isolation
Physical Configuration

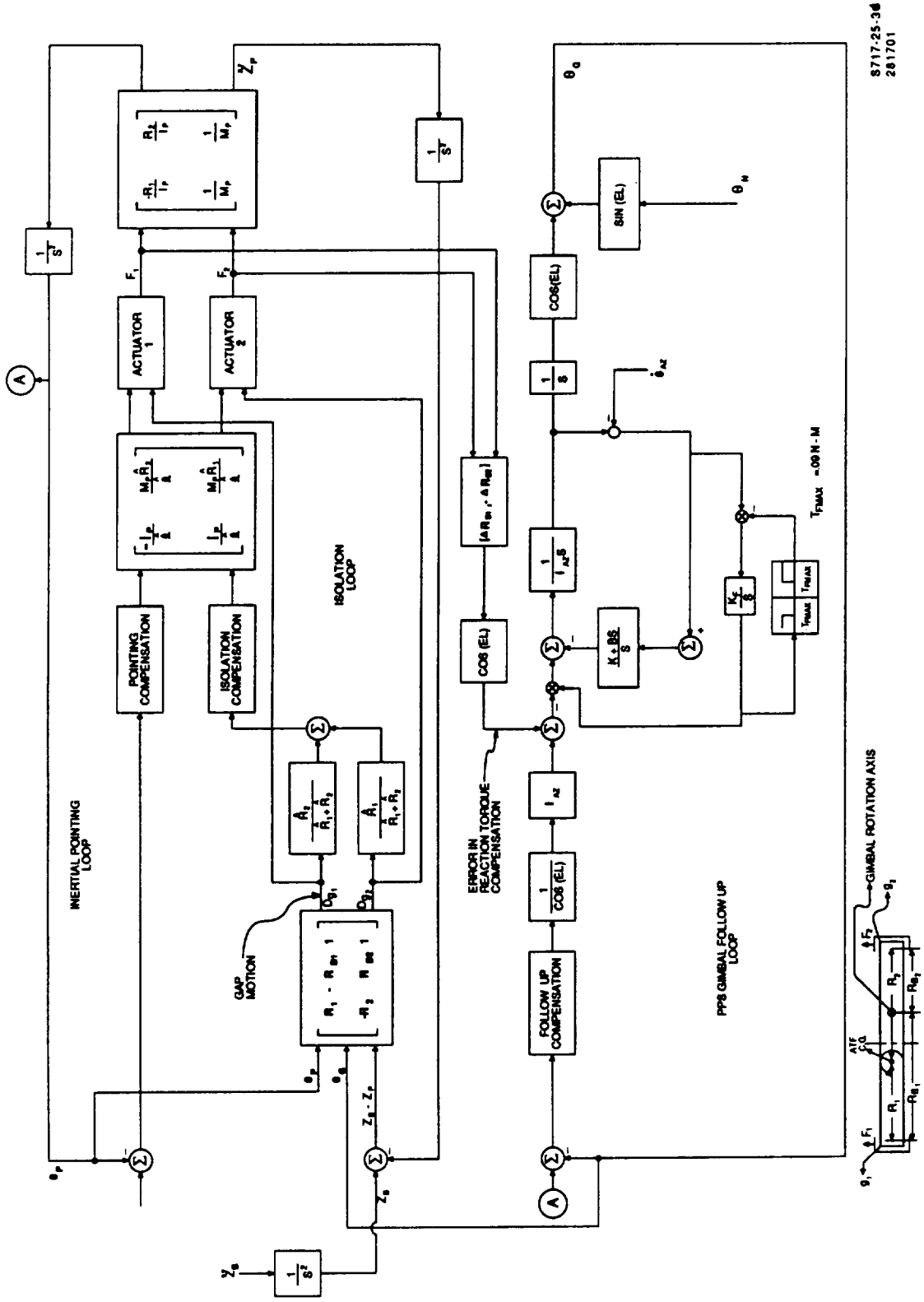

Figure 4-2
Magnetic Pointing and Isolation
Block Diagram

ORIGINAL PAGE IS
OF POOR QUALITY

The functional block diagram of the planar model is given in Figure 4-2. The control loops corresponding to θ_p, Z_p and θ_G are labelled Inertial Pointing Loop, Isolation Loop, and PPS Gimbal Follow-up Loop respectively. Other details of the model include;

- Two magnetic actuators for inertial pointing and isolation. Actuator models are included to show high frequency isolation response.
- Interface stiffness and damping (K and B) due to cabling across the azimuth gimbal.
- Bearing breakaway friction torque on the azimuth gimbal (T_{fmax}). Linear spring, K_F, up to breakaway.
- Effect of payload and PPS rotations (θ_p, θ_G), and payload and base translation (Z_p, Z_b) on the gap motion (armature to stator relative motion) at each actuator.
- Errors in knowledge of payload c.g. offset from the two actuators; actual R_1 versus assumed R_1; same for R_2.
- Errors in knowledge of gimbal rotation axis offset from the two actuators; ΔR_{B1}, ΔR_{B2}.
- Disturbance inputs due to base translations Z_b, base rotation around the azimuth gimbal θ_{AZ}, and base normal axis rotation, θ_N.

The block diagram for the actuator model is provided in Figure 4-3. Note that actuator force control is based on magnetic flux feedback. As shown, actuator force output is determined by both the force command and variations in the actuator gap from its nominal value. Parameters appearing in the diagram include, bias coil current I_{10}, nominal coil inductance, Lgo, bias flux corresponding to I_{10}, B_b, actuator pole force area, A, flux sensor gain, K_H, and flux control loop compensator gain, Kc, among others. Kc is set to produce a 500Hz closed loop bandwidth. Table 4-1 provides a symbol table for this model.

Table 4-2 lists the compensation forms and control bandwidths for the control loops appearing in Figure 4-2. The inertial pointing loop bandwidth limit, 10 rad/sec, is conservatively consistent with the assumed first mode frequency of the ATF telescope, i.e. 20 Hz. The form of the isolation compensation is chosen to produce a very fast ideal high frequency roll-off, (-100 dB/decade). As results in Section 5.0 show, however, the actuator dynamics limit the frequency range over which the -100 dB roll-off is actually produced.

Table 4-3 lists numeric values for several of the model parameters.

TABLE 4-1

MAGNETIC ACTUATOR MODEL
SYMBOL TABLE

L_{GO}	- Coil Inductance
R_A	- AC Coil Resistance
R_D	- DC Coil Resistance
L_L	- Actuator Leakage Inductance
A	- Actuator Pole Face Area
N	- Number of Coil Windings
K_1	- Actuator Gain Constant
K_H	- Flux Sensor Gain
μ	- Actuator Core Permeability
K_{PWM}	- Pulse Width Modulator Gain
K_C	- Flux Loop Compensator Gain
B_B	- Bias Flux
g_o	- Nominal Gap
I_{10}	- Bias Current

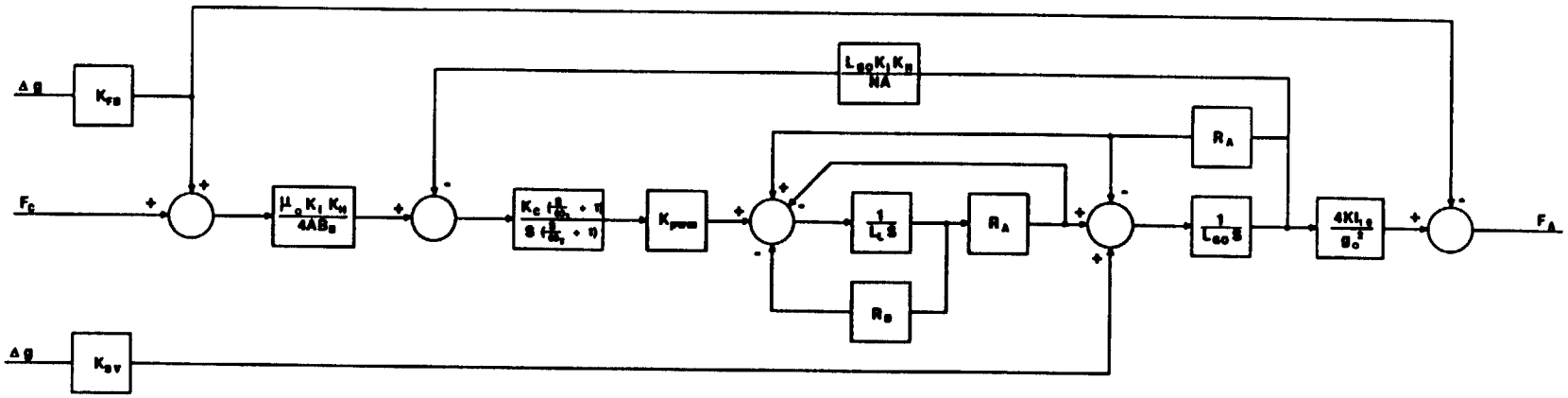

$$K_{FB} = 8 L_{GO} \left(\frac{B_B}{\mu_o N}\right)^2 \quad N/M \qquad K_{SV} = \frac{L_{GO} I_{10}}{g_o} \quad V/M/S$$

S717-25-46
281702

Figure 4-3
Linearized Magnetic Actuator

TABLE 4-2

SIMULATION MODEL COMPENSATION FORMS

- POINTING COMPENSATION:

$$\text{PID:} \quad \frac{K_R S^2 + K_P S + K_P K_I}{S}$$

WITH OPEN LOOP BW < 10 RAD/SEC

- ISOLATION COMPENSATION:

$$\frac{\frac{\omega_C^3}{32}\left(\frac{S}{(\omega_C/4)} + 1\right)\left(\frac{S}{(\omega_C/8)} + 1\right)}{S\left(\frac{S^2}{(5\omega_C)^2} + \frac{S}{5\omega_C} + 1\right)^2}$$

ω_C BETWEEN 7 AND 4 RAD/SEC

- GIMBAL FOLLOW-UP COMPENSATION:

LEAD/LAG

$$\frac{K_{PG}S + K_{PG}K_{IG}}{S\left(\frac{S}{\omega_{LAG}} + 1\right)} \qquad 1 \text{ RAD/SEC}$$

- ACTUATOR BANDWIDTH 3140 RAD/SEC

S717-25-5
267701

TABLE 4-3

SIMULATION PARAMETERS

θ_P — PAYLOAD INERTIAL ANGULAR MOTION

θ_G — GIMBAL ANGULAR MOTION

Z_B — BASE TRANSLATIONAL MOTION ON Z AXIS

Z_P — PAYLOAD TRANSLATIONAL MOTION ON Z AXIS

θ_N — BASE ROTATIONAL MOTION NORMAL AXIS

θ_{AZ} — BASE ROTATIONAL MOTION AZIMUTH AXIS

POINTING COMPENSATION: $K_R = 10$, $K_P = 35$, $K_I = 1.7$
FOR 10 RAD/SEC POINTING LOOP

ISOLATION COMPENSATION: ω_C = OPEN LOOP BANDWIDTH

GIMBAL FOLLOWUP: $\omega_{LAG} = 4$, $K_{PG} = (.25\ I_{AZ})$, $K_{IG} = .25$

I_P - 160,000 Kg-m^2 (~120,000 SLUG-FT^2) } PAYLOAD INERTIA AND MASS

M_P - 3660 Kg (250 SLUGS) }

I_{AZ} - 2050 Kg-m^2 (~1500 SLUG-FT^2) - INERTIA AROUND AZIMUTH GIMBAL - PPS ONLY

L - 1.85m (~6 FT) - ACTUATOR SPAN, $\hat{L}$ - ESTIMATE OF SPAN, ALSO 1.85m.

$R_1 - \hat{R}_1$ - MISKNOWLEDGE IN CG OFFSET = 2 CM - INCLUDES THE EFFECT OF ACTUATOR FORCE RESPONSE ERRORS

$\Delta R_{B1}, \Delta R_{B2}$ - MISKNOWLEDGE IN LOCATION OF MAGNETIC ACTUATOR FORCE APPLICATION POINTS WITH RESPECT TO THE GIMBAL CONTROL AXIS = 5 CM (~2 INCHES)

EL - 45°

K - AZIMUTH GIMBAL (CONTROL GIMBAL FOR THE MODEL) INTERFACE STIFFNESS --1700 N•m/RAD (~ 1250. FT-LBS/RAD)

B - 23100 (N•m-SEC)/RAD (~ 17000 FT-LBS-SEC/RAD)

S717-25-6

SECTION 5.0

MAGNETIC SYSTEM POINTING STUDY RESULTS

SECTION 5.0
MAGNETIC SYSTEM POINTING STUDY RESULTS

5.1 POINTING ERROR AND FORCE AND MOTION REQUIREMENTS

The primary results of the study conducted with the simulation described in Section 4.0 relate to the payload pointing errors obtained in response to base acceleration disturbances, $\ddot{Z}_b$ in Figure 4-2, and base rotational motion, θ_{AZ} and θ_N in the same figure. In addition to pointing performance results, however, the simulation was used to define system response characteristics required to specify magnetic actuator force and gap parameters. These characteristics include required control force (sum of the actuator outputs, F_1 and F_2 in Figure 4-2) and actuator gap motion, Dg_1 (or $(Z_b - Z_p)$ since gap motion is dominated by $(Z_b - Z_p)$). The three items below summarize these main study objectives.

- Define pointing performance for magnetic pointing system--high and low frequency disturbances--as a function of input disturbance level and pointing and isolation bandwidths.
- Define peak actuator gap motion as a function of input disturbance level and isolation and pointing loop bandwidths.
- Define control force requirements as a function of input disturbance level.

While space station linear and rotational disturbances were expected to have the greatest effect on ATF pointing performance, there was some concern that magnetic actuator noise might, also, produce a significant error component. Consequently, the magnetic pointing study has investigated the effects of actuator force noise, input as a disturbance at F1 in Figure 4-2, on pointing error.

As described in the requirements section above (Section 2), pointing performance for the ATF magnetic pointing and isolation system is defined by the pointing error generated by single frequency sinusoidal disturbances, (both linear acceleration and base rotations) in the frequency regions below and above 5 Hz. Pointing error levels are determined with the simulation by generating the magnitude frequency response curves for the transfer functions from the various disturbance sources to θ_p. At any particular frequency (corresponding to the frequency of the disturbance input) the magnitude of θ_p depends on the magnitude of the disturbance input and the bandwidths of the pointing and isolation control loops.

Figures 5-1 and 5-2 show frequency response curves for the $\ddot{Z}_b$ to θ_p transformation. The $\ddot{Z}_b$ magnitude used in generating the curves is the nominal 0.01 g. In each figure curves are shown for pointing loop bandwidths spanning the range 5 to 10 rad/sec.

In Figure 5-1 the isolation bandwidth is 5 rad/sec, in Figure 5-2 it is 7 rad/sec. The two figures together show that the peak pointing error for frequencies below 5 Hz is determined by the pointing loop bandwidth and is relatively unaffected by the isolation bandwidth. In each figure the 1 arcsec pointing spec for frequencies below 5 Hz is satisfied for pointing loop bandwidths above 7 rad/sec. Note, also, that the frequency at which the peak error below 5 Hz occurs depends on the pointing loop BW.

For frequencies above 5 Hz the peak error, which occurs at 5 Hz, is determined by the isolation bandwidth. The pointing loop spec is satisfied for both the 5 and 7 rad/sec isolation BW's.

The frequency response of relative motion at the actuator, $(Z_b - Z_p)$, corresponding to a 0.01 g value of $\ddot{Z}_b$ is shown in Figure 5-3. The different curves in the figure were generated with the different levels of isolation BW indicated. Pointing bandwidth has much less of an effect on the curves. Only the peak value on the curves are of interest in determining potential effects on the actuator gap. If we set 0.5 inch (1.27 cm) as the desirable relative motion limit, then the isolation bandwidth must be 5 rad/sec or higher.

Control force requirements in response to a 0.01 g translational acceleration, $\ddot{Z}_b$, are determined from the curves in Figure 5-4. As with the relative motion response curves, the control force frequency response is sensitive to the isolation BW. Indeed, the curves essentially define the transmissibility of the isolation loops. The peak force magnitude is the same for each isolation BW, but the frequency at which the peak occurs moves out as the BW is increased. Between 20 and 50 Hz the response curves transitions from the ideal isolation roll off characteristics to a much less rapid decline as the actuator dynamics interact with the control loop.

Pointing error in response to normal axis and azimuth axis disturbance motions are illustrated in Figures 5-5 and 5-6 respectively. The curves were generated assuming a 1 rad. disturbance magnitude and 5 rad/sec isolation bandwidth. At low frequencies, below 5 Hz, the curves show a sensitivity to pointing loop BW although the peak errors do not vary significantly. At 5 Hz the azimuth disturbance response curve is a factor of 3 or more lower than the normal axis disturbance curve at the same frequency. This difference is attributed to the isolation characteristics of the azimuth gimbal. In fact, above 10 Hz the azimuth curve roll off is -40 dB/decade compared with -20 dB/decade for the normal axis curve.

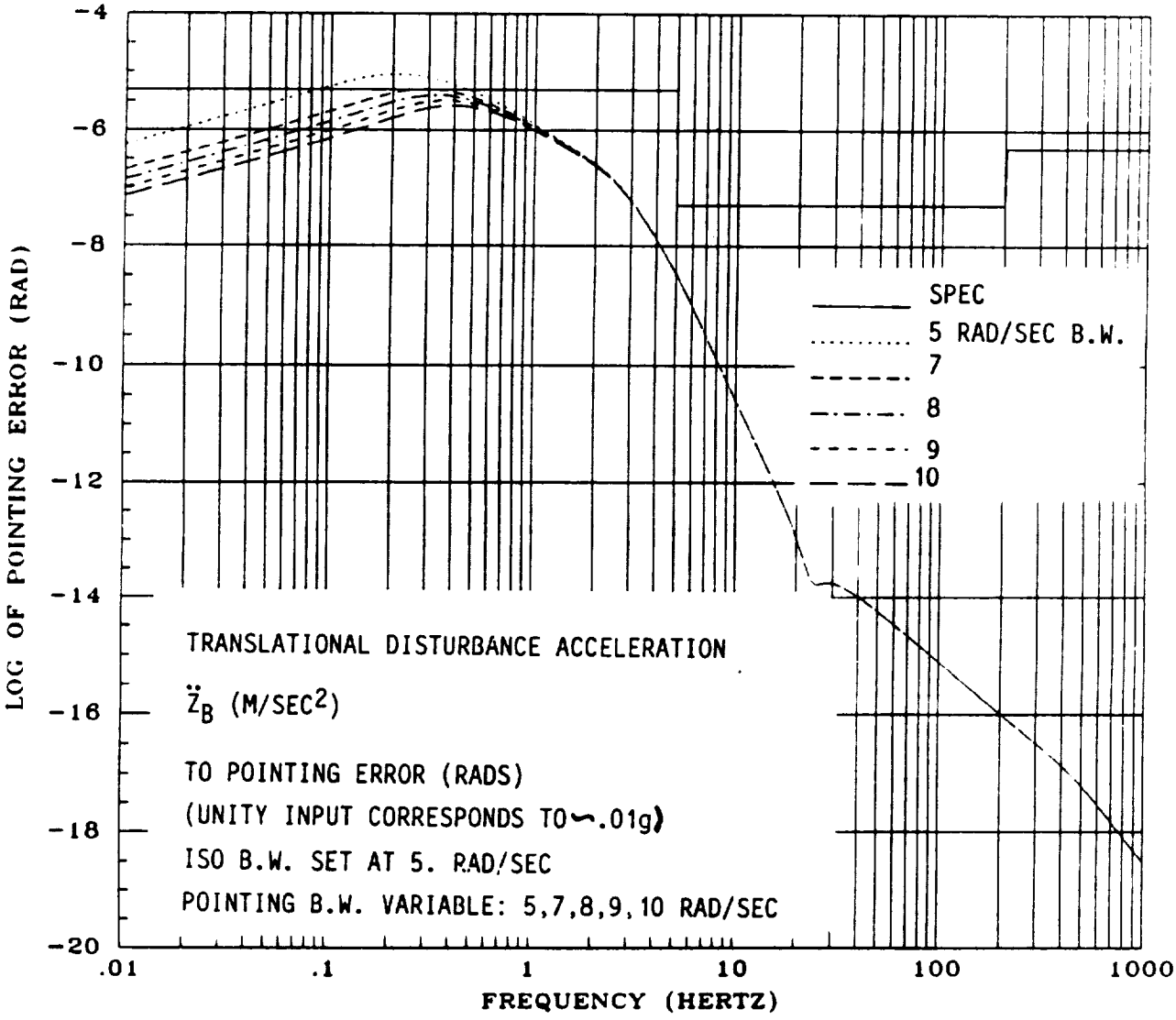

S717-25-7

Figure 5-1
Frequency Response Curves, Translational
Disturbance Acceleration to Pointing Error
ISO BW = 5 rad/sec

ORIGINAL PAGE IS
OF POOR QUALITY

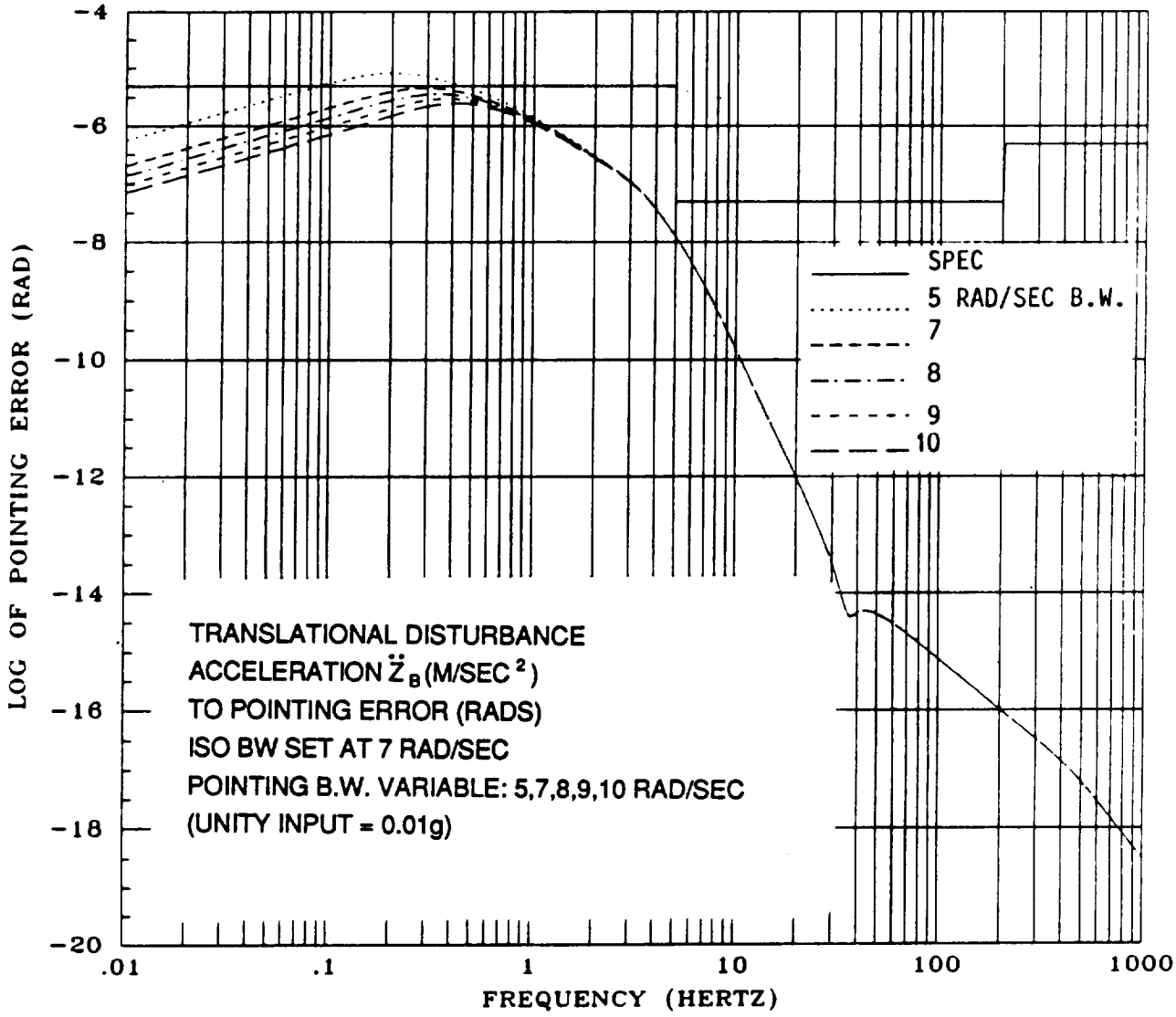

S717-25-8

Figure 5-2
Frequency Response Curves, Translational
Disturbance Acceleration to Pointing Error,
ISO BW = 7 rad/sec

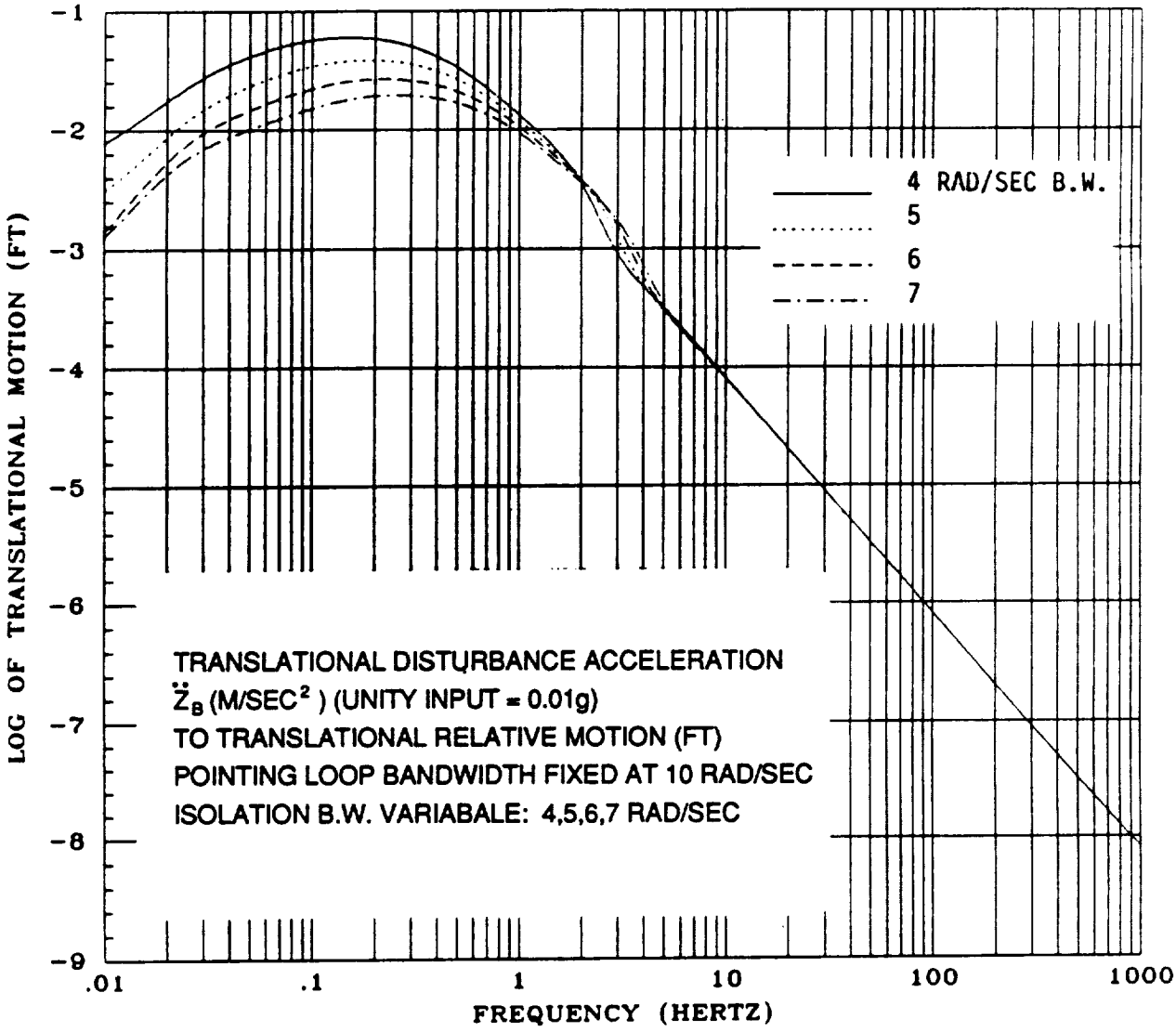

Figure 5-3
Frequency Response Curves, Translational Disturbance
Acceleration to Translational Relative Motion

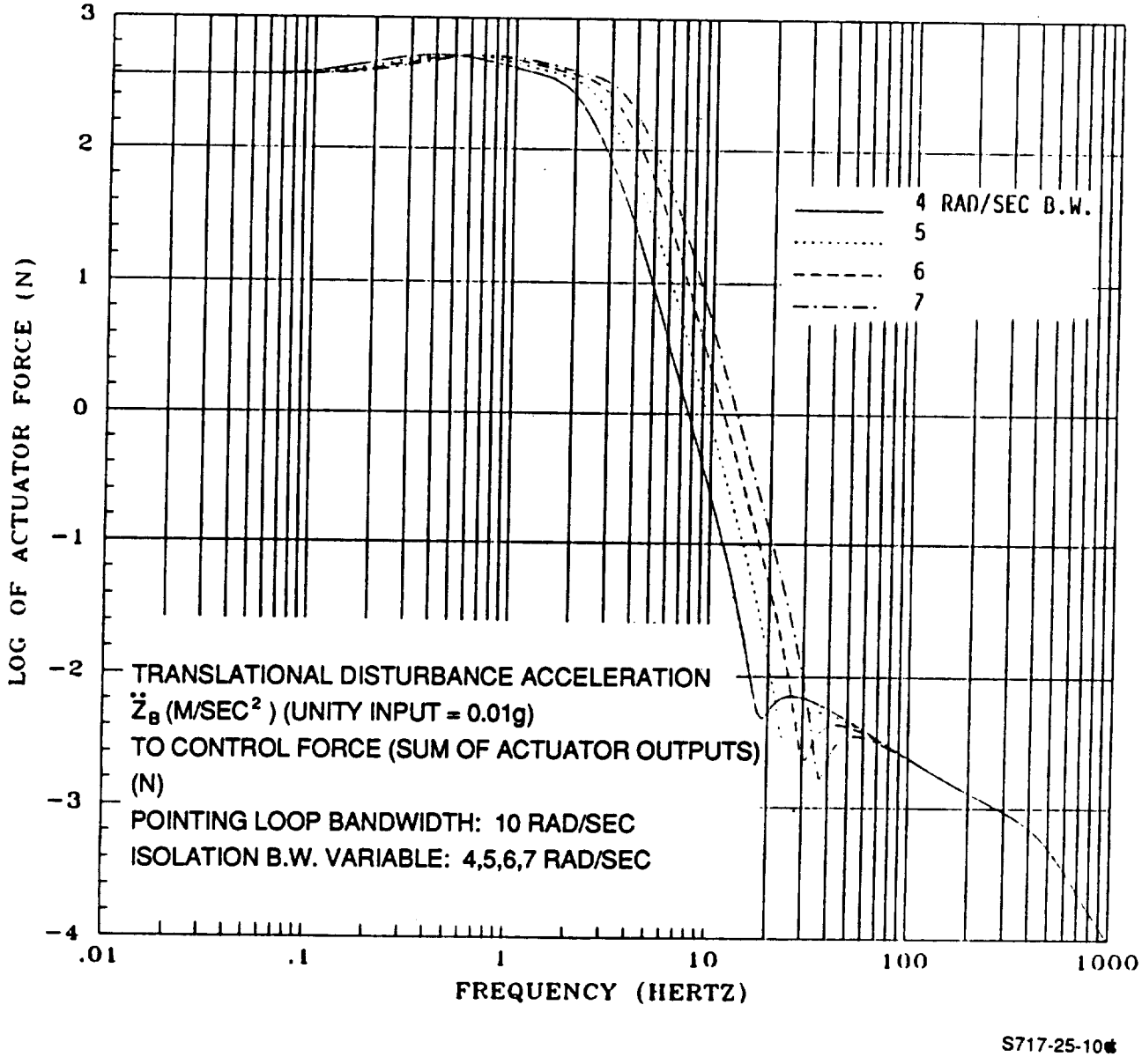

Figure 5-4
Frequency Response Curves, Translational Disturbance
Acceleration to Control Force

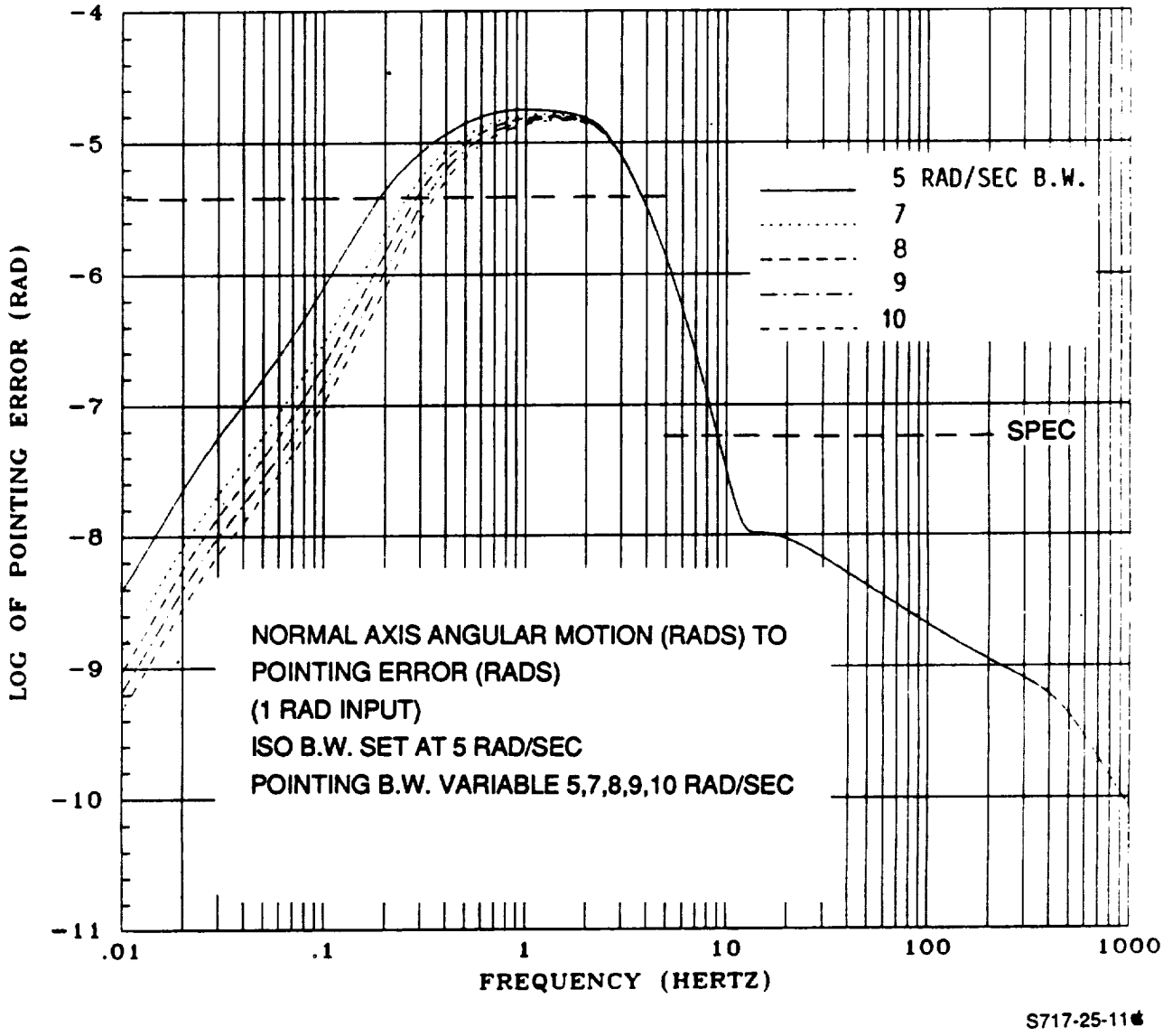

Figure 5-5
Frequency Response Curves, Normal Axis
Angular Motion to Pointing Error

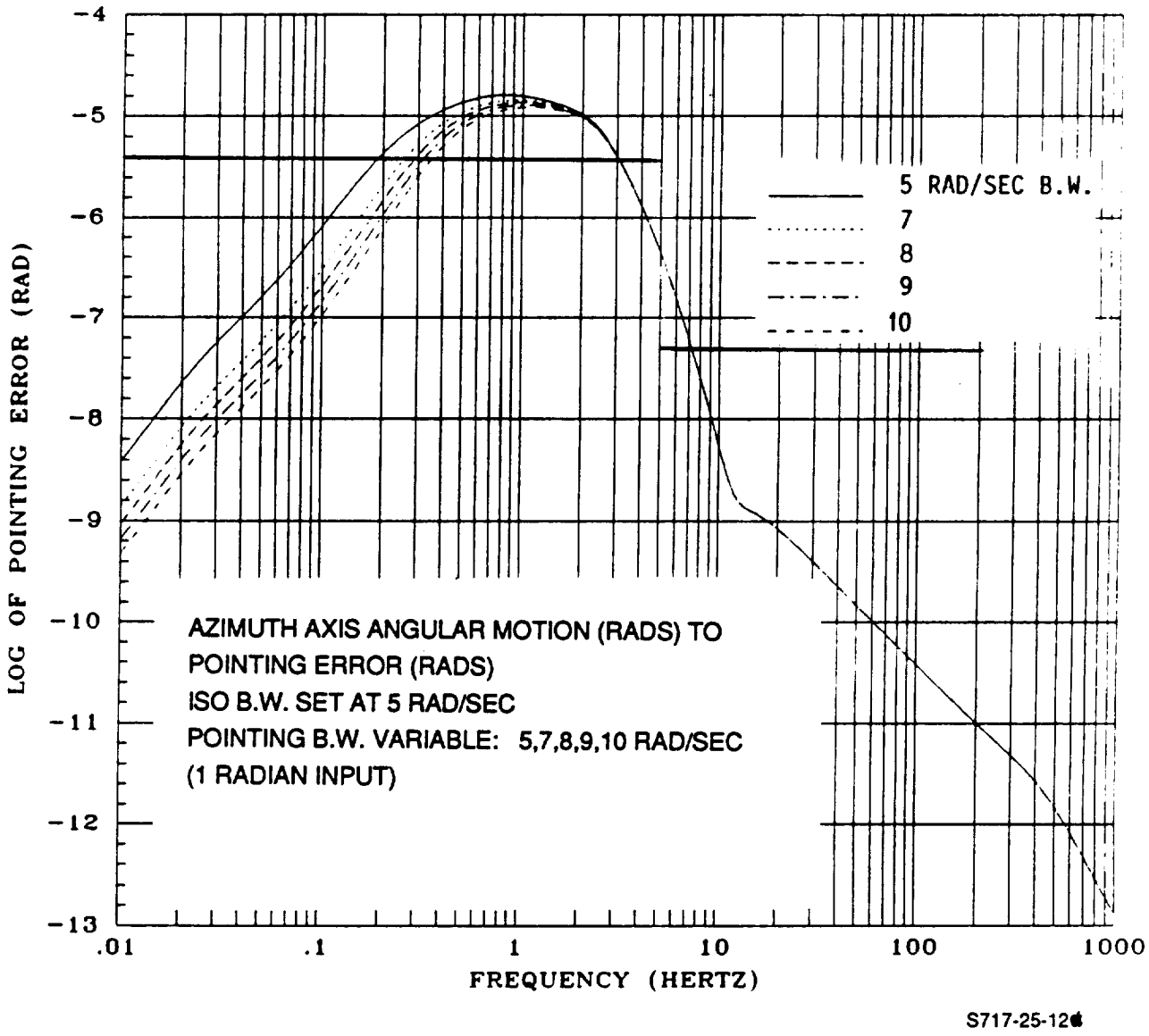

Figure 5-6
Frequency Response Curves, Azimuth Axis
Angular Motion to Pointing Error

While the error levels in Figures 5-5 and 5-6 are significant, they are also very unrealistic in that they are based on a 1-rad. disturbance. If the curves are scaled down to reflect a 1-arcmin disturbance, the resulting errors are, in fact, much smaller than those produced by the linear acceleration disturbances. Table 5-1 summarizes the high and low frequency pointing errors based on the curves in Figures 5-5 and 5-6 scaled to reflect a 1-arcmin input. In all cases the errors are more than an order of magnitude below the requirement spec values.

In order to emphasize the effect of the variation in translational disturbance magnitude on pointing error, gap motion and control force, data from Figures 5-1, 5-2, 5-3 and 5-4 has been used to generate linear curves for high and low frequency pointing errors, gap motion and control force versus disturbance magnitude.

Figure 5-7 shows pointing error (at 5 Hz and below 5 Hz) versus disturbance magnitude for different levels of isolation bandwidth. Pointing loop bandwidth is fixed at 10 rad/sec. The figure indicates that both high and low frequency pointing requirements are met out to a disturbance magnitude of more than 0.018 g if a 5 rad/sec isolating BW is used. Figure 5-8 shows similar error curves except that pointing BW is varied and isolating BW is fixed at 5 rad/sec. In this case, a pointing BW of more than 10 rad/sec (see Figure 5-8) is required to meet pointing specifications out to the 0.018 input level.

Gap motion versus disturbance magnitude is illustrated in Figure 5-9. The sensitivity to isolation BW is even more evident in this figure than in Figure 5-3 because of the linear scale. The curves in the figure indicate that a 0.5-inch motion limit can not be maintained out to 0.02 g without increasing the isolation BW beyond 6 rad/sec.

The linear force versus disturbance magnitude curve, based on the results in Figure 5-4, is shown in Figure 5-10.

5.2 ACTUATOR NOISE INDUCED POINTING ERROR

In order to evaluate the expected effect of magnetic actuator force noise on ATF pointing error, two data items are required; an estimate of the PSD of the actuator noise, and the magnitude frequency response curve for the transfer function from actuator disturbance force to pointing error. Available actuator force noise data obtained using a 7 lb-force (31 N) (peak) actuator indicates that the noise PSD is much less than 1 N^2/Hz. The performance simulation based on the model of Figure 4-2 has been used to generate the required frequency response curve, illustrated in Figure 5-11.

The response curve in Figure 5-11 is used to determine the RMS of the pointing error below 5 Hz as a function of the noise PSD (assumed constant) in that frequency region, and the RMS of the pointing error above 5 Hz and below 1000 Hz, again as a function of the noise PSD in that region. These functions, illustrated in Figures 5-12 and 5-13, are evaluated using the following expressions:

$$\left(\int_0^5 K_{psd}\, H^2(\omega)d\omega\right)^{1/2} \quad \text{and} \quad \left(\int_5^{1000} K_{2psd}\, H^2(\omega)d\omega\right)^{1/2}$$

$H(\omega)$ is the square of the magnitude frequency response, approximated from the curve in Figure 5-11, and K_{psd} is the actuator noise PSD in (N^2/Hz).

TABLE 5-1

ERROR RESPONSE TO 1 ARCMIN AZIMUTH AND NORMAL
AXIS ROTATION DISTURBANCES
(Isolator BW = 5 rad/sec)

Pointing Loop Bandwidth (rad/sec)	Pointing Error w/ 1 arcmin disturbance			
	θ_{AZ}		θ_{N}	
	Below 5 Hz ($\widehat{sec}$)	At 5 Hz ($\widehat{sec}$)	Below 5 Hz ($\widehat{sec}$)	At 5 Hz ($\widehat{sec}$)
5	0.0011	0.0001	0.0012	0.0003
7	0.0009	0.0001	0.0011	0.0003
8	0.0009	0.0001	0.0011	0.0003
9	0.0008	0.0001	0.0010	0.0003
10	0.0008	0.0001	0.0010	0.0003

S717-25-13
275701A

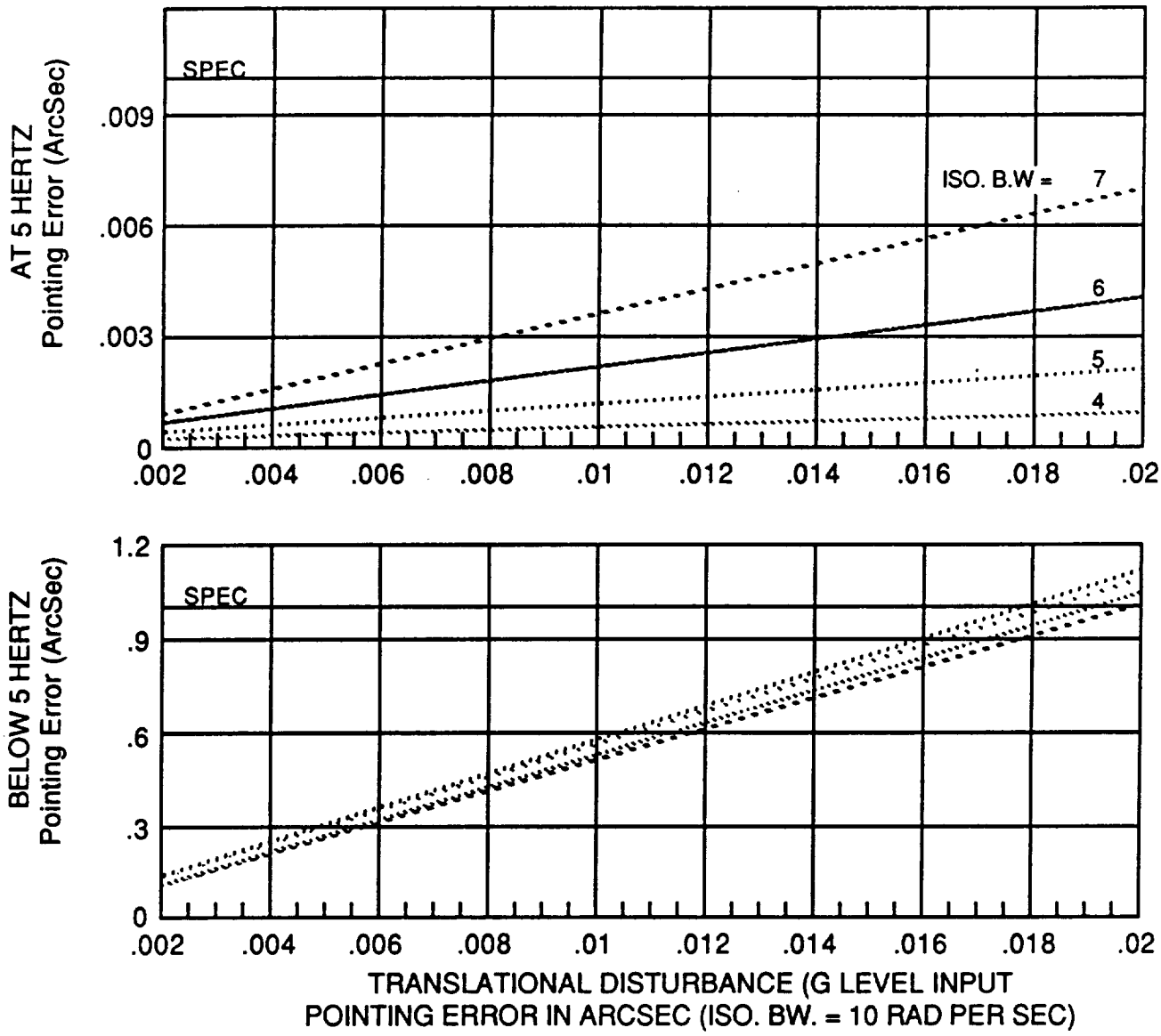

Figure 5-7
Pointing Error Versus Linear Acceleration Disturbance Level
ISO BW - Variable, PT BW - 10 rad/sec

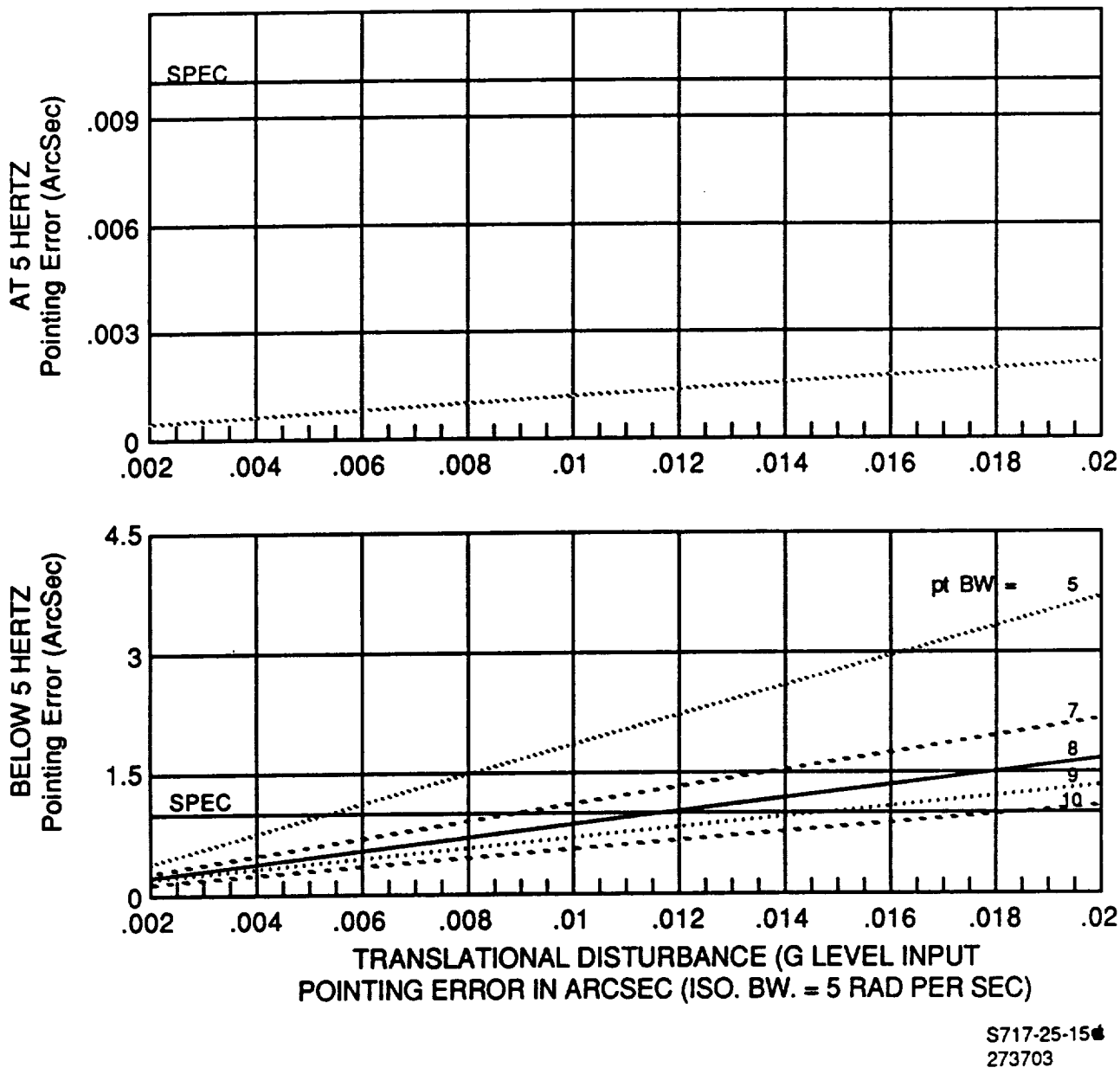

Figure 5-8
Pointing Error Versus Linear Acceleration Disturbance Level
ISO BW - 5 rad/sec, PT BW - Variable

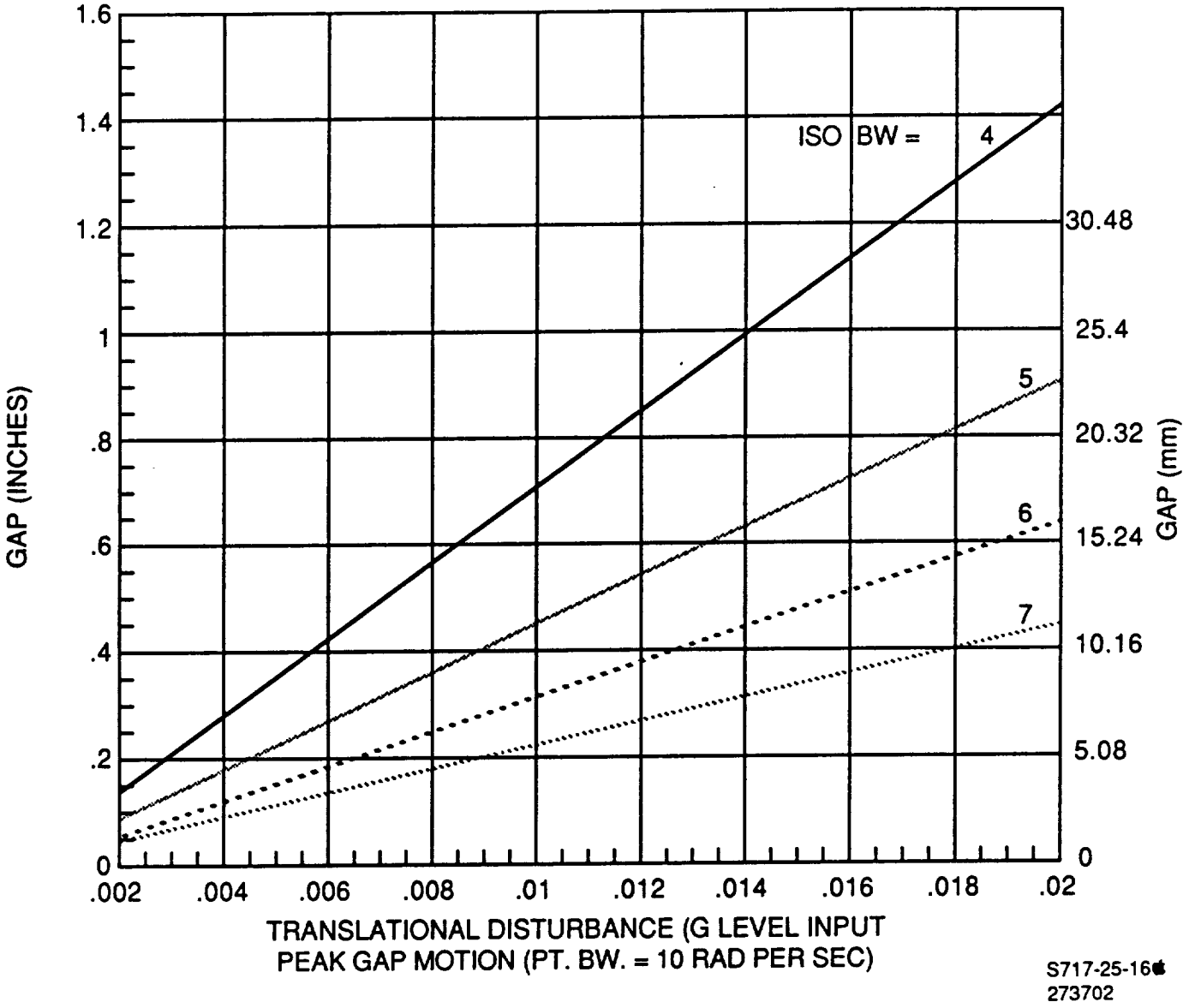

Figure 5-9
Actuator Gap Motion Requirements Versus Linear
Acceleration Disturbance Level, Isolation BW-Variable

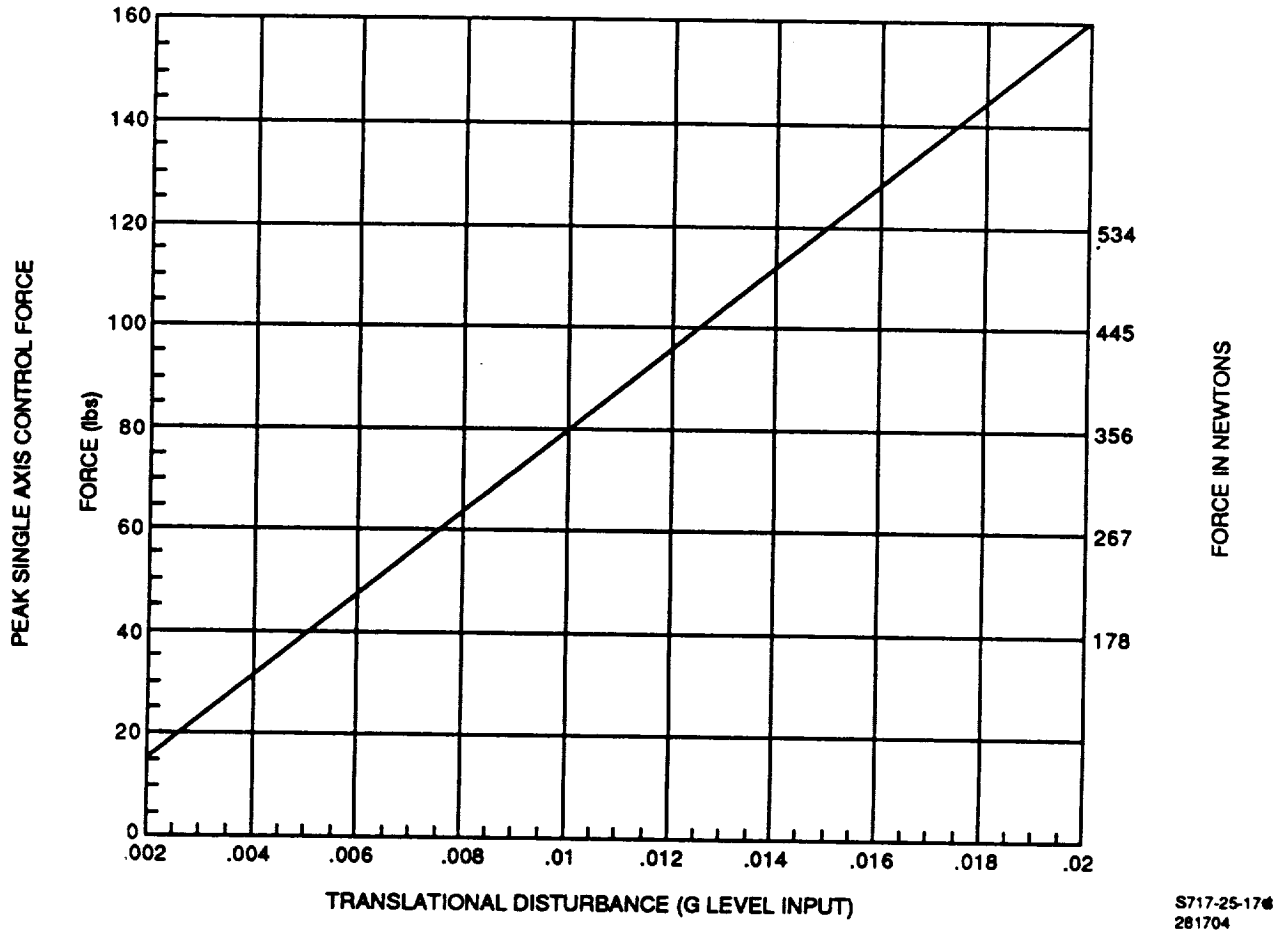

Figure 5-10
Control Force Requirements

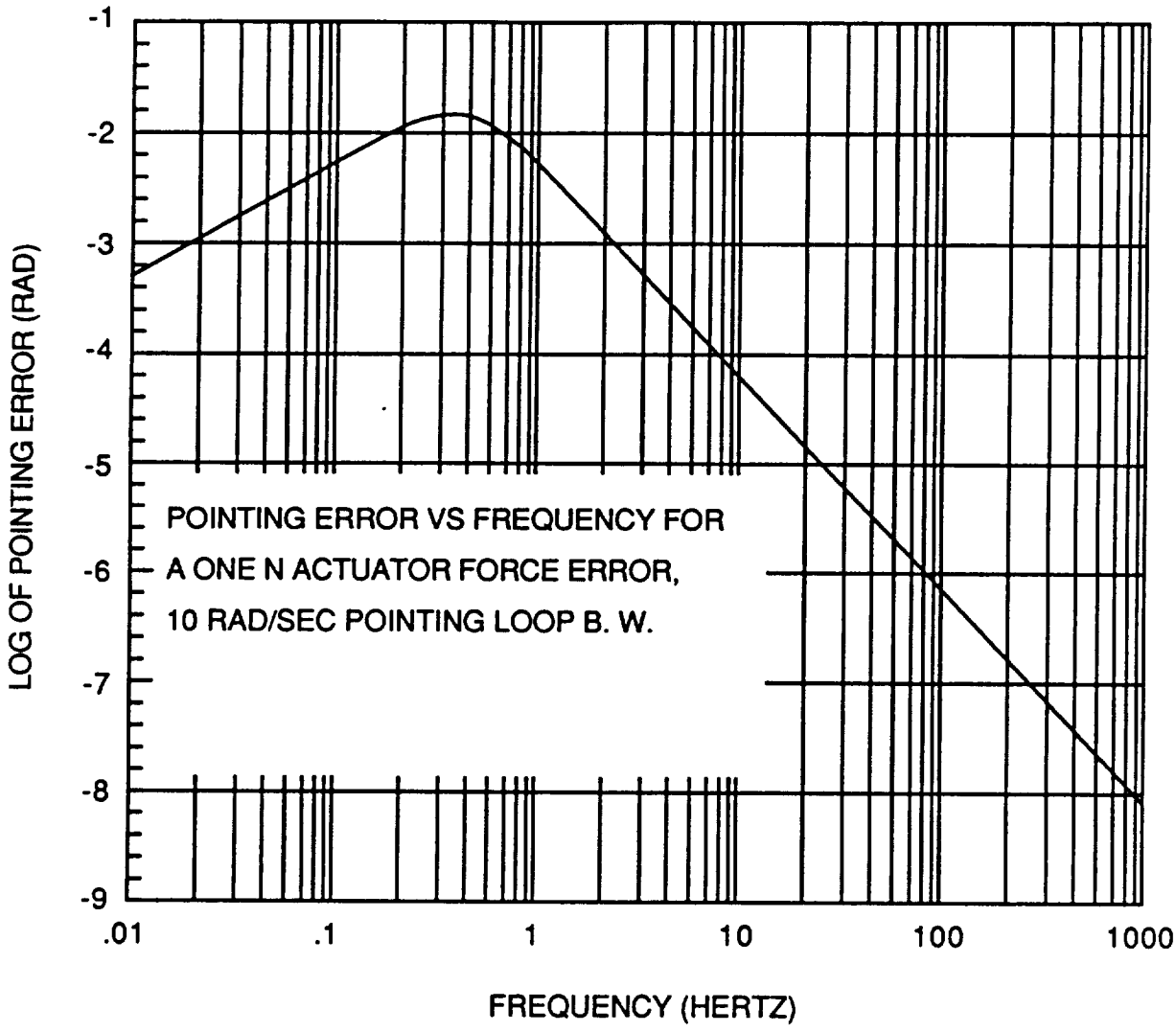

Figure 5-11
Pointing Error vs Frequency for a One N Actuator Force Error

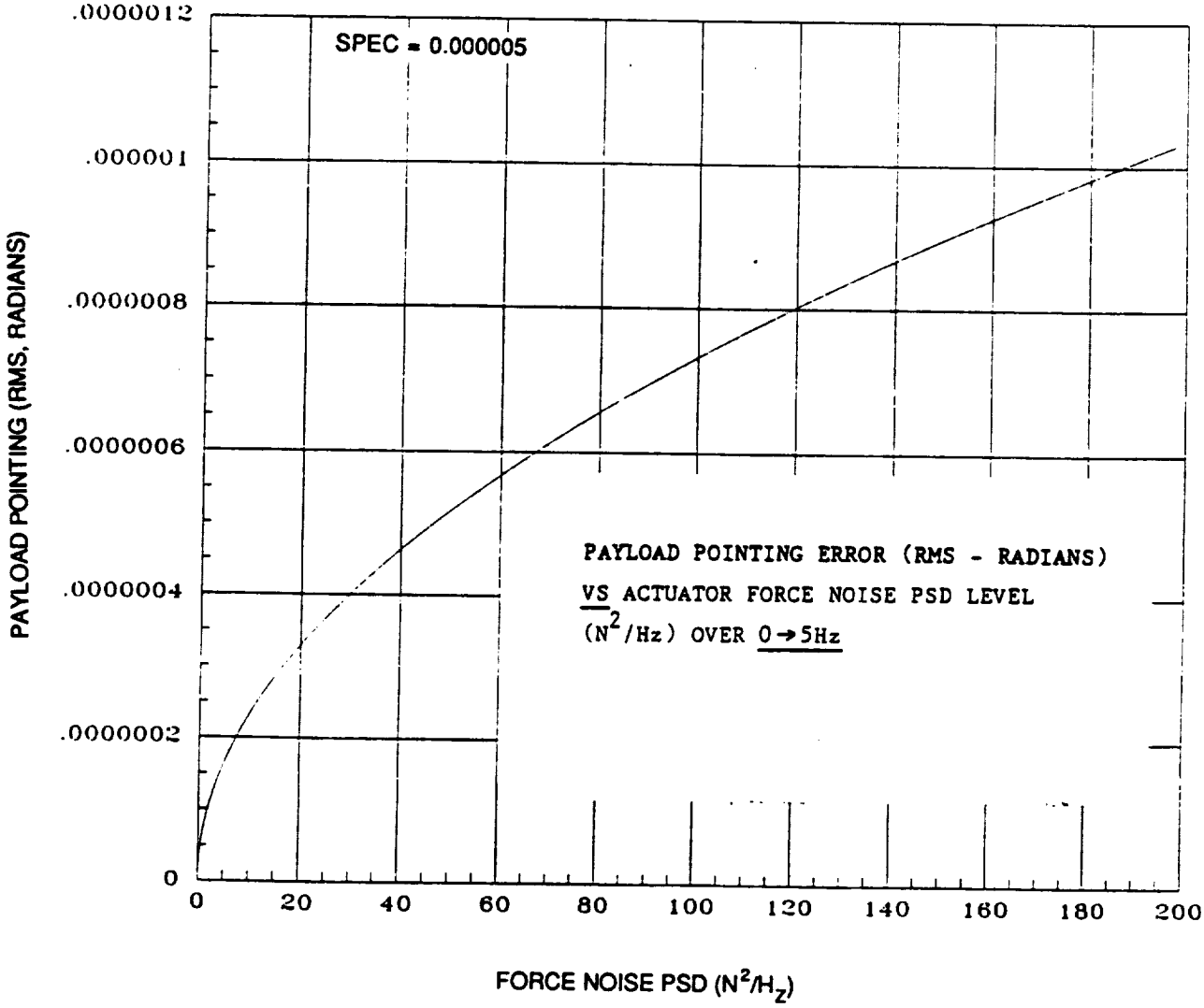

Figure 5-12
Payload Pointing Error vs Actuator Force Noise
PSD Over 0 to 5 Hz

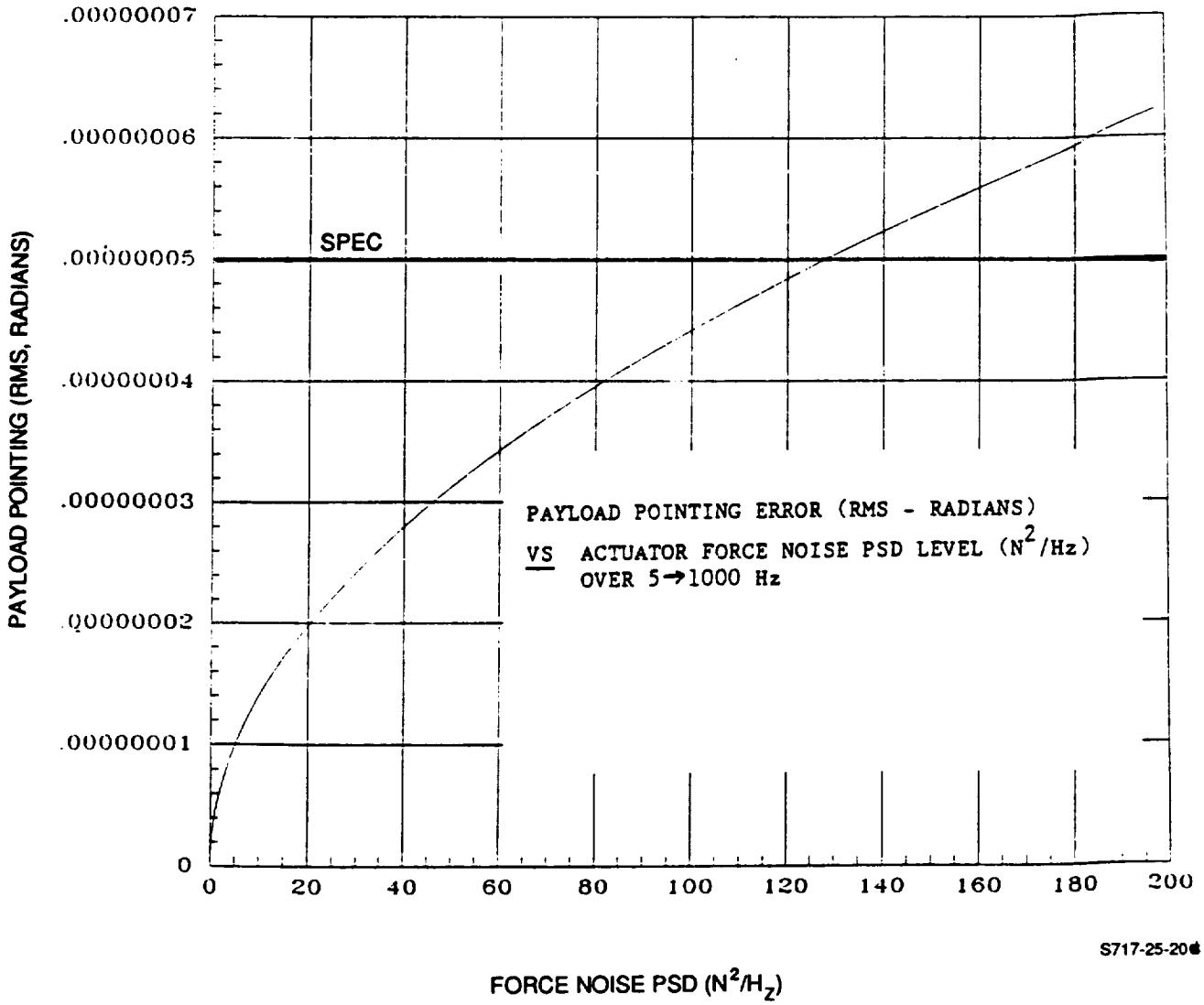

Figure 5-13
Payload Pointing Error vs Actuator Force Noise
PSD Over 5 to 1000 Hz

Obviously, even a 1 N^2/Hz actuator noise PSD level results in an insignificant pointing error contribution, both below and above 5 Hz.

5.3 STUDY SUMMARY

The following items summarize the results from the magnetic pointing and isolation study.

- Low frequency pointing performance is affected most by pointing loop BW--high frequency performance by the isolator BW.
- A 10 rad/sec pointing BW and 6 rad/sec iso BW satisfy low and high frequency pointing requirements for single axis disturbances <0.018g.
- For the nominal disturbance input level, 0.01g, gap motion is less than 0.5 inch. (1.27cm).
- Angular motion disturbances at the 1 arcmin level are insignificant in their effect on pointing error.
- Actuator force noise is an insignificant contributor to pointing error.

SECTION 6.0

PASSIVE BASE ISOLATOR MODEL

SECTION 6.0

PASSIVE BASE ISOLATOR MODEL

As with the magnetic pointing study, evaluation of ATF pointing performance assuming a PPS/Base Isolator pointing configuration was performed with a simple planar model. In contrast to the definition of a full 6 DOF magnetic actuator configuration (Section 8.0), however, no candidate 6 DOF configuration is presented for the base isolator. The study defines the pointing performance that can be achieved for various levels of isolation of both base linear accelerations and base rotations. Other assumptions related to the base isolator model include:

- PPS includes only the azimuth and elevation gimbal. The cross elevation gimbal is replaced with a roll mechanism.
- The isolator configuration is made up of spring-fluidic damper elements.
- The PPS pointing loop bandwidth is limited by the assumed gimbal structure first modal frequency, 5 Hz.
- Dynamic interactions between the base isolator elements and flexibilities in the PPS, i.e., gimbal structure, gimbal interface stiffness, have been ignored.

6.1 ISOLATOR ELEMENT

The passive isolator element is assumed to have the ideal form shown in Figure 6-1. Such a device may be implemented using a fluidic viscous damper design proposed by Sperry Satellite Systems Division for other space isolation applications, including isolation of the space telescope (ST) reaction wheels. The ST device is shown in Figure 6-2. Using the parameters defined in Figure 6-1, the frequency response functions from base acceleration, $\ddot{X}_B$, to payload acceleration, $\ddot{X}_p$, (transmissibility), and from $\ddot{X}_B$ to relative motion across the actuator, $X_p - X_b$, (relative transmissibility), are defined in Table 6-1. Figure 6-3 illustrates the effect of variation in N with ω_0=1 and Q selected (as a function of N) to minimize peaking. The effective isolation bandwidth increases as N increases. At the same time, the achievable minimum low frequency peaking (optimum Q) decreases. In performing the passive isolator study, it has been assumed that a fluid damper can be configured to achieve any required Q level.

A large value of N indicates a significant difference in the stiffness of the parallel springs in the isolator element. From a practical standpoint, it may be difficult to build an element with parallel spring components that both deflect the same amount and yet have a large stiffness ratio. For example, the limit on N for a ST type design is estimated to be about 3. This value has, thus, been used as a limit in defining a best case isolator for the ATF pointing study.

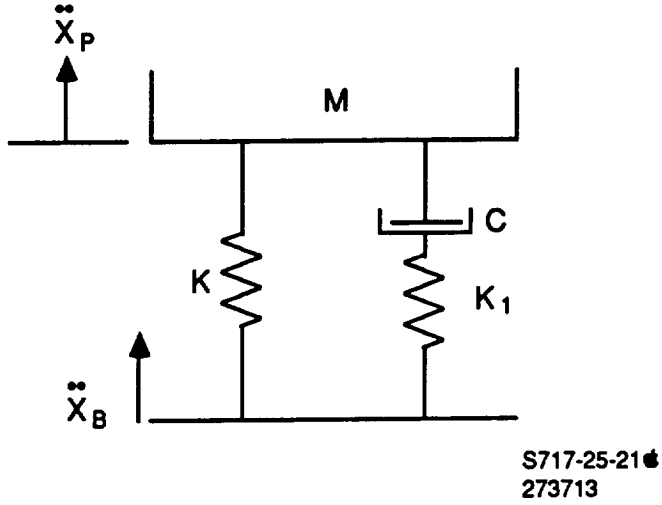

Figure 6-1
Passive Isolator Lumped Mass Model

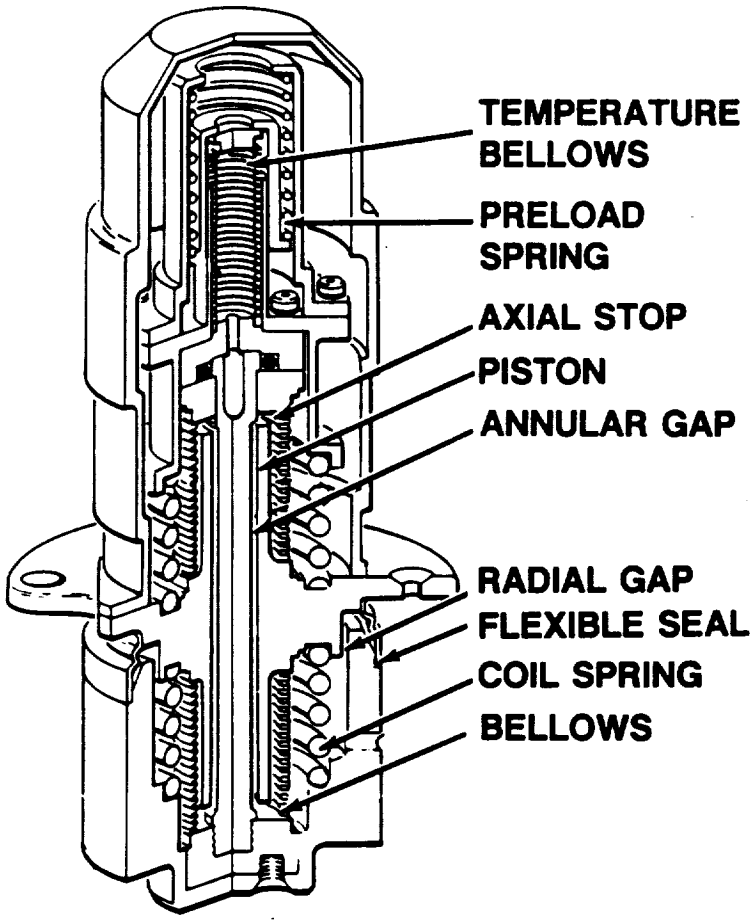

- Damping and stiffness are deterministic and independently controlled
- Viscous fluid damping gives zero hysteresis, zero stiction effects

S717-25-22

Figure 6-2
Unit Isolator

TABLE 6-1

PASSIVE ISOLATOR TRANSMISSIBILITY
AND RELATIVE TRANSMISSIBILITY

DIRECT TRANSMISSIBILITY

$$\frac{\ddot{X}_P}{\ddot{X}_B} = \frac{\left(\frac{S}{\omega_o}\right)\left(\frac{N+1}{NQ}\right) + 1}{\left(\frac{S}{\omega_o}\right)^3\left(\frac{1}{NQ}\right) + \left(\frac{S}{\omega_o}\right)^2 + \frac{S}{\omega_o}\left(\frac{N+1}{NQ}\right) + 1}$$

RELATIVE TRANSMISSIBILITY

$$\frac{X_P - X_B}{\ddot{X}_B} = \frac{1}{S^2} \frac{\left(\frac{S}{\omega_o}\right)^3\left(\frac{1}{NQ}\right) + \left(\frac{S}{\omega_o}\right)^2}{\left(\frac{S}{\omega_o}\right)^3\left(\frac{1}{NQ}\right) + \left(\frac{S}{\omega_o}\right)^2 + \left(\frac{S}{\omega_o}\right)\left(\frac{N+1}{NQ}\right) + 1}$$

WHERE $\omega_o = \sqrt{\frac{K}{M}}$ $\quad N = \frac{K_1}{K}$ $\quad Q = \sqrt{\frac{K_1 M}{C}}$

S717-25-23
274701

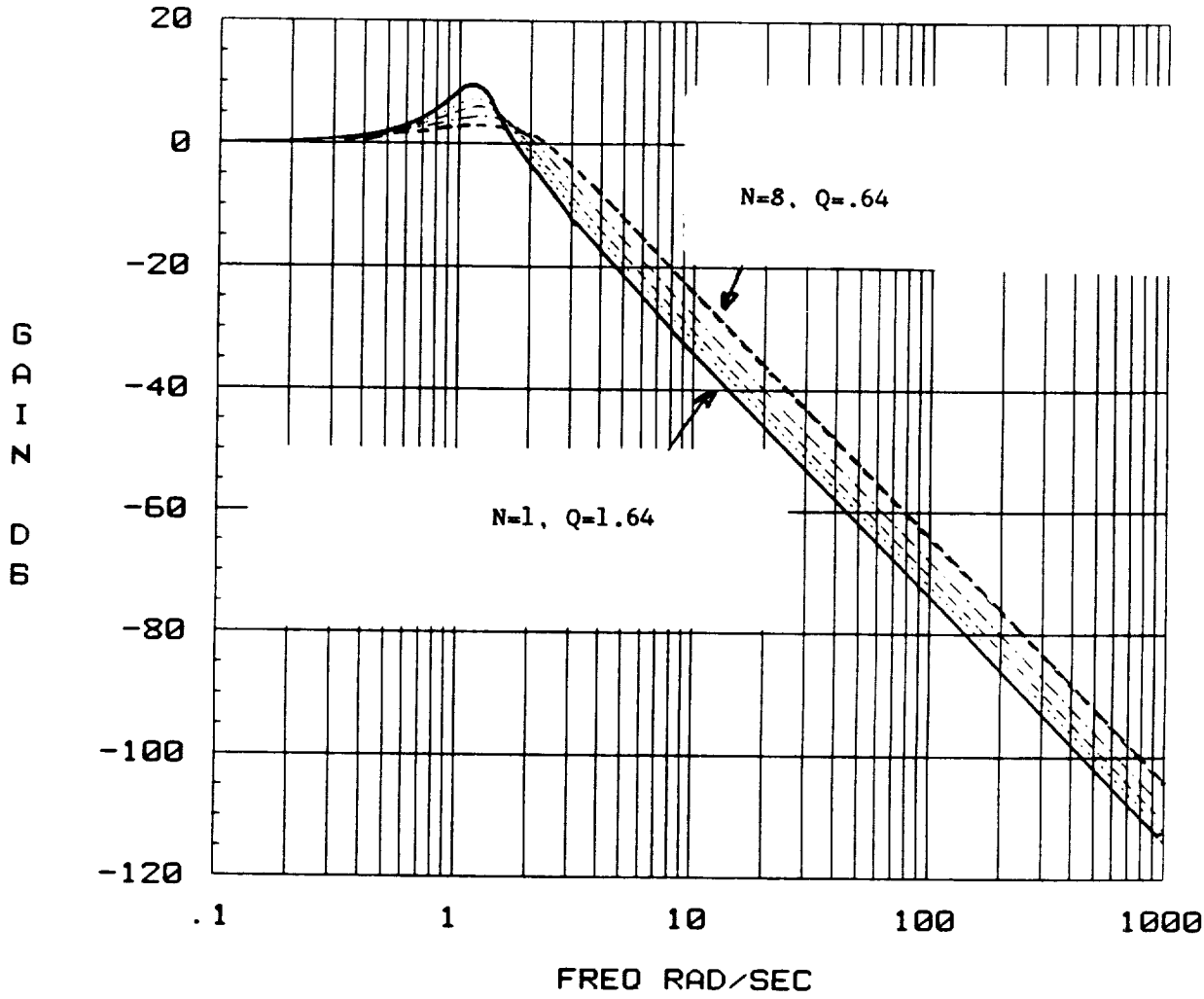

Figure 6-3
Passive Isolator Transmissibility as a Function
of N, Optimal Q (Minimum Peak)

From the relative transmissibility formula in Table 6-1, the relative motion across the isolator element at low frequency is shown to be determined by $1/\omega_0^2$ and by the magnitude of the base acceleration, $\ddot{X}_b$. Figures 6-4 through 6-6 illustrate the relative transmissibility function, dashed line, and the direct transmissibility function, solid line, for three values of ω_0: 3, 1 and 0.3 rad/sec. At ω_0=1, the relative motion gain is one. Thus, for a 0.01 g base acceleration, the relative motion is approximately 9.8 cm. Since the estimated upper limit on actuator deflection for a reasonably sized (1 to 2 feet long) isolator element of the ST type design is about 3 cm, ω_0 must be set at a higher value than 1 rad/sec. For ω_0=3 rad/sec, the element deflection is about 1 cm.

In actuality, the base acceleration (space station acceleration) will not be constant for arbitrarily low frequencies. In assessing the effect of ω_0 on isolator deflection, however, it is assumed that the constant acceleration applies at frequencies below ω_0 so that the peak relative motion from the relative transmissibility function in Table 6-1 actually occurs.

The above discussion has centered on limitations imposed on the linear isolation characteristics as a result of isolator element design restrictions. However, the passive system must also provide PPS rotational isolation. The degree to which isolator element design influences limitations in rotational isolation transmissibility is more difficult to assess. The difficulty arises because the rotational isolation bandwidth is influenced by the geometry of isolator element placement as well as the element spring-damper characteristics. In addition, the relative transmissibility function for the rotational motion does not contain the $1/S^2$ factor because the disturbance is constant angle rather than constant acceleration. Thus, the low frequency relative rotation across the isolation system is defined by S^2/ω_0^2 rather than $1/\omega_0^2$.

In the absence of a candidate 6 DOF actuator configuration, the passive isolator performance study makes no assumption about limitations on parameters in the rotational transmissibility functions. In this regard, the rotational disturbance performance results are more parametric (in ω_0) than the translational results.

6.2 PERFORMANCE MODEL

The linear model on which the PPS/Base Isolator simulation is based is represented in the block diagram of Figure 6-7. The model itself is based on the PPS configuration of Figure 6-8.

Pointing error in the PPS/Base Isolator model is defined by payload motion around the payload X axis. Disturbances which influence this error are illustrated in the diagram and include payload linear acceleration, Z_p, acting through the offset L_{OF} (payload c.g. to gimbal control axis), base rotation around the gimbal normal axis, θ_N, and base rotation around the azimuth gimbal, θ_{AZ}. Control on the payload X axis is provided by the PPS azimuth gimbal.

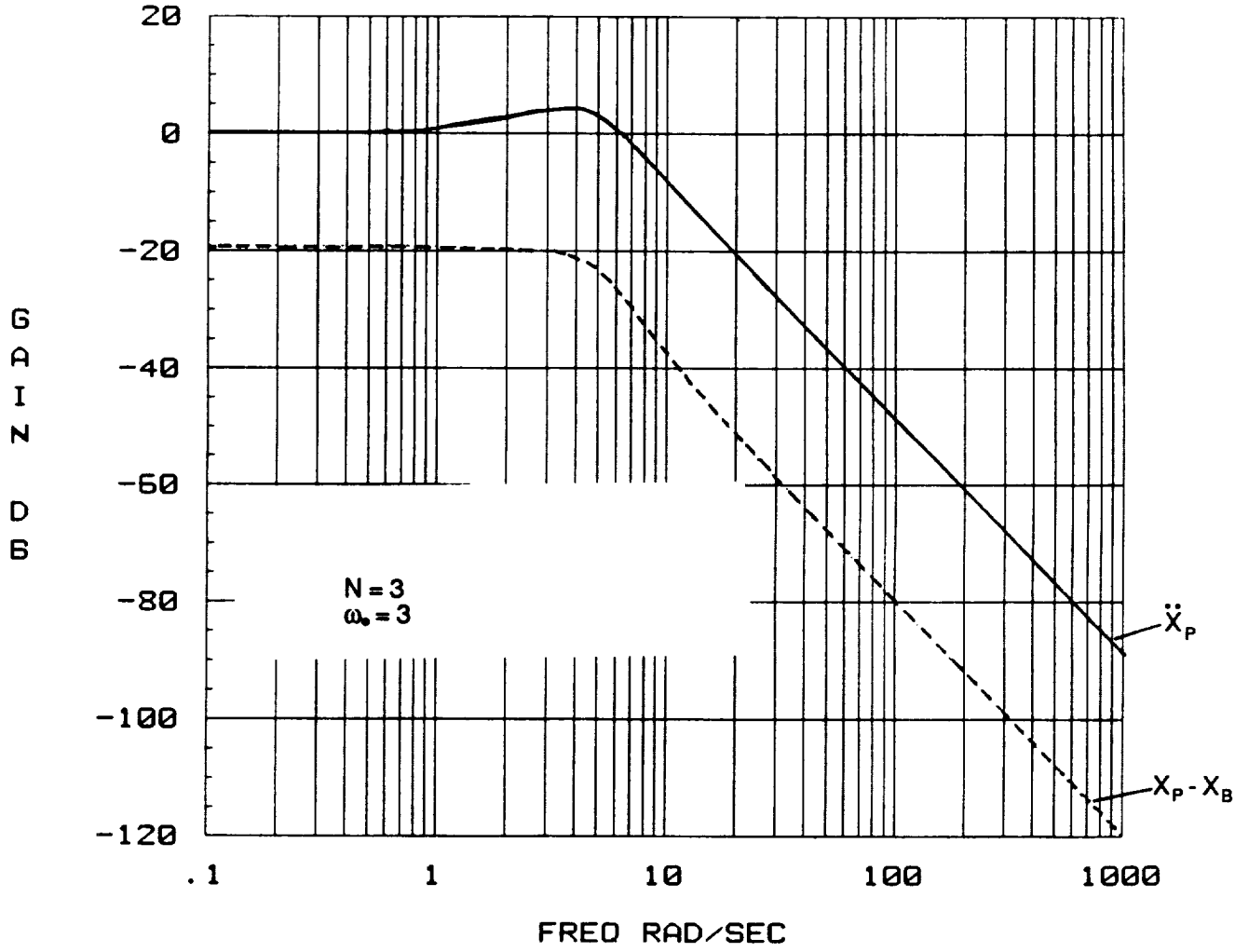

Figure 6-4
Isolator Transmissibility and Relative Motion
N = 3, ω_0 = 3

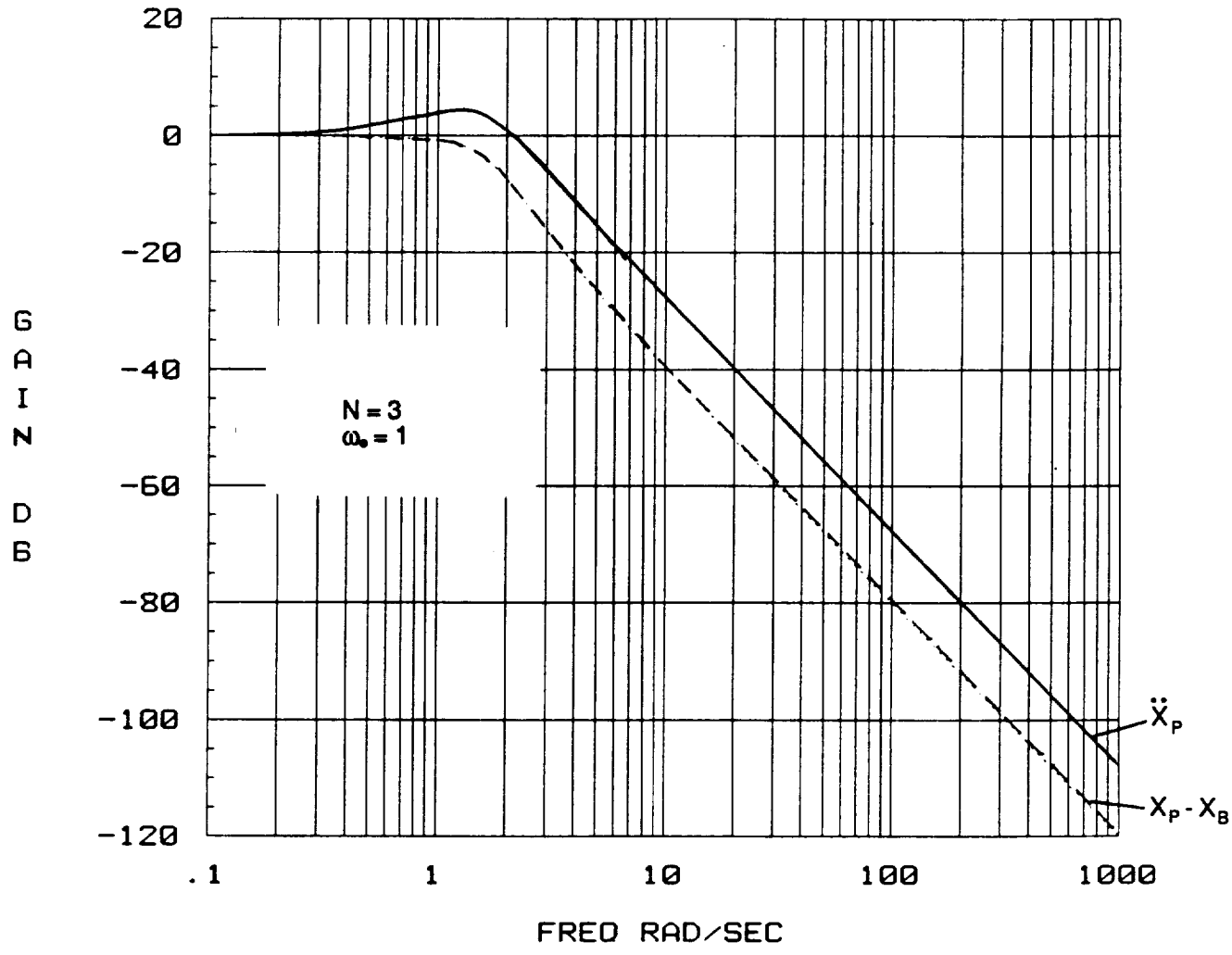

Figure 6-5
Isolator Transmissibility and Relative Motion
N = 3, ω_0 = 1

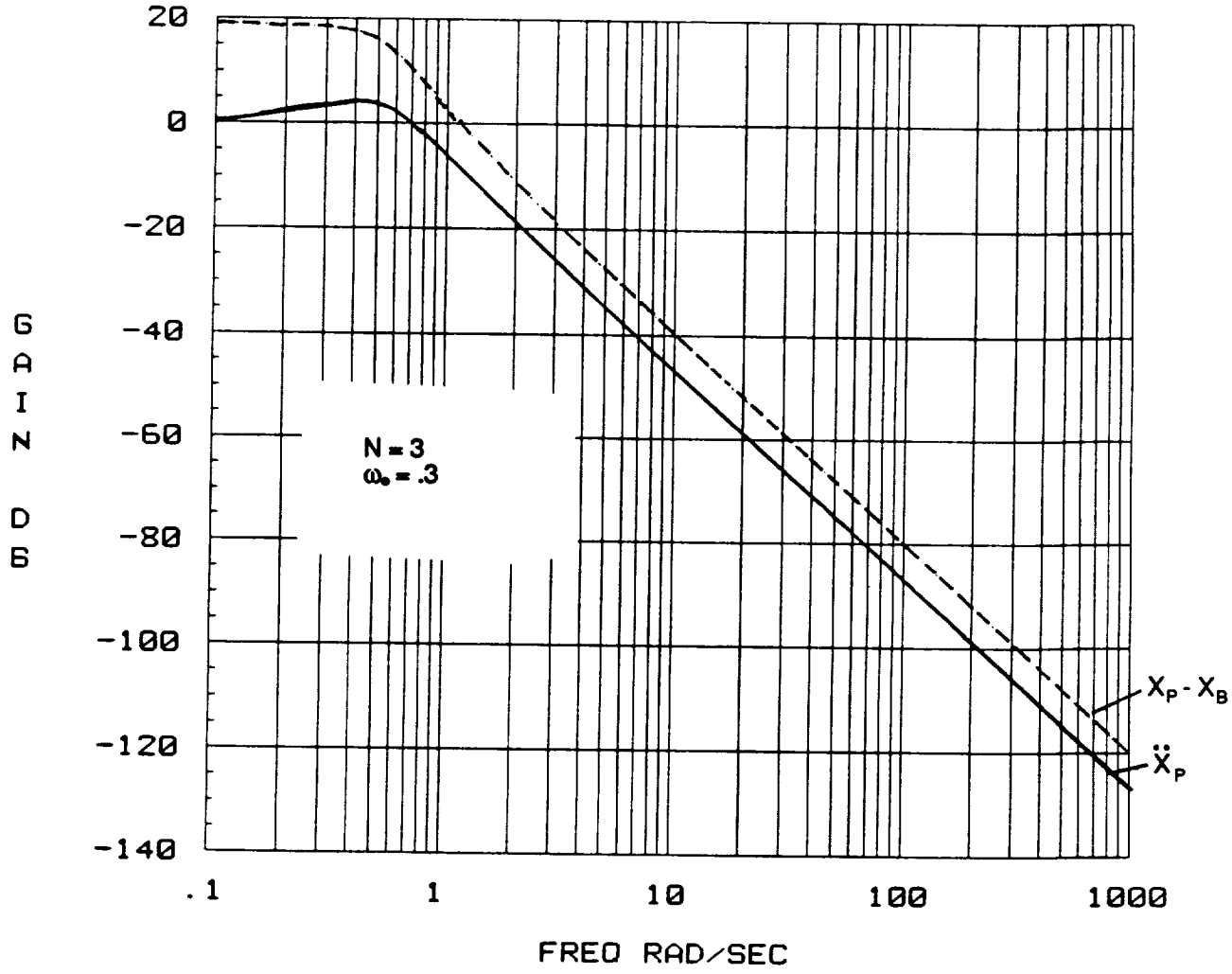

Figure 6-6
Isolator Transmissibility and Relative Motion
$N = 3$, $\omega_0 = 0.3$

ORIGINAL PAGE IS
OF POOR QUALITY

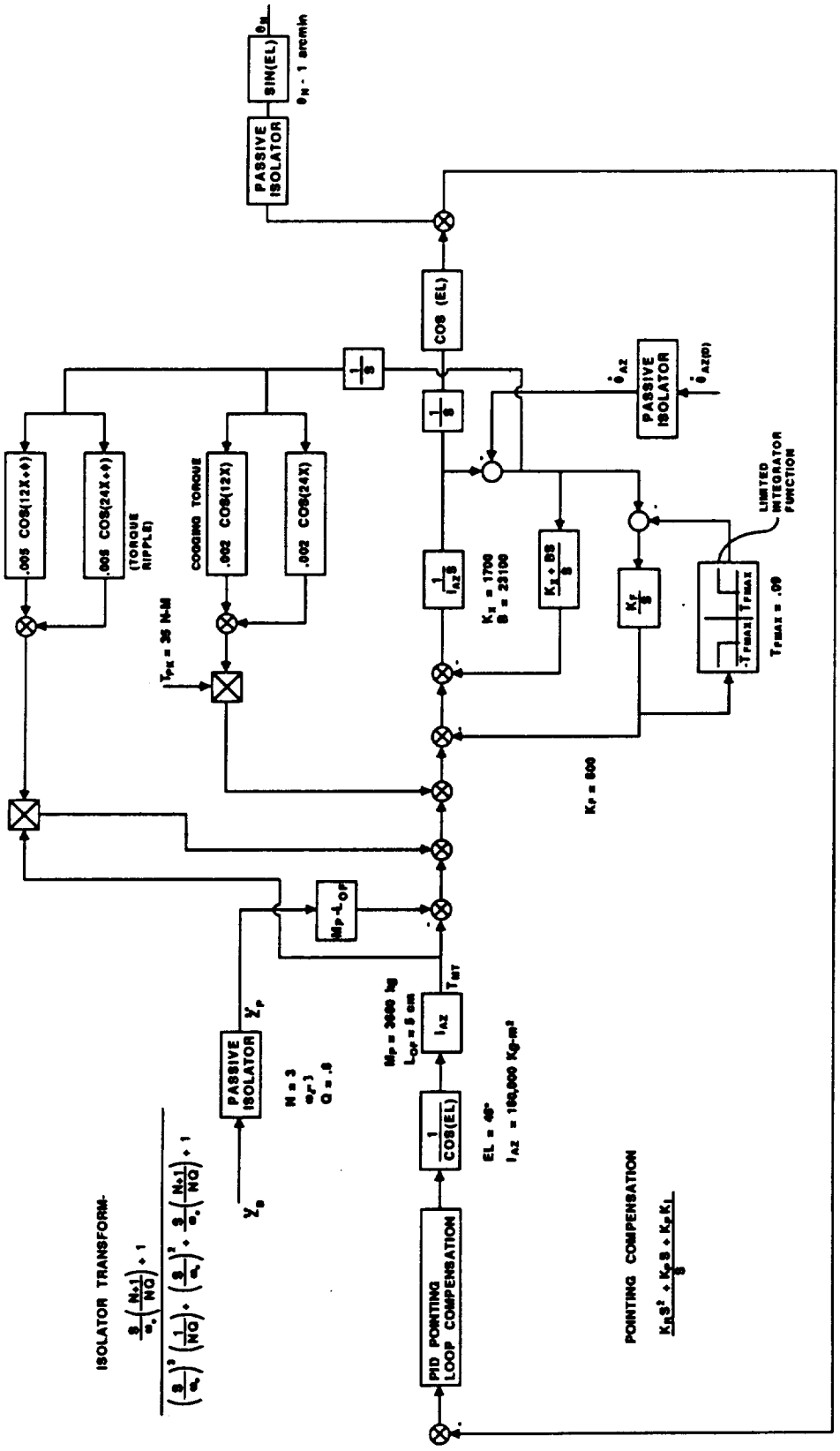

Figure 6-7
Passive Isolator Configuration

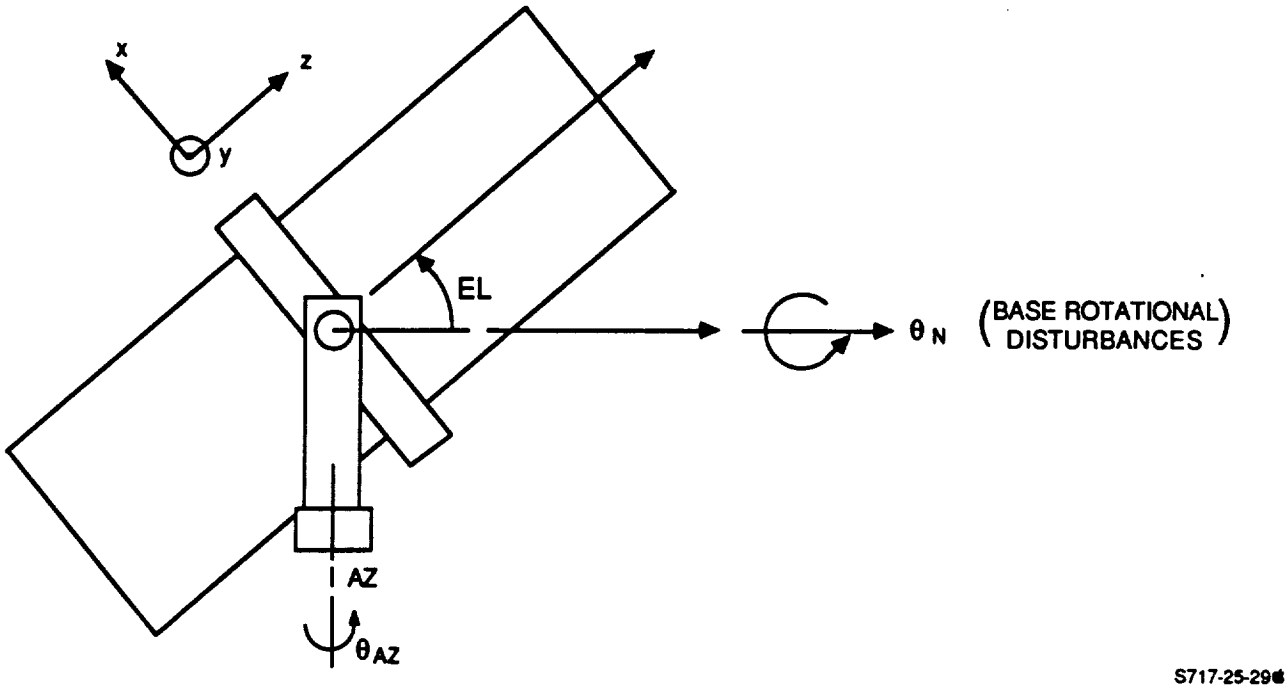

Figure 6-8
PPS Configuration for Passive Isolator Study

The PPS model includes the same level of bearing friction stiffness and interface cabling stiffness assumed in the magnetic system model. In addition, motor cogging and ripple anomaly torques have been added. These torques are direct disturbances to the ATF pointing loop. However, because of the inertial pointing function of ATF, gimbal motion should not be significant. Thus, the cogging torque will appear primarily as a bias. The ripple torque effect will appear as a small open loop gain error.

The parameters used in the passive model (Figure 6-7) are summarized in Table 6-2.

TABLE 6-2
PASSIVE ISOLATION MODEL DATA

M_p - Payload mass - 3666 kg

I_{AZ} - Payload + azimuth gimbal inertia - 160,000 kg-m^2

L_{OF} - Offset from payload cg to gimbal control axis - 5 cm

K_x - Azimuth gimbal interface stiffness- 1700 N.m/rad

B - Azimuth gimbal damping factor - 23100 (N.m-sec/rad)

K_F - Gimbal breakaway friction stiffness - 600 N.m/rad

T_{FMAX} - Maximum gimbal friction torque - 0.09 N.m

$\ddot{Z}_B$ - Translational acceleration below passive isolation

$\ddot{Z}_P$ - PPS base translational acceleration - above passive isolator

EL - Elevation angle - 45°

$\theta_{AZ(D)}$ - Azimuth base angular motion - below passive isolator

θ_{AZ} - Azimuth base angular motion - above isolator

θ_N - Normal axis base angular motion - below passive isolator

T_{PK} - Peak gimbal motor torque - 35 N.m

K_R - Pointing loop rate gain = open loop crossover frequency

K_P - Pointing loop position gain - $=\sqrt{2/3}\ K_R^2$

K_L - Pointing loop integral gain = $K_R/3\sqrt{2}$

The model of Figure 6-7 assumes that the base isolation and gimbal interface spring/damper around the azimuth axis are uncoupled and that they produce a payload isolation that is the sum of the separate isolation effects. Because of the large magnitude of the payload inertia in comparison with the isolated inertia below the gimbal, the decoupled isolator assumption is valid only if the stiffness of the base isolator is large compared with the gimbal interface stiffness. We might expect this condition to exist. However, even if it does not, the base to payload isolation results from a coupled or an uncoupled analysis should be similar. In a coupled analysis, the isolation frequency associated with the gimbal interface drops while the effective base isolation frequency increases. These two changes tend to cancel each other in their effect on payload isolation. The exact effect, of course, depends on the interface inertia and the base isolator rotational stiffness.

SECTION 7.0

PPS/BASE ISOLATION POINTING PERFORMANCE

SECTION 7.0

PPS/BASE ISOLATION POINTING PERFORMANCE

7.1 TRANSLATIONAL DISTURBANCE ACCELERATIONS

ATF pointing performance in the presence of translational disturbance accelerations transmitted by a passive base isolator with the spring damper structure described in Section 6.0 and with ω_0=3 rad/sec and N=3, is defined by the frequency response curves of Figure 7-1. The curves were generated for pointing loop BW's between 2 and 5 rad/sec assuming a 0.01g disturbance level.

The straight line segments in the figure represent the ATF pointing stability spec for frequencies below and above 5 Hz. Evidently, the high frequency pointing spec is satisfied with ample margin. However, below 5 Hz all four of the curves peak above 1 arcsecond. In view of the assumption that the pointing system's assumed first modal frequency is 5 Hz, increasing the BW beyond 5 rad/sec is probably not viable.

Some performance benefit can probably be realized by decreasing ωo to 2 rad/sec. This value produces an isolator element deflection of around 2.5 cm. However, as Figure 7-2 shows, a significant decrease in ω_0 is required to provide any low frequency performance margin, and only then for a control BW of 5 rad/sec. As discussed in Section 6.0, such a low ω_0 is inconsistent with allowable isolator deflection.

7.2 NORMAL AXIS DISTURBANCE MOTION

Pointing error frequency response curves reflecting PPS pointing error sensitivity to normal axis base motions are shown in Figures 7-3 through 7-5 for different levels of base isolation ω_0. The curves were generated assuming a 1 arcminute motion. Together the figures show that the response curves are very sensitive to variations in ω_0. For ω_0=3 and 1 rad/sec, pointing errors are significantly higher than the specification values, both below and above 5 Hz. When ω_0 is reduced to 0.3, the specifications are still not met; however, the out of spec margin is very small, at least when using a 5 rad/sec pointing loop BW.

7.3 AZIMUTH AXIS DISTURBANCE MOTION

The azimuth gimbal interface stiffness, (K_χ in the block diagram of Figure 6-7) provides low frequency (<0.1 rad/sec) payload isolation from rotational motions transmitted by the base isolator. Because of this additional isolation, the frequency response curves for the pointing error produced by disturbance rotations around the azimuth gimbal, Figures 7-6 through 7-8, are lower than the corresponding normal axis response curves (Figures 7-3 through 7-5) for frequencies >0.1 rad/sec. In fact, the azimuth axis response curves are lower than the high frequency ATF pointing error specifications at frequencies >5 Hz for each value of ω_0 (0.3 to 3 rad/sec). Below 5 Hz the pointing specification is satisfied for ω_0=1 with a pointing loop BW of 5 rad/sec and for ω_0=0.3 with the pointing BW >1 rad/sec.

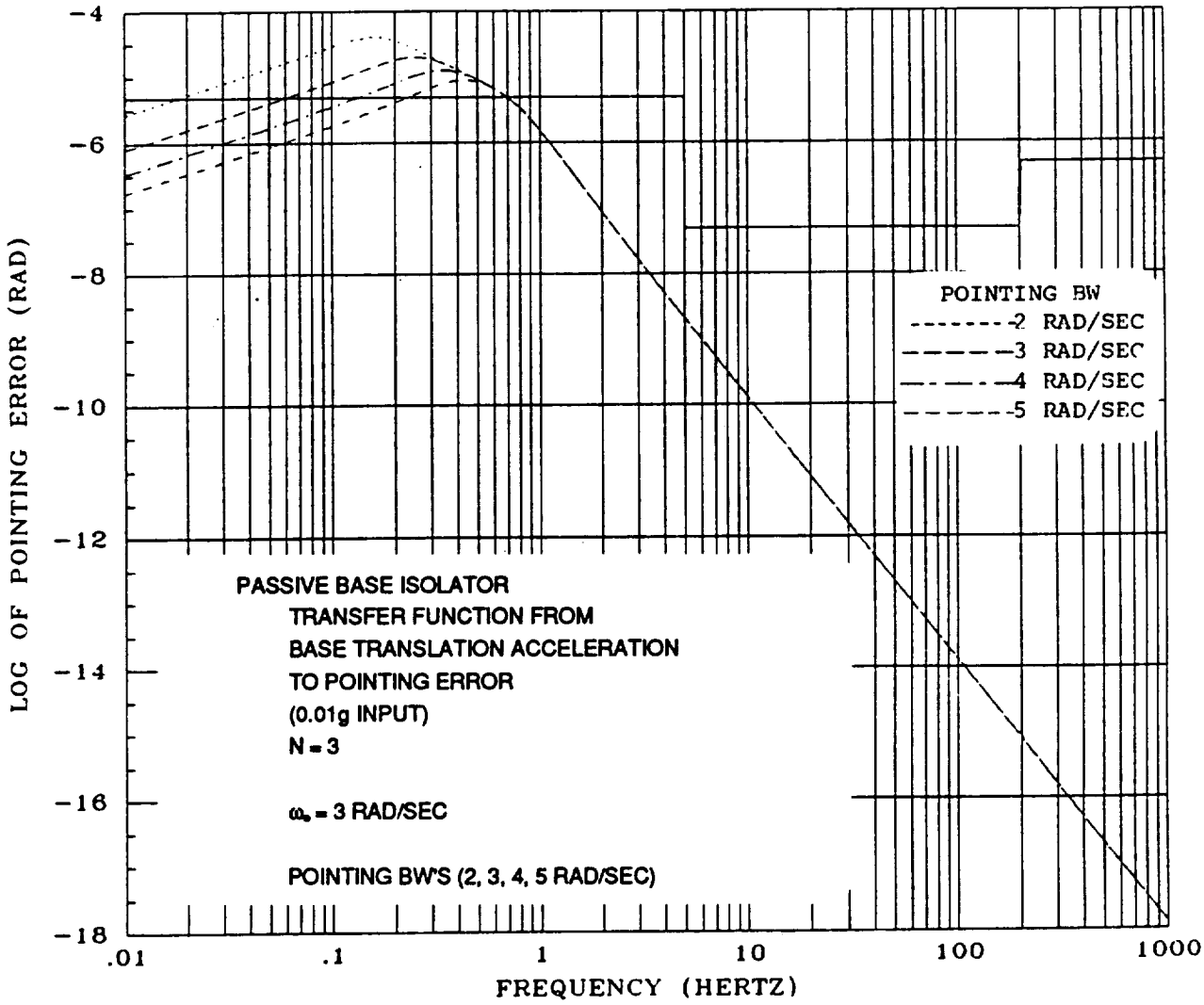

Figure 7-1
Passive System Frequency Response Curves
Base Translational Acceleration to Pointing Error
$N = 3$, $\omega_0 = 3$

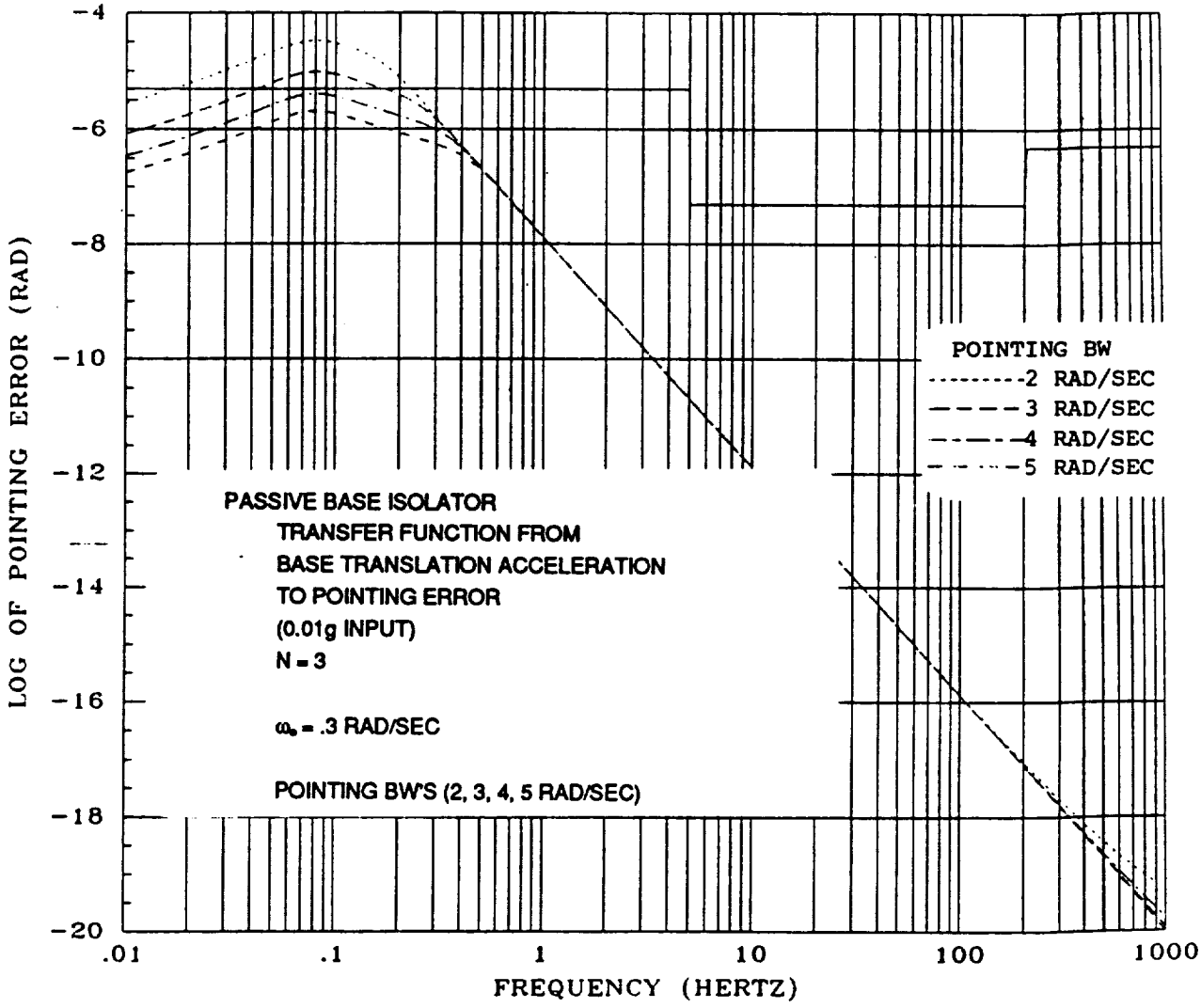

S717-25-31

Figure 7-2
Passive System Frequency Response Curves,
Base Translational Acceleration to Pointing Error
N = 3, ω_0 = 0.3

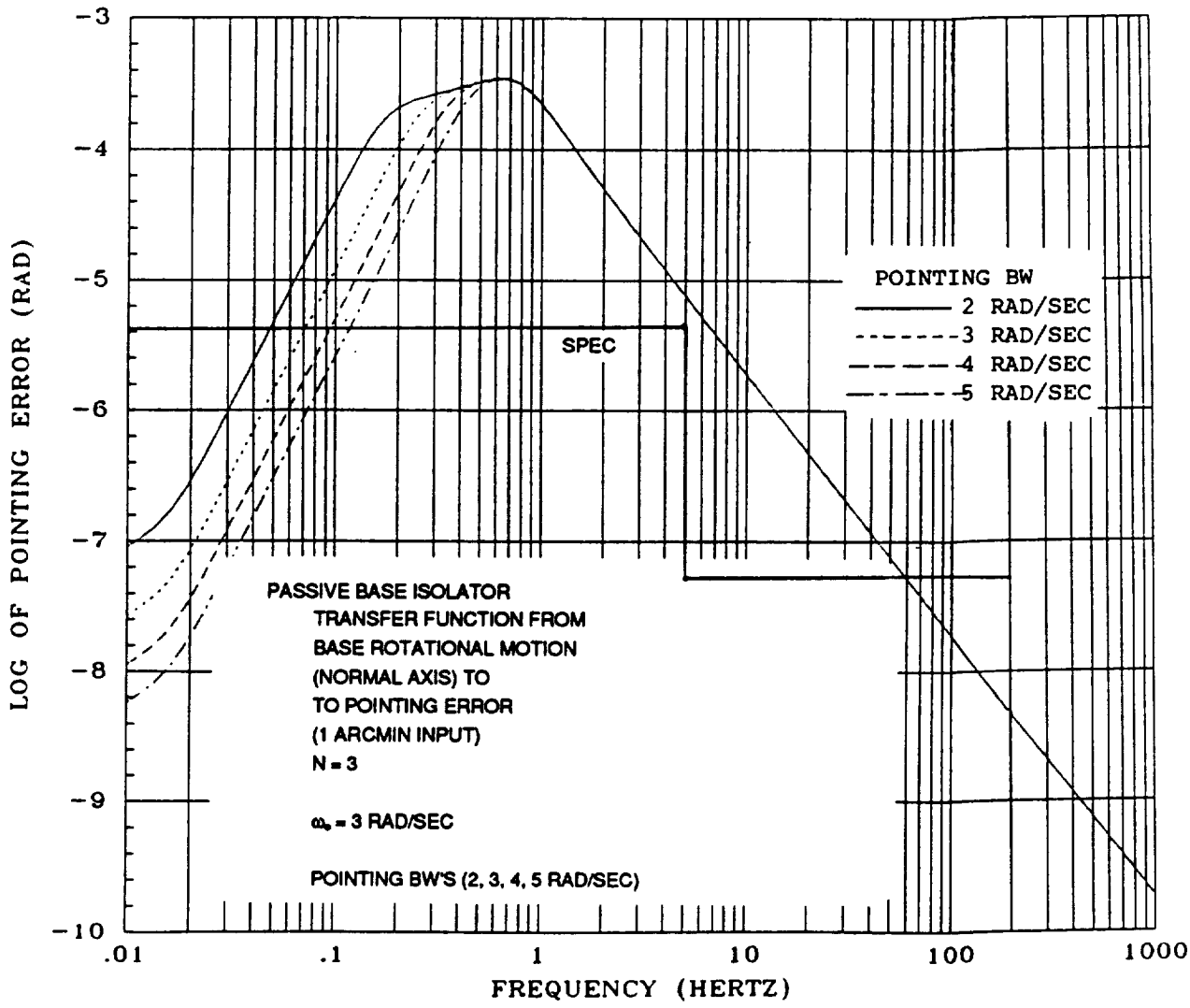

Figure 7-3
Passive System Frequency Response Curves,
Normal Axis Motion to Pointing Error
$N = 3$, $\omega_0 = 3$

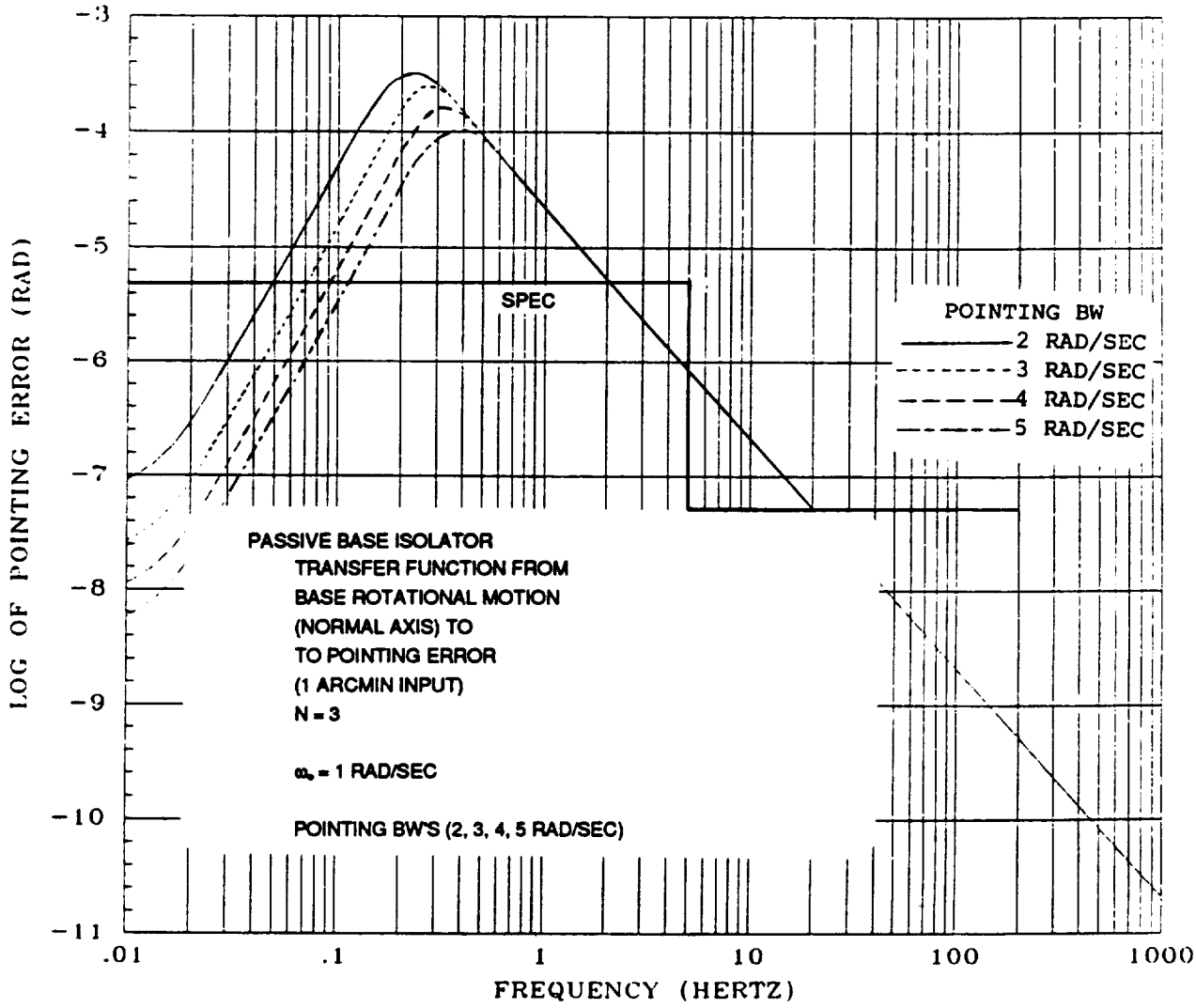

Figure 7-4
Passive System Frequency Response Curves,
Normal Axis Motion to Pointing Error
N = 3, ω_0 = 1

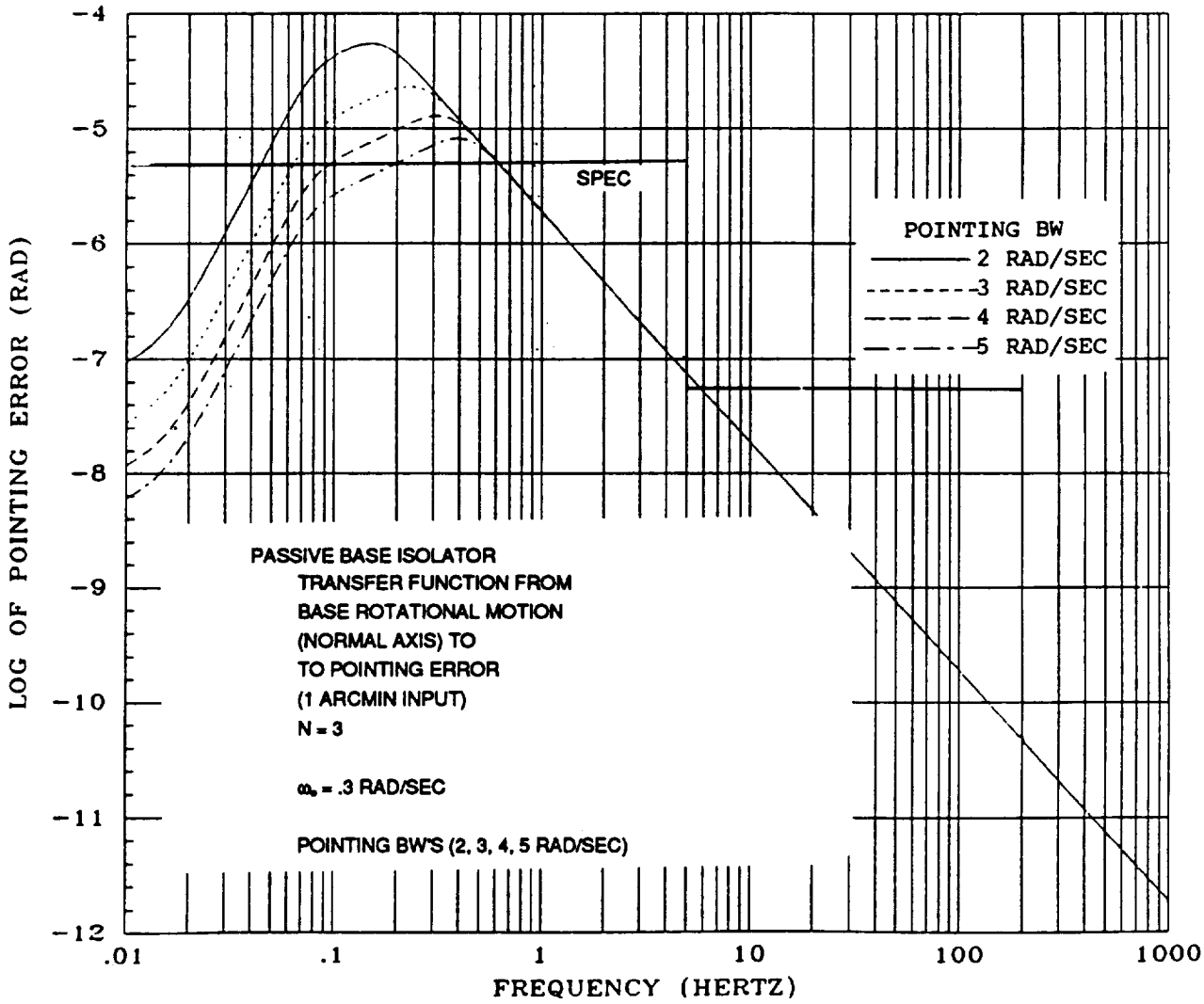

S717-25-346

Figure 7-5
Passive System Frequency Response Curves,
Normal Axis Motion to Pointing Error
$N = 3, \omega_0 = 0.3$

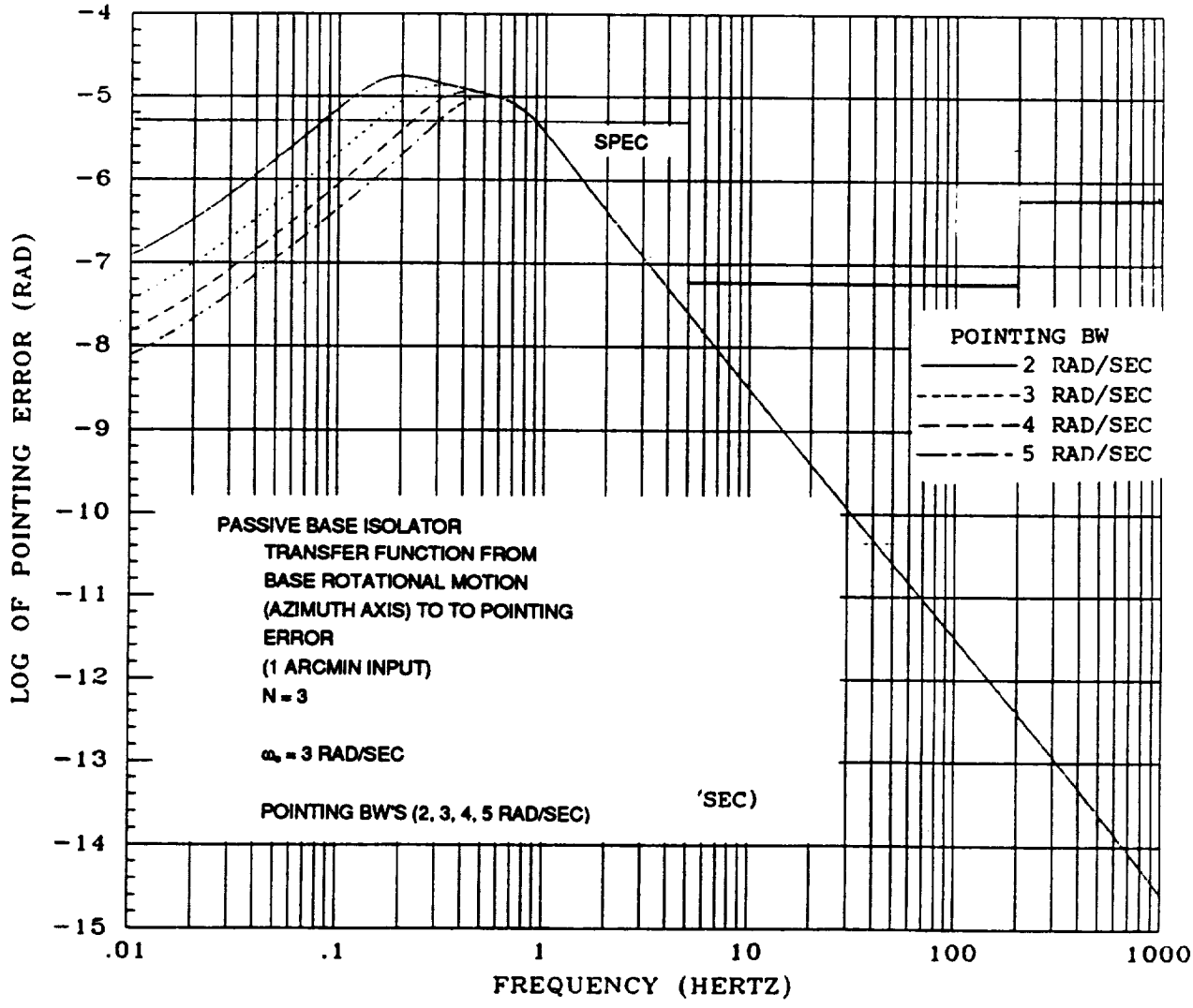

Figure 7-6
Passive System Frequency Response Curves,
Azimuth Axis Motion to Pointing Error
N = 3, ω_0 = 3

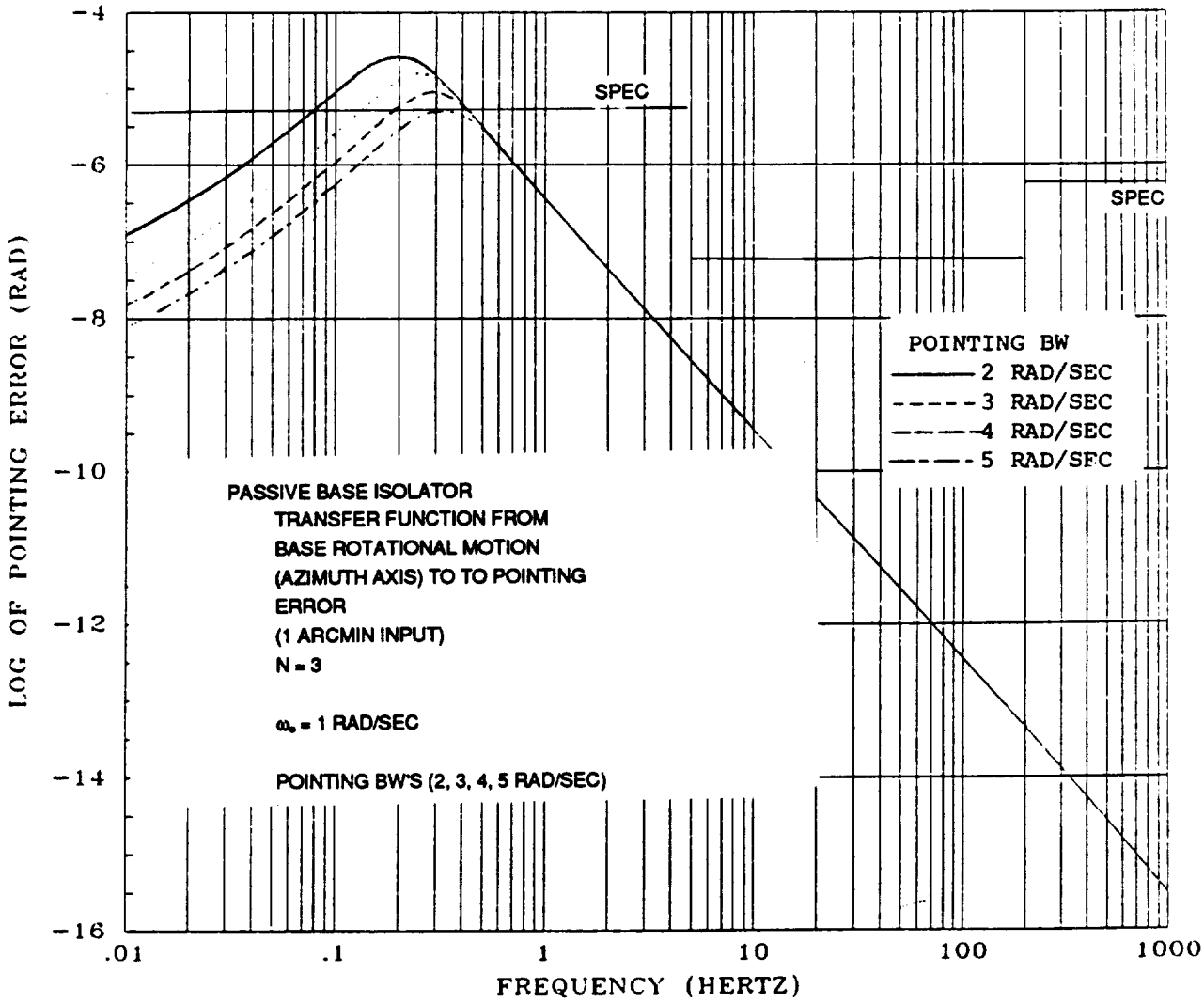

Figure 7-7
Passive System Frequency Response Curves,
Azimuth Axis Motion to Pointing Error
N = 3, ω_0 = 1

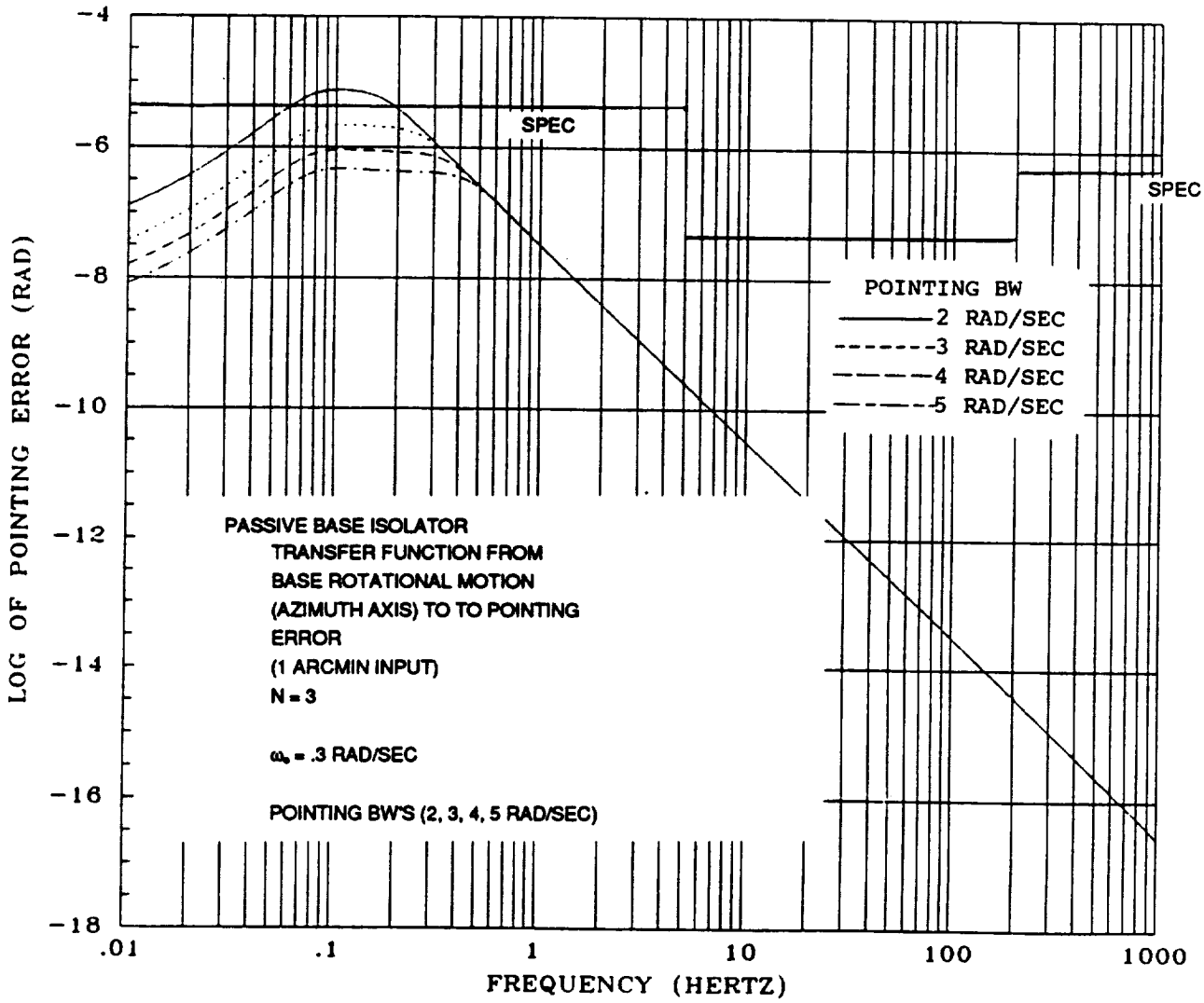

S717-25-37B

Figure 7-8
Passive System Frequency Response Curves,
Azimuth Axis Motion to Pointing Error
N = 3, ω_0 = 0.3

7.4 PASSIVE ISOLATION STUDY CONCLUSIONS

The PPS requires very low base isolation bandwidths, both in translation and rotation, in order to satisfy ATF pointing requirements under the assumption that space station linear acceleration disturbances are at least 0.01g and that rotational motions are 1 arcminute. There may be a significant challenge both in defining the required isolator configuration to meet these low bandwidth requirements and in fabricating the isolator elements.

SECTION 8.0

CANDIDATE MAGNETIC POINTING AND ISOLATION SYSTEM

SECTION 8.0
CANDIDATE MAGNETIC POINTING AND ISOLATION SYSTEM

A candidate ATF magnetic pointing and isolation system, including all potential sources of power and weight, has been defined in order to establish a power, weight, and size budget for such a system. In addition, system reliability has been addressed. To place a limit on the peak force required of the magnetic actuators, a peak control force of 80 lbs. (356 N) corresponding to a 0.01 translational disturbance acceleration input has been assumed.

8.1 DESIGN REQUIREMENTS

The following items summarize the requirements and assumptions imposed on the magnetic system design,

- A 356 N control force can be required in any direction.
- A 34 N.m control torque is required normal to the ATF line of sight.
- Relative motion at any actuator is limited to ±0.5 inch (1.27 cm).
- A full ring armature attached to the ATF is required to provide ±200 degrees roll motion.
- A noncontacting roll motor providing 7 N.m (5 ft-lbs) of roll torque is required.
- The magnetic system must fit within an annular region between the PPS and ATF that has a 1.8 M inside diameter and a 2.5 M outside diameter.
- The system must provide a non-contacting power and signal transfer to the ATF.

8.2 ACTUATOR PLACEMENT SIZING

Several actuator configurations were considered for the candidate design. Figure 8-1, (A, B, C) illustrates three such options. The number of actuators in the configuration is important because a large number of actuators implies a small peak actuator force and, thus, a small actuator. A small actuator makes it easier to fit the system in the available radial space. However, each actuator requires separate drive electronics, gap sensors, and flux sensors. Since it is undesirable to make the system any more complicated than necessary, a balance is found between accommodating the radial space limitation and minimizing the number of actuators. While five actuators and a roll motor are adequate for providing ATF control, 8 actuators (plus roll motor) were selected for the candidate system.

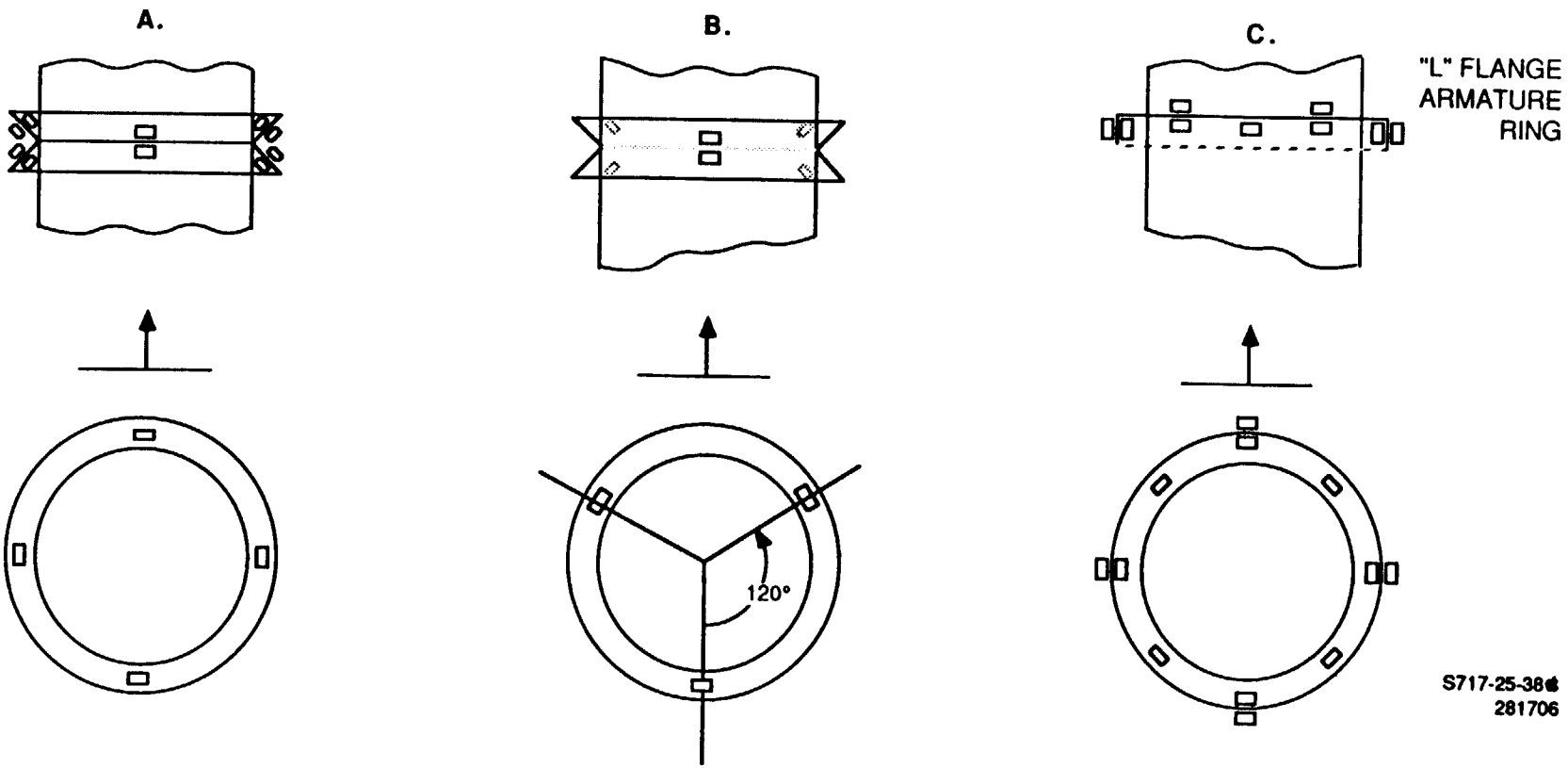

Figure 8-1
Candidate ATF Actuator Layouts

For configurations A and C, simple models were developed relating peak (of the 8 actuators) single actuator force to control force and torque magnitudes and directions and, for configuration A, to the inclination angle of the armature, ϕ_A. Figure 8-2 shows the angles used to define the force and torque directions as well as the armature inclination angle. An optimization procedure was implemented with each configuration model to define the maximum peak single actuator force and torque. For configuration A, the angle ϕ_A was varied in a min-max. procedure to define the ϕ_A value producing the minimum maximum peak single actuator force.

Between configurations A and C, A requires the smallest peak actuator force. Because of this advantage in actuator force requirements and because it makes more efficient use of the available radial space, configuration A was selected for the candidate system. Figure 8-3 illustrates this peak force as a function of ϕ_A and θ_F. It shows a min-max value of 156 N (35 lbs) at a ϕ_A of 52 degrees and a θ_F value of 45 degrees.

In order to provide force margin, a peak actuator force of 220 N (or 50 lbs) was chosen for the candidate system. Figure 8-4 shows the results of the actuator force sizing process carried out for other values of control force. The circled point on the graph corresponds to the nominal configuration values (80 lb, 50 lb) or (356 N, 220 N).

The selected actuator design, providing 50 lbs peak force and allowing ±0.5 inch of relative motion is described in the values of Figure 8-5. For given values of peak force and motion, an actuator design allows a trade-off between actuator weight and peak power. The design of Figure 8-5 is tilted somewhat to saving weight at the expense of power.

The circled point in Figure 8-6 places the nominal actuator design in an array of possible actuator force, motion, peak power and weight options. The curves in the figure relate total system actuator weight (8 actuators) to peak actuator force for different levels of actuator gap motion and single actuator peak power. The curves can be used to determine how an increase in actuator force and motion, or an emphasis on power rather than weight, can be expected to affect the actuator system weight.

8.3 ACTUATOR SYSTEM OPERATIONAL POWER

In Figure 8-5 the quiescent and peak power requirements for a single actuator are given as 32 and 199 watts, respectively. The quiescent power requirement corresponds to the situation where the force command to the actuator is zero and the armature is centered in the actuator gap, i.e. no gap motion. The peak power is required when the actuator is driven to its peak force level while the gap motion is at its limit. In normal operation an actuator's power requirement, determined by the command force and gap motion, is somewhere in between these extremes. The actuator system's power requirement is, of course, the sum of the individual values.

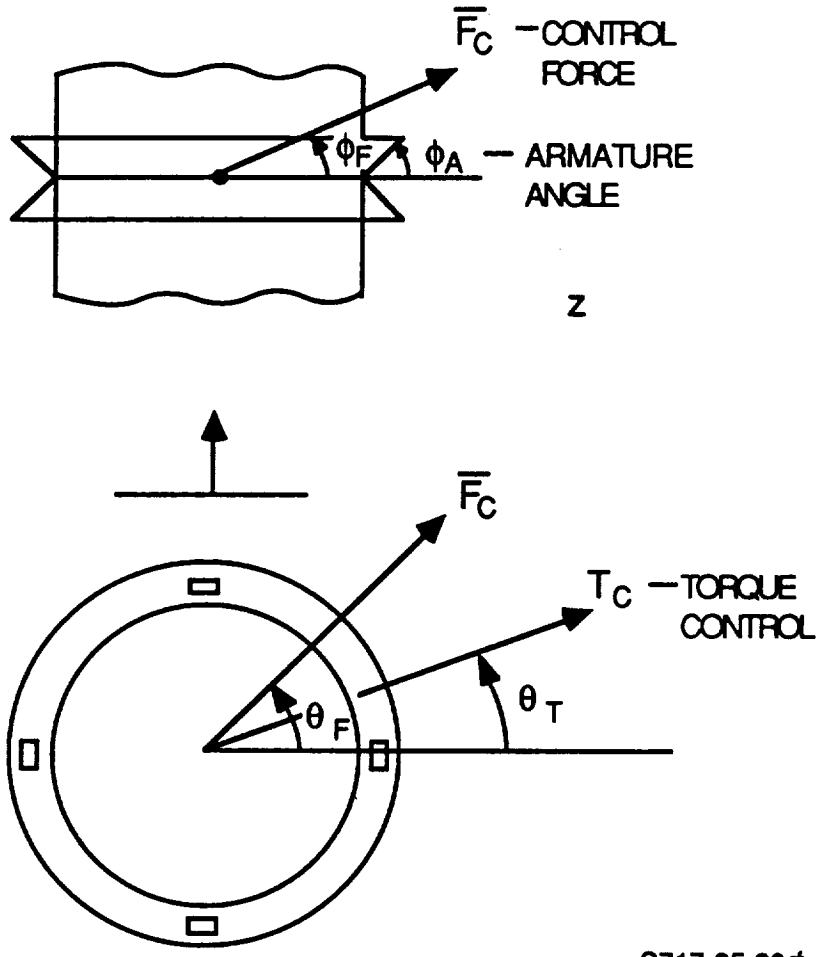

Figure 8-2
Control Force and Torque With Respect to Actuator Configuration

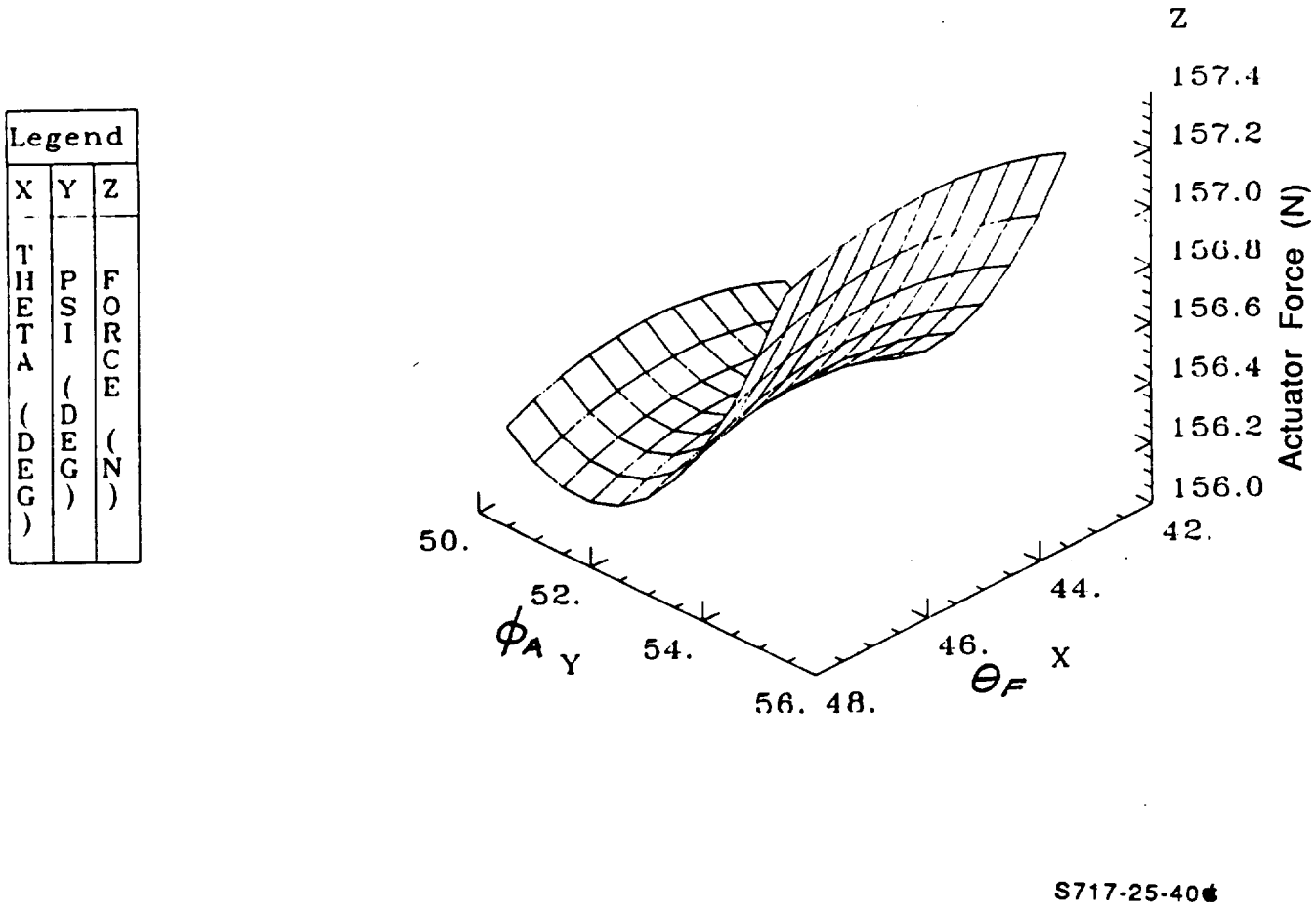

Figure 8-3
Peak Single Actuator Force Versus Armature Angle
and Force Direction

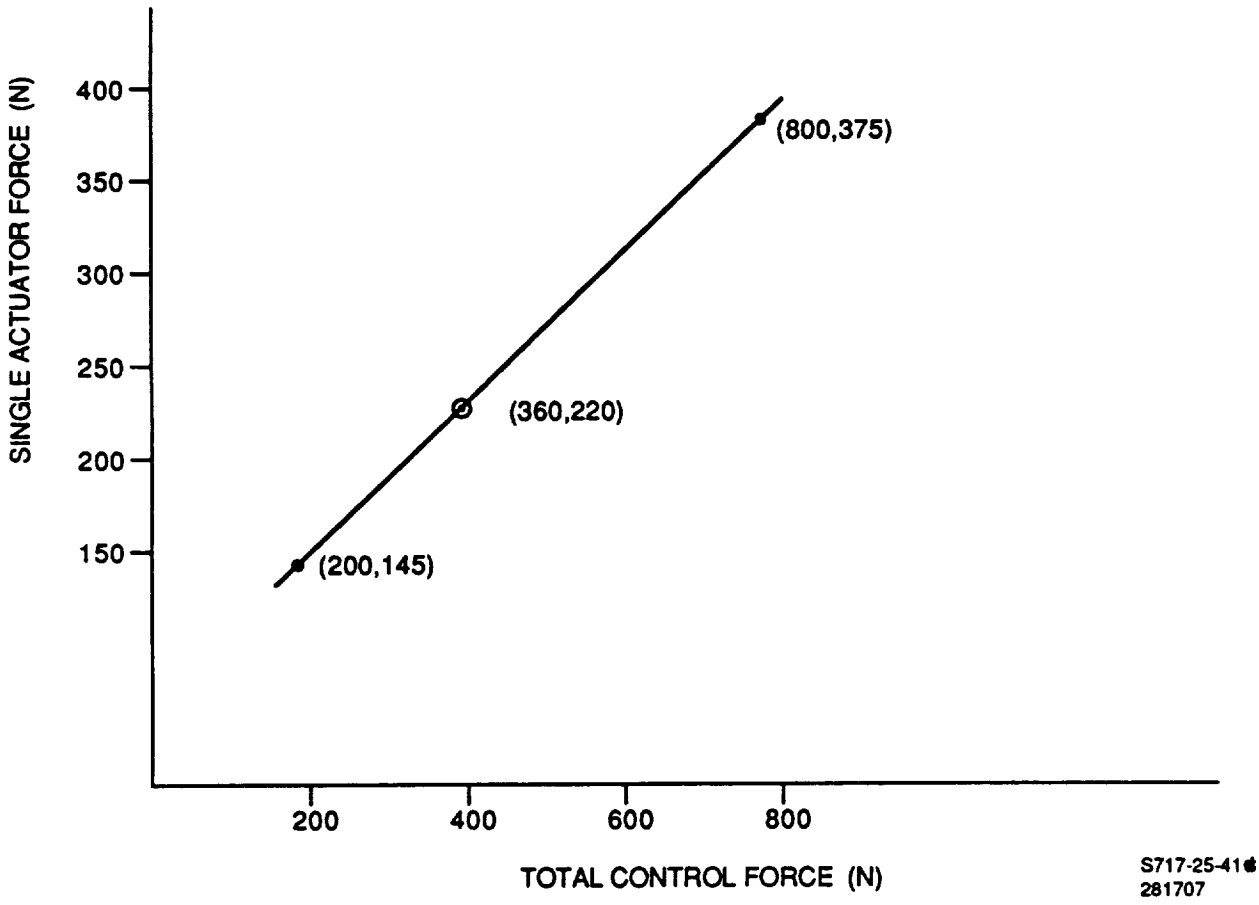

Figure 8-4
Single Actuator Force Requirement (+ Margin) Versus Control Force

Force (lbs.)	50	(222 N)
Motion Range (inches)	±0.50	(12.7 mm)
Nominal Gap (inches)	0.625	(15.9 mm)
Peak Power (watts)	199	
Quiescent Power (watts)	32	
Stator Weight - Each (lbs.)	29	(13.2 Kg)
a) Stator length (inches)	12.1	(.307 m)
b) Stator width (inches)	3.8	(.097 m)
c) Stator height (inches)	5.2	(.132 m)
d) Armature length (inches)*	16.6	(.422 m)
e) Armature width (inches)	8.3	(.211 m)
f) Armature height (inches)	0.33	(.0084 m)
g) Actuator Station height (inches)	12.0	(.305 m)

* MIN REQUIRED LENGTH

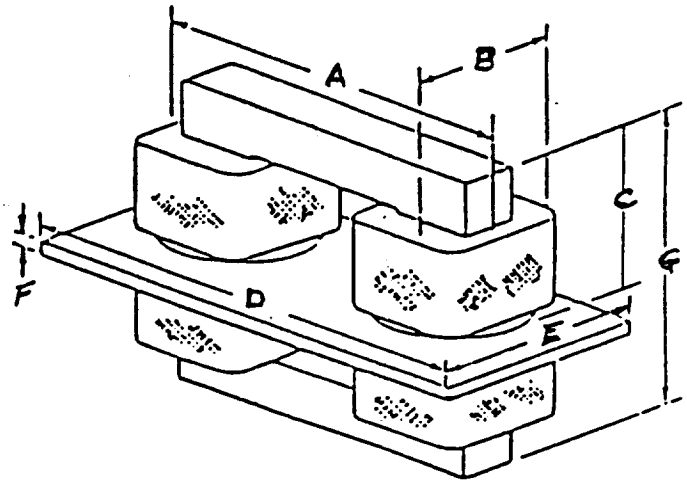

S717-25-42
274702

Figure 8-5
ATF Actuator

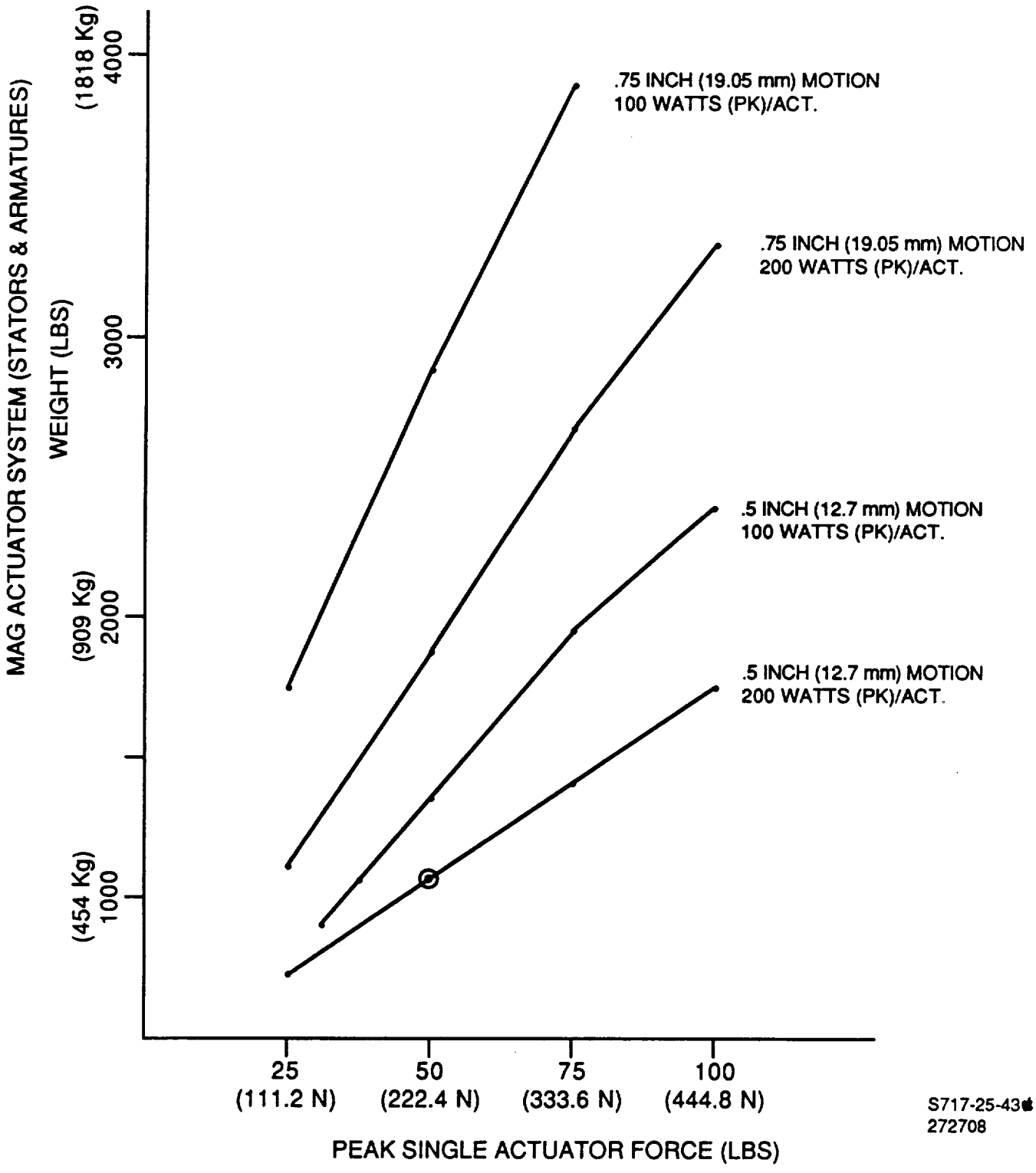

Figure 8-6
Actuator System Weight Versus Actuator Force

In order to define operational power needs of the proposed actuator configuration, a simulation was developed to compute the power for each of the configuration actuators as a function of its commanded force and gap motion. The command forces and gap motions were based on the payload control forces and torques (magnitudes and directions) and on the relative motion between the ATF payload and the actuator stator ring. Figure 8-7 illustrates the model. In the figure, θ_X and ϕ_X define the direction of the relative motion. The θ angles are measured in the plane of the actuators; the ϕ angles are measured out of the actuator plane and define the components of force (ϕ_F) and motion (ϕ_X) normal to the actuator plane.

The simulation was used with an optimization procedure to define the maximum operational system power and the corresponding values for ϕ_X, θ_X, ϕ_F etc. Figures 8-8 and 8-9 show the variation in system power as a function of (θ_X, ϕ_X) and (θ_F and ϕ_F) respectively. The vertical scales in the figures indicate that the maximum operational power is approximately 448 watts.

Using the same simulation, a system power time profile was generated in response to 0.8 rad/sec sinusoidal force (356 N) and motion (1.27 cm) inputs (in phase) along their maximum power directions. The frequency of the inputs corresponds, approximately, to the frequency at which the peak relative motion occurs in response to a translational disturbance input; Figure 5-3. The power profile is shown in Figure 8-10. The frequency of the profile is twice that of the input because total actuator power is a function of the square of force command and gap motion.

8.4 MECHANICAL LAYOUT

Based on the actuator dimensional parameters listed in Table 8-1 and the actuator-armature configuration of Figure 8-1, a mechanical layout for the proposed magnetic system has been generated, Figure 8-11, that shows the system can fit easily into the available radial space. The cross section also indicates how the actuators might be placed relative to the optical signal coupler channel, the rotary power transformer, and a power off caging mechanism. The coupler and transformer are described below. The caging mechanism has not been defined. Presumably it would operate on an annular ring and operate when power is lost or on command.

A similar cross section of the roll motor placement with respect to the same armatures used by the pointing and isolation actuators is shown in Figure 8-12. The overall layout is shown in Figure 8-13.

8.5 ATF ROLL CONTROL

ATF roll control is provided by two AC induction motors reacting against the two actuator rings. The motors are placed as indicated in Figure 8-14 to balance disturbance forces produced by the motors. Each motor produces a torque of 2.5 ft-lbs (3.4 N.m). The weight and power requirements of the system are listed at the bottom of the figure.

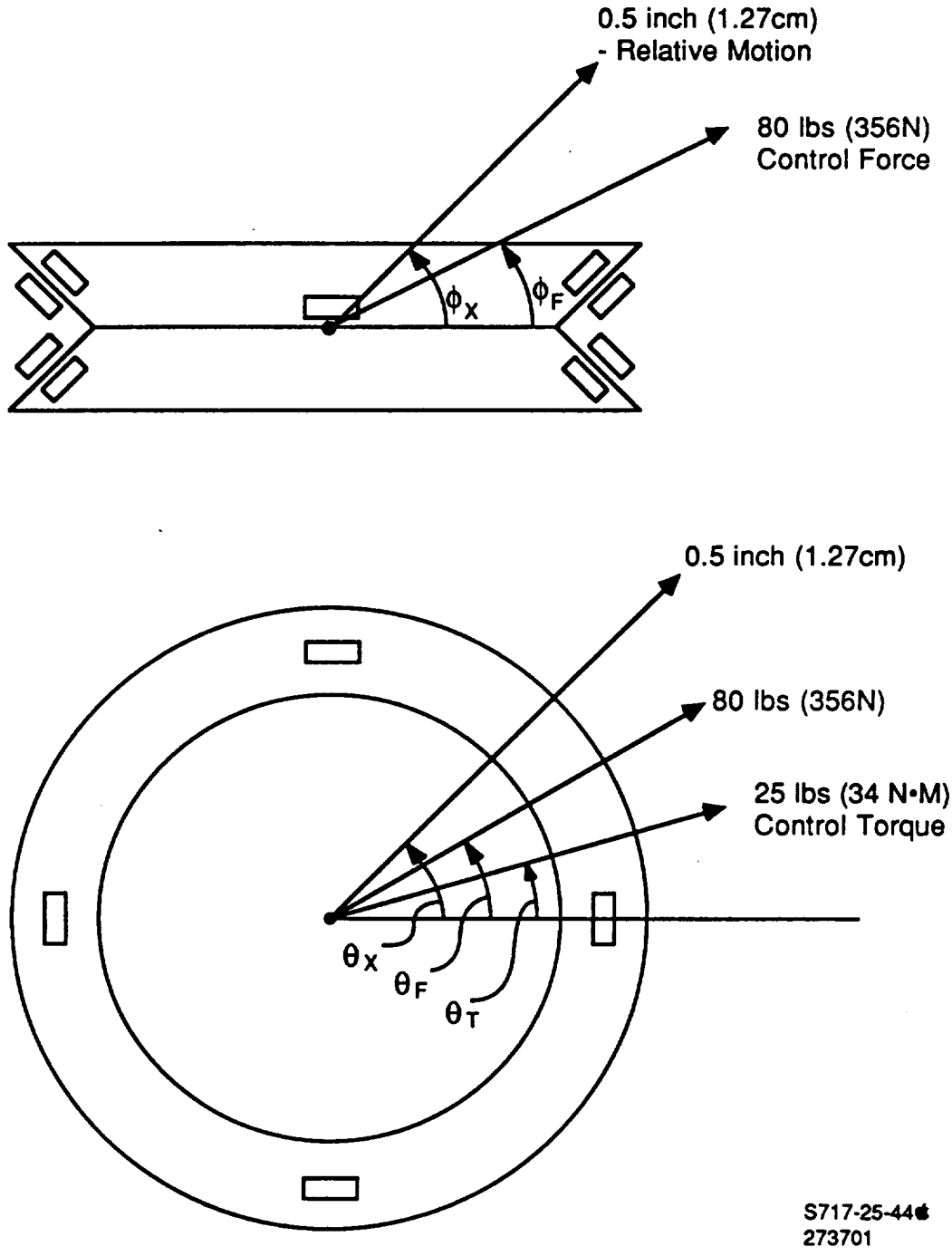

Figure 8-7
Control Force, Torque and Relative Motion

ORIGINAL PAGE IS
OF POOR QUALITY

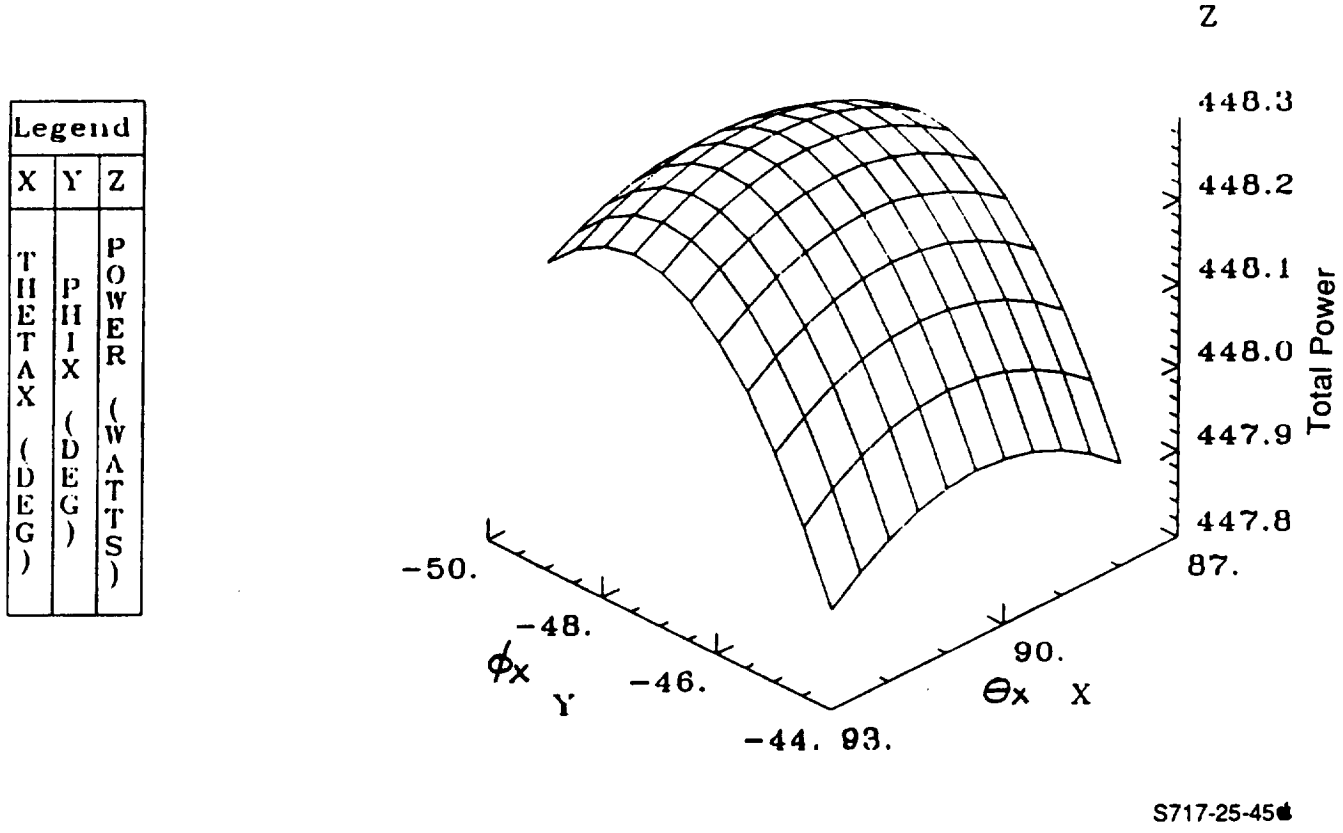

Figure 8-8
Operational Total Actuator Power Versus Relative Motion Parameters

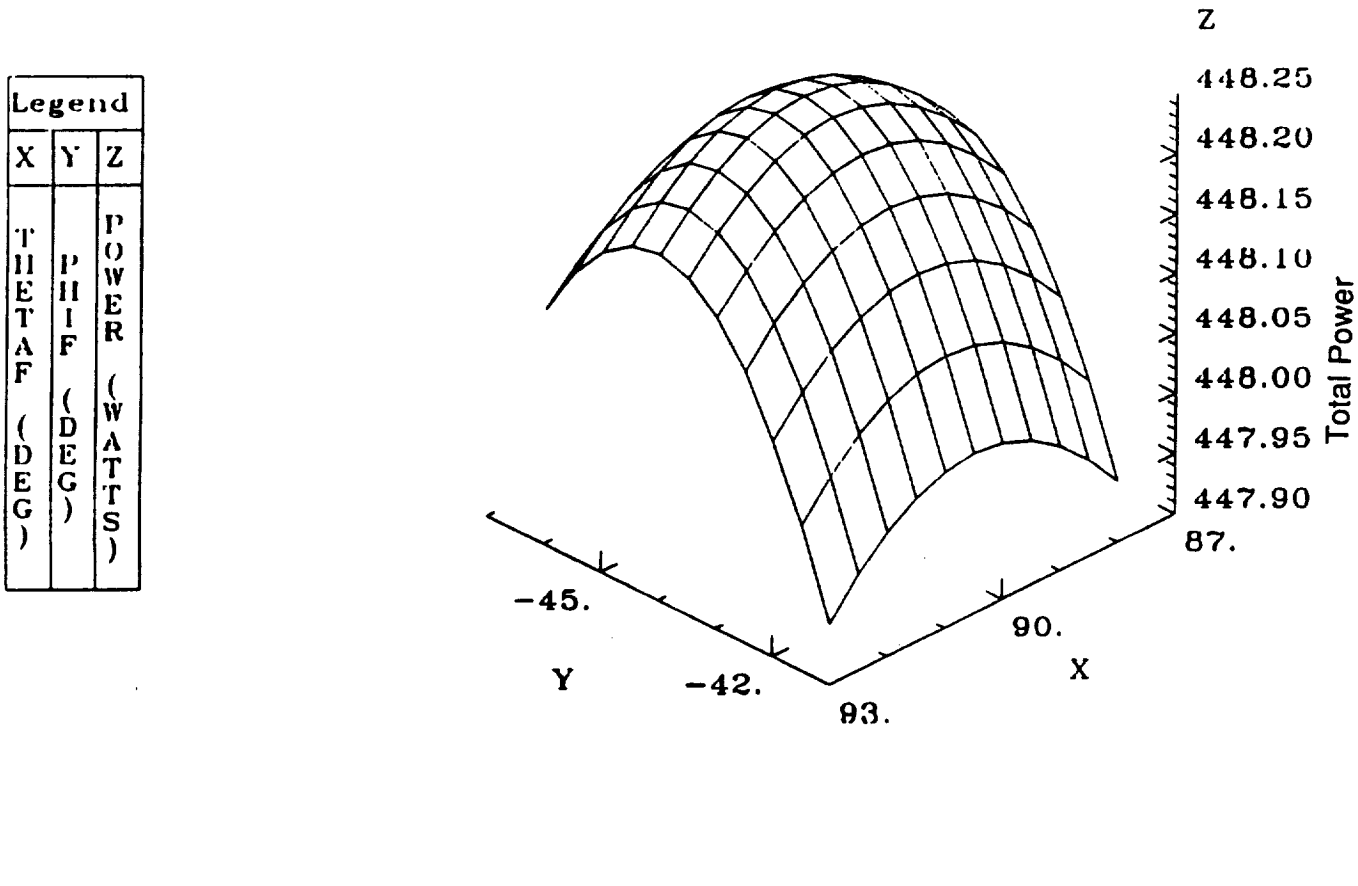

Figure 8-9
Operational Total Actuator Power Versus Force Direction Parameters

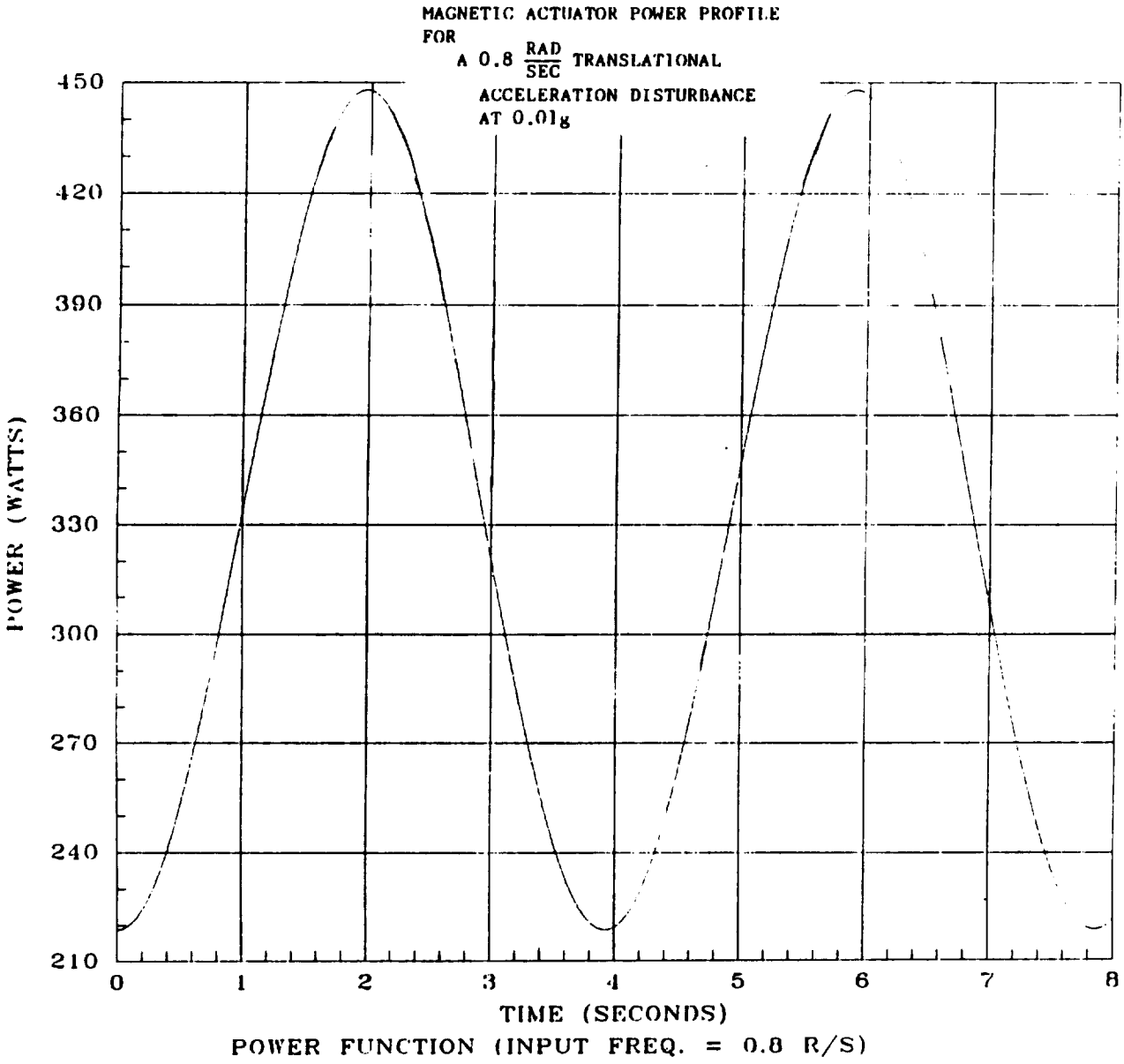

Figure 8-10
Magnetic Actuator Power Profile

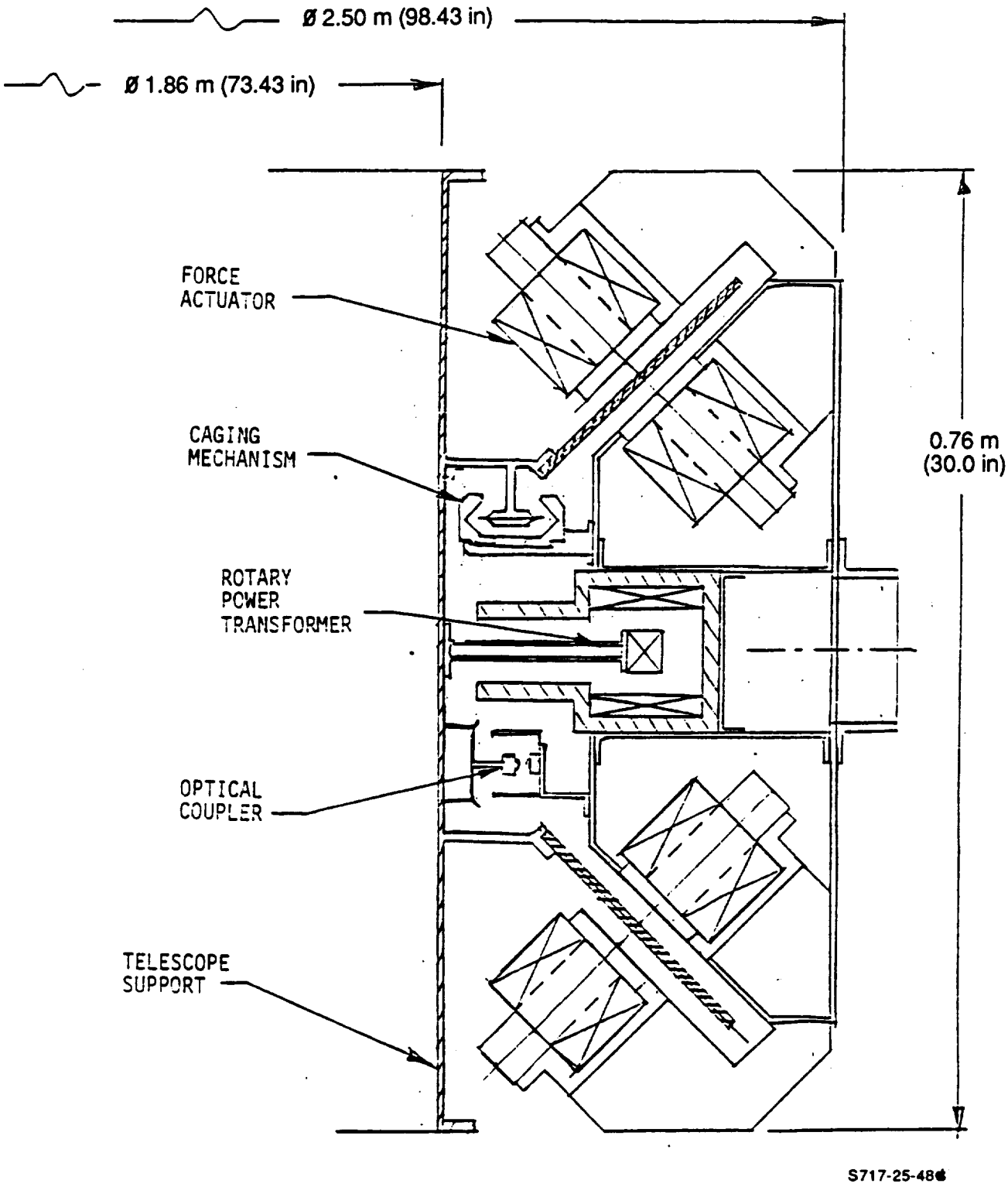

Figure 8-11
Actuator Cross Section

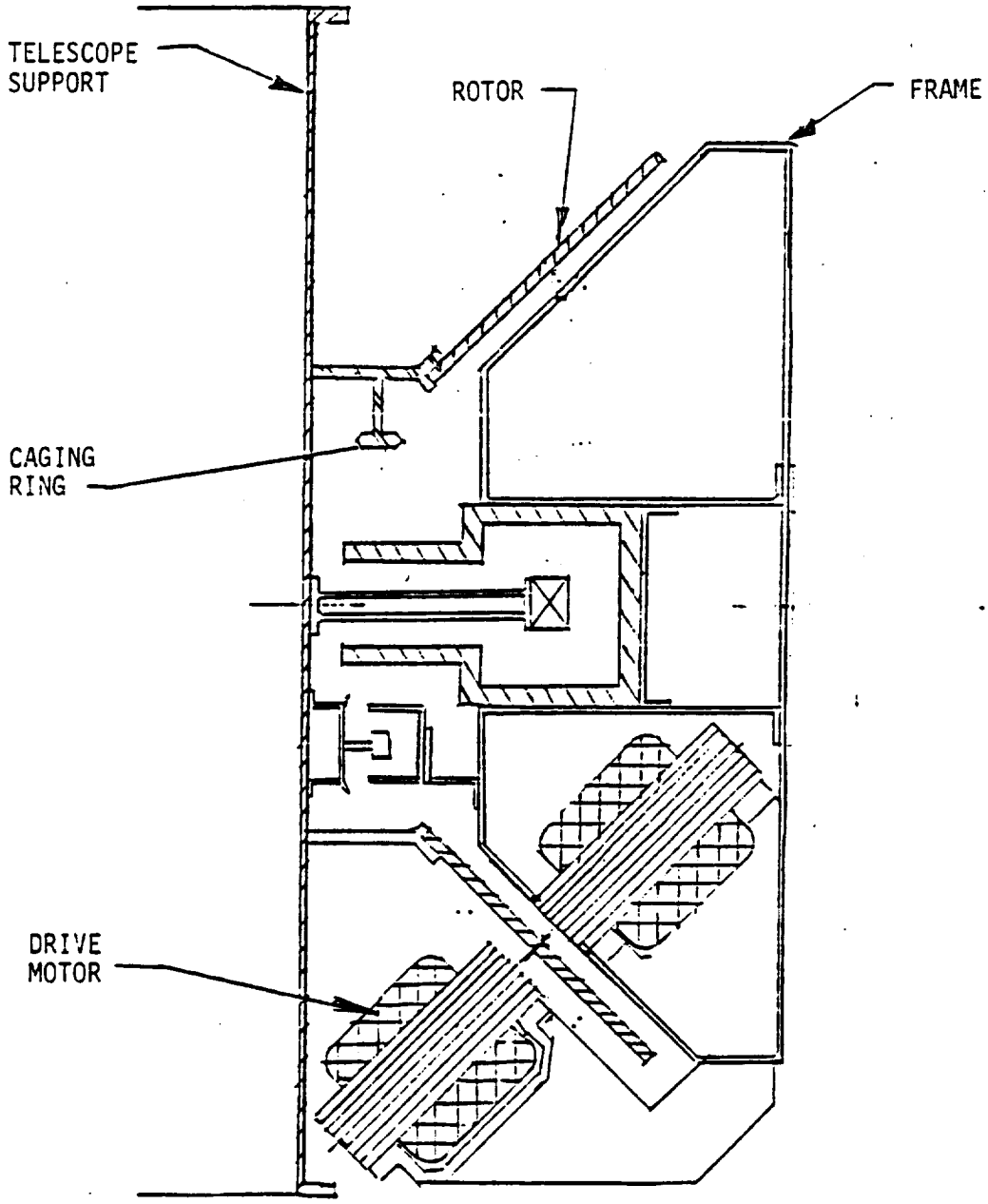

Figure 8-12
Roll Motor Cross Section

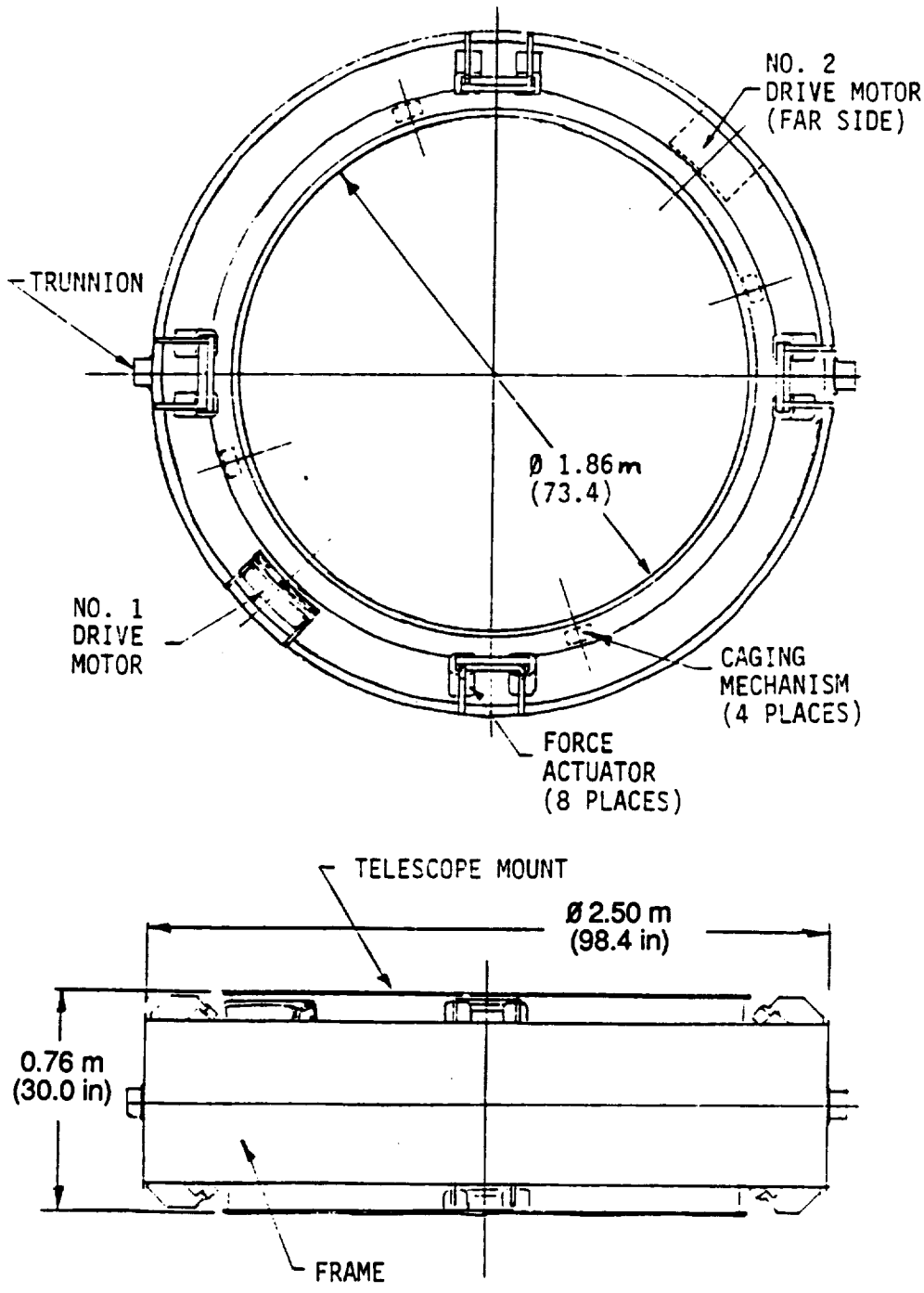

Figure 8-13
Actuator Layout

AC INDUCTION MOTOR

± 0.6 " MOTION, 5 FT LBS (TOTAL), FULL ROTATION

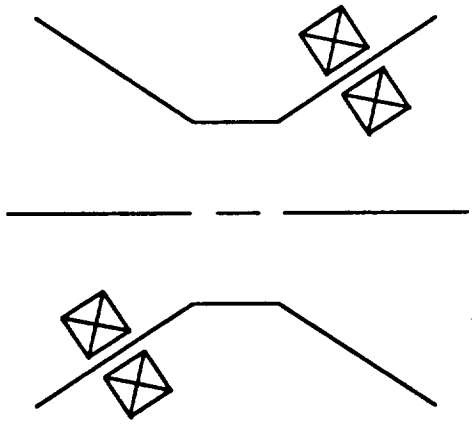

TWO SETS OF STATORS USING MBA ROTOR PLATED:
(TO BALANCE FORCES ABOUT CG)

		WT	Power	Torque
EARTH STATOR SET		36 Kg	100 Watts	3.4 N•m
TOTAL	x 2	72 Kg	200 Watts	6.8 N•m

S717-25-516
273707

Figure 8-14
ATF Roll Motors Summary

8.6 POWER TRANSFORMER

The rotary transformer designed to transfer power to the ATF from the PPS is illustrated in Figure 8-15. The majority of the weight is placed on the stator side of the transformer. Dimensions are shown in inches.

The transformer is designed to supply 2400 watts peak at 120 V and 20 KHz. The efficiency is 94 percent. The equivalent passive element circuit diagram for the device is shown at the bottom of the figure.

8.7 OPTICAL COUPLER

The concept design for signal transfer between the PPS and ATF is shown in Figure 8-16. The device consists of a reflective channel around the ATF with optical transmitters (LEDs) and receivers (photodetectors) placed on both rotor and stator sides of the channel. Information is transmitted as sequences of optical pulses, from the ATF to the PPS and vice versa. Multi-information channels can be supported by multiplexing on both sides of the channel as illustrated in the block diagram at the top of the figure.

8.8 ATF ELECTRONICS

Support and drive electronics are required for each of the magnetic system components described above: control actuators, roll motors, rotary transformer, and opto coupler. In addition, gap sensor and support electronics are required to support the isolation and PPS follow-up control. Finally, an ATF processor is required to connect all of the functions. The functional and signal interface diagram of Figure 8-17 shows these various electronic subsystems. Table 8-1 gives additional details about the make-up and operation of the subsystems. All electronics are redundant. Figure 8-18 shows this redundancy for the processor, actuator and roll drive electronics.

8.9 WEIGHT AND POWER SUMMARY

Table 8-2 supplies an estimated breakdown of total system weight and operational power. The values in parentheses refer to changes in power and weight resulting from a change to 100 W peak power actuators (without a change in motion limit or maximum actuator force). No dimensional layouts were defined to determine whether or not the larger system will actually fit in the available radial space.

8.10 SYSTEM RELIABILITY

The intended twenty-year operational life of the ATF experiment mandates that all major electronic components of the magnetic pointing and isolation system be redundant. A summary of the system component failure rates is provided in Table 8-3. The redundant electronics components are non-operational prior to a primary component failure and therefore are assigned a failure rate of 1/10 of the primary failure rate. A single actuator failure is viewed as a system failure. Fewer than eight actuators can be used to control the ATF (with modification to the control software), but the system was sized assuming eight actuators. Thus, an actuator failure may result in unacceptably degraded performance.

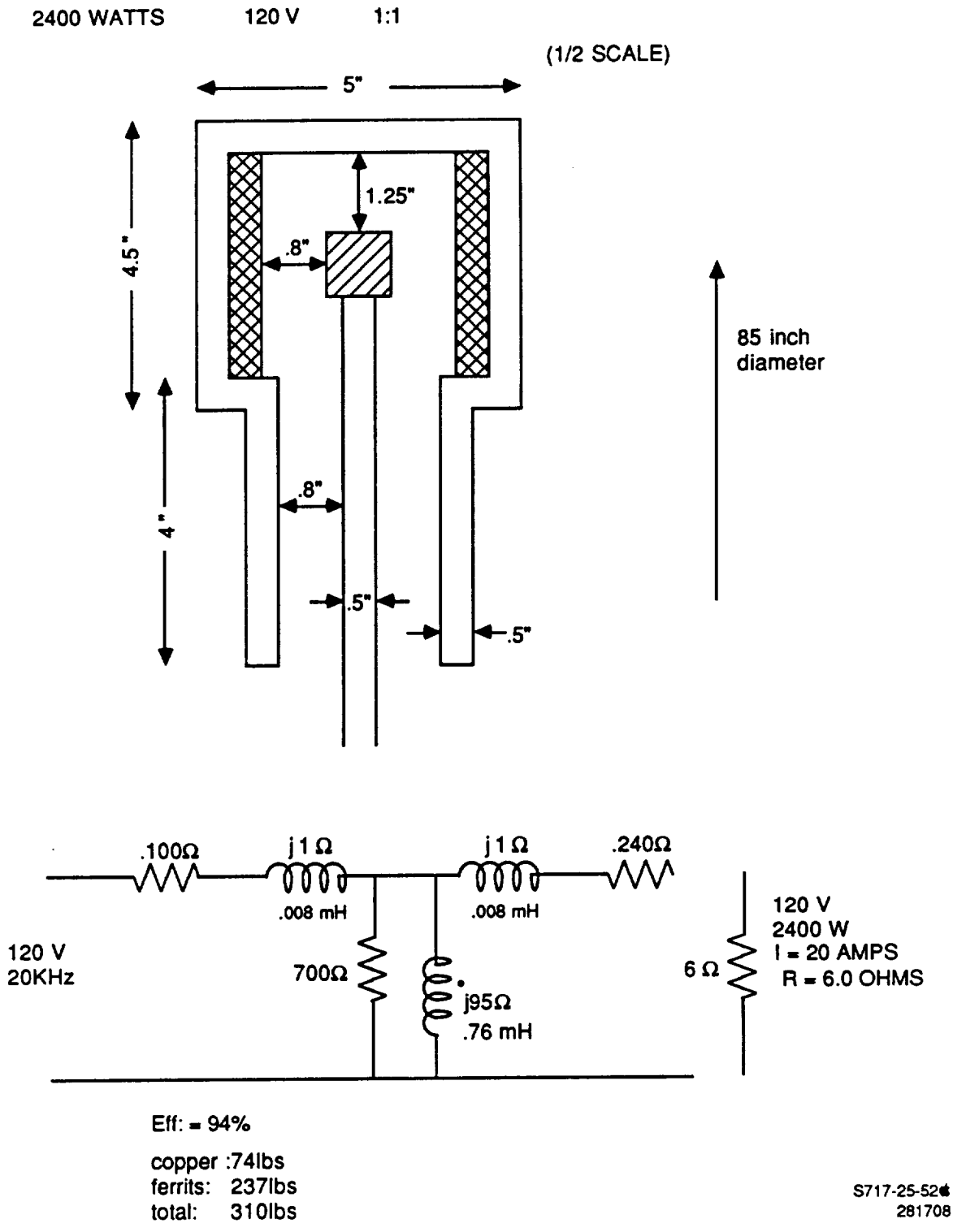

Figure 8-15
ATF Power Transformer

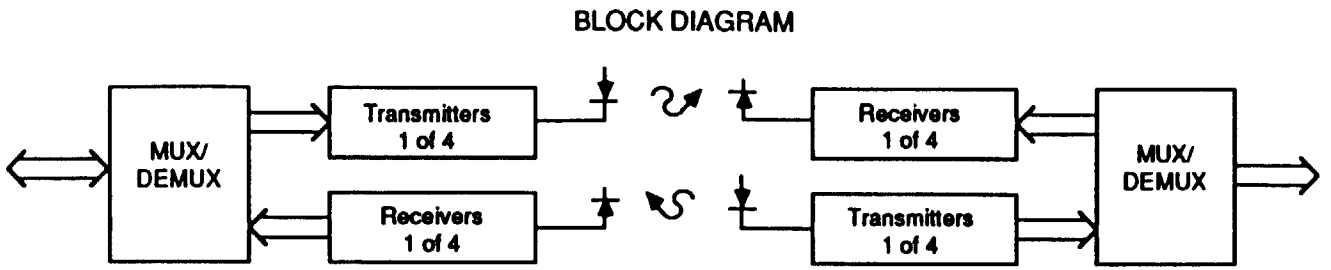

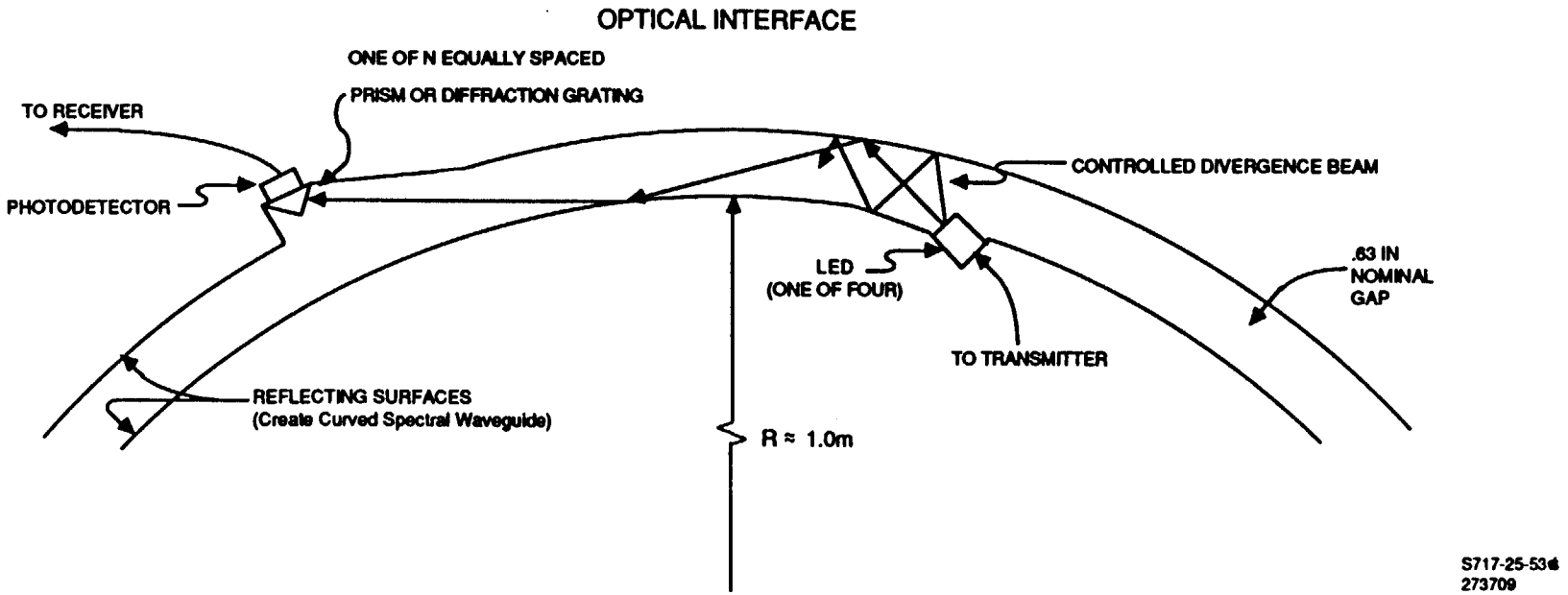

Figure 8-16
Opto Coupler

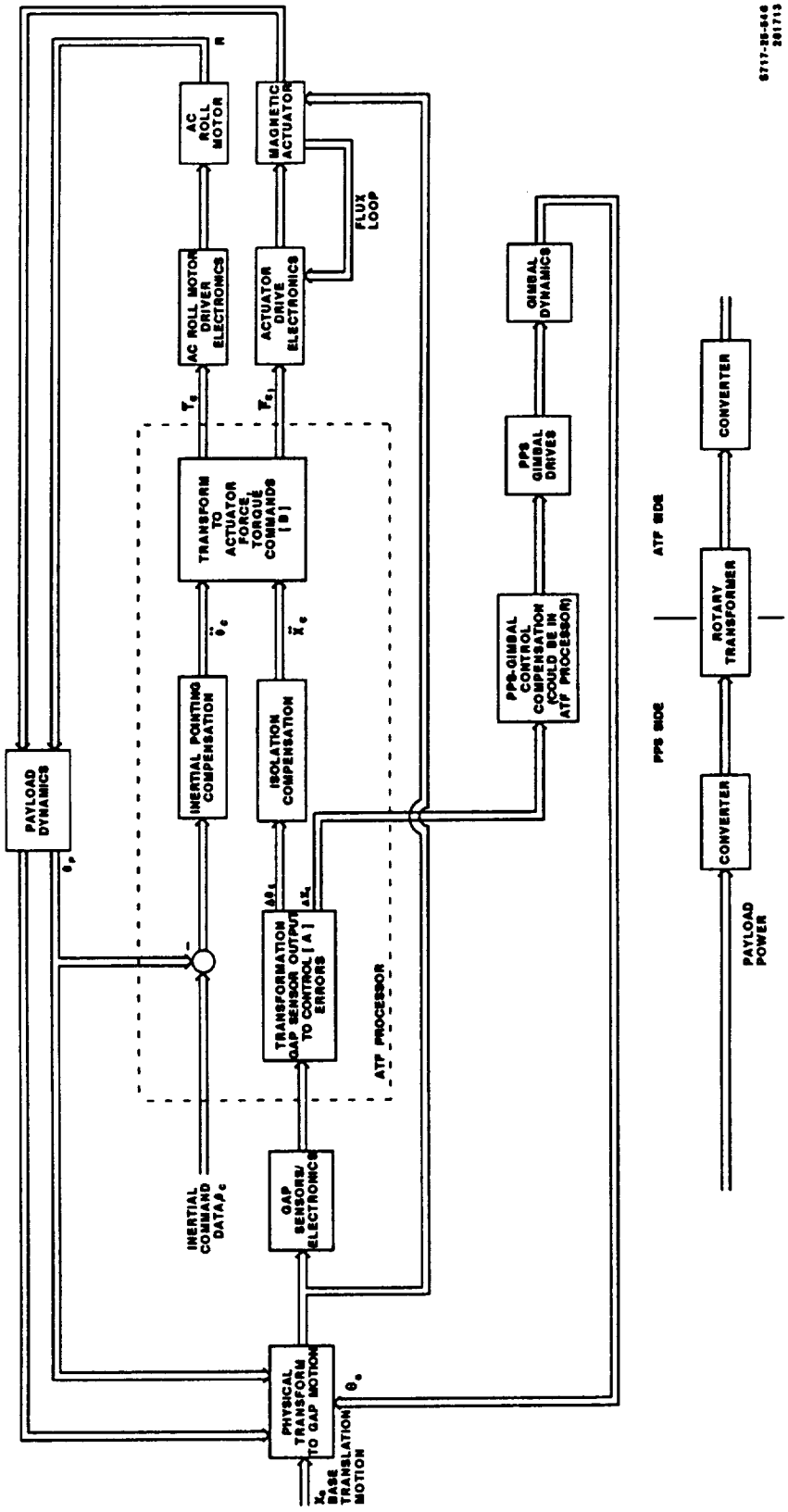

Figure 8-17
ATF Magnetic Pointing and Isolation-Functional
Signal Interface Diagram

TABLE 8-1

ATF ISOLATOR ELECTRONICS

- **ATF Processor**
  - Redundant Electronics Assemblies
  - Host Communication
  - Coordinate Transforms
  - Multirate Digital Control
  - Health/Status Telemetry
  - Candidate Processor RCA SPC-050

Throughput	- 500 KIPS Gibson Mix
Memory	- 48 K Words
I/O	- 1.6 sec/word
Weight	- 16 LBS
Power	- 16 Watts
Reliability	- 0.99 for Two Years

- **Suspension Electronics**
  - Redundant Electronics Assemblies
  - Local EMI Filtering
  - Eight Actuator Drives With Corresponding Flux Loops
  - Local Gap Sensing And Anti-Aliasing Filters
  - ATF Processor Interface
  - Health/Status Telemetry
  - Primary/Redundant Relay Switching

S717-25-55
281709

TABLE 8-1 (cont)

ATF ISOLATOR ELECTRONICS

- **Roll Motor Electronics**
  - Redundant Electronics Assemblies
  - Local EMI Filtering
  - Two AC Induction Motor Segment Drives
  - Local Gap Sensing Electronics
  - ATF Processor Interface
  - Health/Status Telemetry
- **Opto-Coupler Assembly**
  - Redundant Assemblies
  - Four Optical Channels In Each Direction
  - ~ 20 MBPS /Channel Data Rates
  - LED Light Sources
  - Manchester Coded Optical Pulses
  - Internal Multiplexing And Demultiplexing
- **Power Transfer**
  - Rotary Transformer
  - DC to AC Inverter (for dc power bus only)
  - AC to DC Converter (for dc power bus only)

S717-25-56
281710

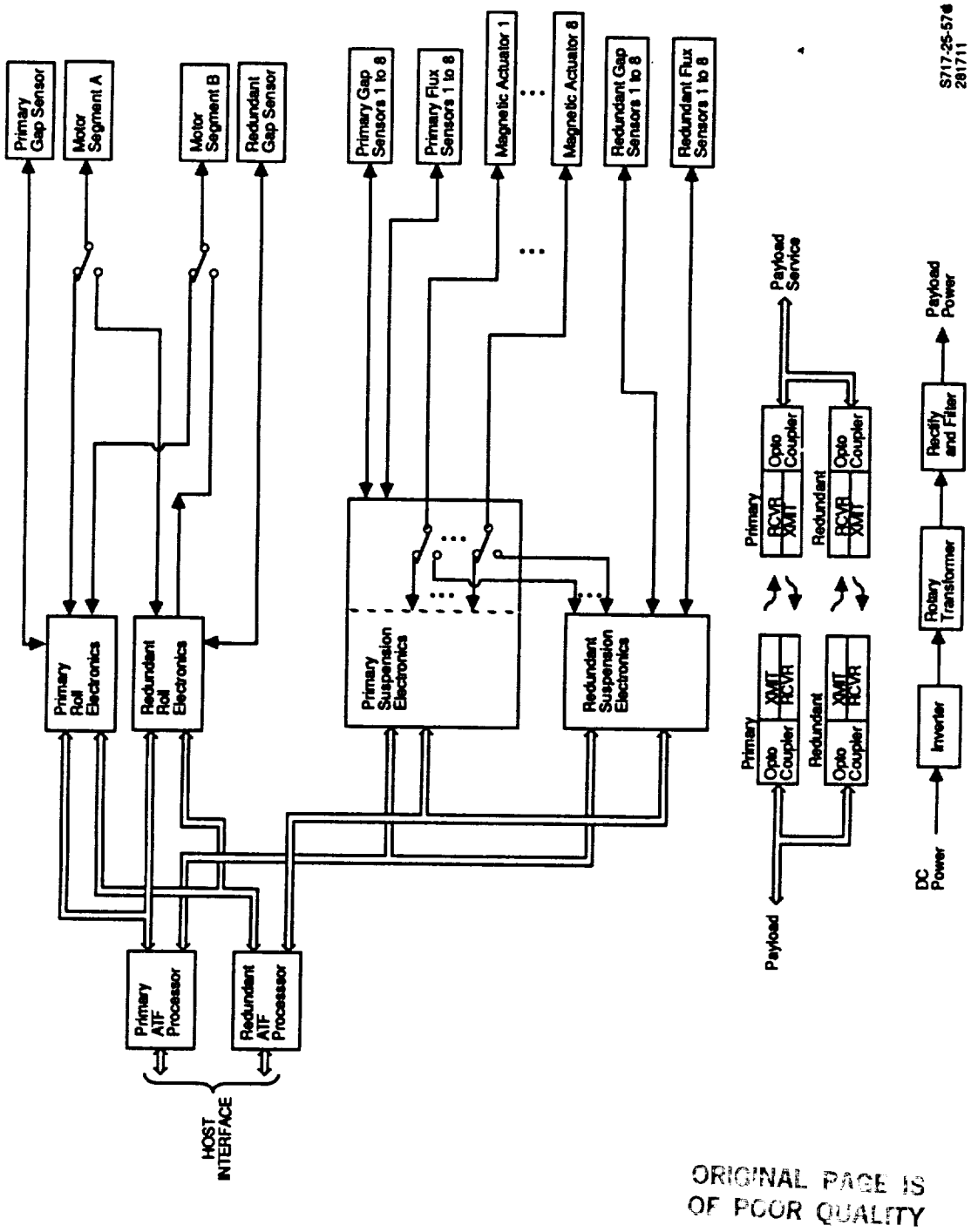

Figure 8-18
AIF Isolator Equipment

TABLE 8-2

CANDIDATE ATF WEIGHT-POWER PREDICTION

	MAX OP. POWER (W)	TOTAL WEIGHT (lbs)	(Kg)
ACTUATORS	450 (225)	1000 (1400)*	(454) (636)
ROLL MOTORS	125	160	(72.7)
SUSPENSION ELECTRONICS (REDUNDANT)	100	120	(54.5)
PROCESSOR	16	32	(14.5)
OPTICAL COUPLER	16	40	(18.2)
ROLL MOTOR ELECTRONICS	80 (BASED ON 60% ROLL MOTOR OP.)	50	(22.7)
STRUCTURE	-	225 (325)	(103.3) (147.7)
ROTARY TRANSPORT	(94% EFFICIENT)	310	(140.9)
	787 (562)	1937 (2437)	(880.5) (1107.7)

* POWER AND WEIGHT VALUES CORRESPONDING TO THE USE OF MAGNETIC ACTUATORS REQUIRING 100 WATTS PEAK POWER.

S717-25-58
273705

TABLE 8-3

ESTIMATED BASELINE SYSTEM RELIABILITY

			Failures per million hours of operation (λ)		
				Primary Electronics	Redundant Electronics
MAGNETIC ACTUATOR ELECTRONICS		Qty		8.29	0.829
Drive Electronics	0.49	8	3.92		
Standby Electronics	3.86	1	3.86		
Flux Sensor	0.002	8	0.016		
Gap Sensor	0.062	8	0.496		
MAGNETIC ACTUATOR	0.015	8		0.12	
ROLL MOTOR	0.03	2		0.06	
ROLL MOTOR ELECTRONICS				4.64	0.464
Drive Electronics	1.05	2	2.10		
Standby Electronics	2.29	1	2.29		
Gap Sensor	0.062	4	0.25		
OPTO-COUPLER	0.3	8		2.40	0.24
COMPUTER	2.4	1		2.40	0.24
ROTARY TRANSFORMER	0.06	1		0.06	
TOTAL MTBF				17.97	

Probability of Success	5 year mission	10 year mission
Non Redundant Electronics	0.455	0.207
Redundant Electronics (Standby)	0.905	0.711

S717-25-59
281712

The magnetic actuator failure rate listed in the table, 0.015, assumes a single coil with discrete insulation between coil winding. The failure rate can be improved to 0.00285 by adding redundant coils, but the effect on overall system reliability is very small. A decision to add redundant coils might be made based on the difficulty of exchanging a failed actuator.

8.11 DESIGN SUMMARY

An ATF magnetic pointing and isolation system design based on requirements imposed by a 0.01 g space station disturbance input has been generated. The design fits in the available annular space and is estimated to weigh less than 2000 lbs. Power requirements for the system are dominated by the magnetic actuator and roll motor requirements. Power numbers presented for these systems do not represent the peak possible power for the system. They do, however, represent the anticipated peak operational power. Based on these peak numbers the total system power requirement is estimated to be < 800 watts.

The full redundancy of the system, except actuator coils, provides a reasonable mean time between system failures (defined by system nonoperation or performance degradation).

Things not studied or requiring more study include: roll control, and power/data.

8.12 ADDITIONAL SYSTEM STUDIES AND TECHNOLOGY DEVELOPMENT

8.12.1 Additional Study Efforts

As noted earlier, the study results described in this report are based on a less than well-defined Space Station disturbance model. Before a Magnetic Isolation and Pointing System (MIPS) can be developed for ATF, additional studies based on better Space Station and MIPS models are required in order to more precisely define system pointing performance, magnetic actuator force and motion requirements, and roll motor torque requirements. These models should include Space Station flexibility, Space Station disturbance time lines, improved PPS characterization, and six DOF dynamics of the ATF payload and magnetic actuator configuration.

8.12.2 Technology Studies/Development

Two areas of technology development have been identified as providing benefits to the ultimate development of a complete magnetic IPS for the ATF: (1) data-signal transfer across a noncontacting, rotating interface and (2) efficient noncontacting rotary power transfer. In neither area is there a perceived technical risk. However, development of a large-scale power transfer device prototype and of a prototype signal transfer device (along the lines of the device described in the report) would provide a significant headstart in the MIPS development and, thereby, reduce development schedule risk.

APPENDIX A

ACTUATOR LEAKAGE FLUX

APPENDIX A

ACTUATOR LEAKAGE FLUX

Leakage flux for a magnetic actuator is determined by the actuator flux density, the geometry of the actuator pole faces and armature, and the actuator gap, (nominal gap plus gap motion). The flux density and gap have the most significant influence.

Most of the HSSD's magnetic actuator designs incorporating flux feedback for force control, as does the ATF design, produce roughly the same high level of flux density when driven to their design force limit. Thus, the difference in leakage flux values between two flux feedback actuators operating at their peak forces, even if the peak forces are significantly different, is determined, primarily, by the difference in actuator gaps.

The two outer curves in Figure A-1 show leakage flux test data obtained using the SAVI (Space Active Vibration Isolator) brassboard actuator operating at peak force for two gap values, 4.78 and 6.6 mm. The center curve shows predicted values for a smaller SAVI device. The data shows that with a 6.6 mm gap the flux density at a distance of 0.4 m from the actuator is less than that of the earth's magnetic field. Since the SAVI brass board actuator has a peak flux density comparable to that of the ATF design, this SAVI data can be used to estimate worst case ATF actuator flux leakage.

The ATF design includes a 0.6-inch nominal gap and 0.5-inch (12.7 mm) gap motion. Therefore, at the extreme motion the total gap is about four times the SAVI peak gap. Obviously, ATF leakage flux at peak force will be greater than the values shown in the figure at comparable distances from the actuator. However, it is estimated that ATF leakage flux density will still be less than earth field density at a distance of less than 0.7 m. Note that this is an absolute worst case condition. Because of actuator force oversizing (approx. 45%), the ATF actuator will never be driven to its maximum flux density under the normal operating conditions defined for the ATF system. Even reaching the maximum force required for control (35 lbs, 156 N) while the gap motion is at its peak in the worst case direction should be an infrequent occurrence for any individual actuator.

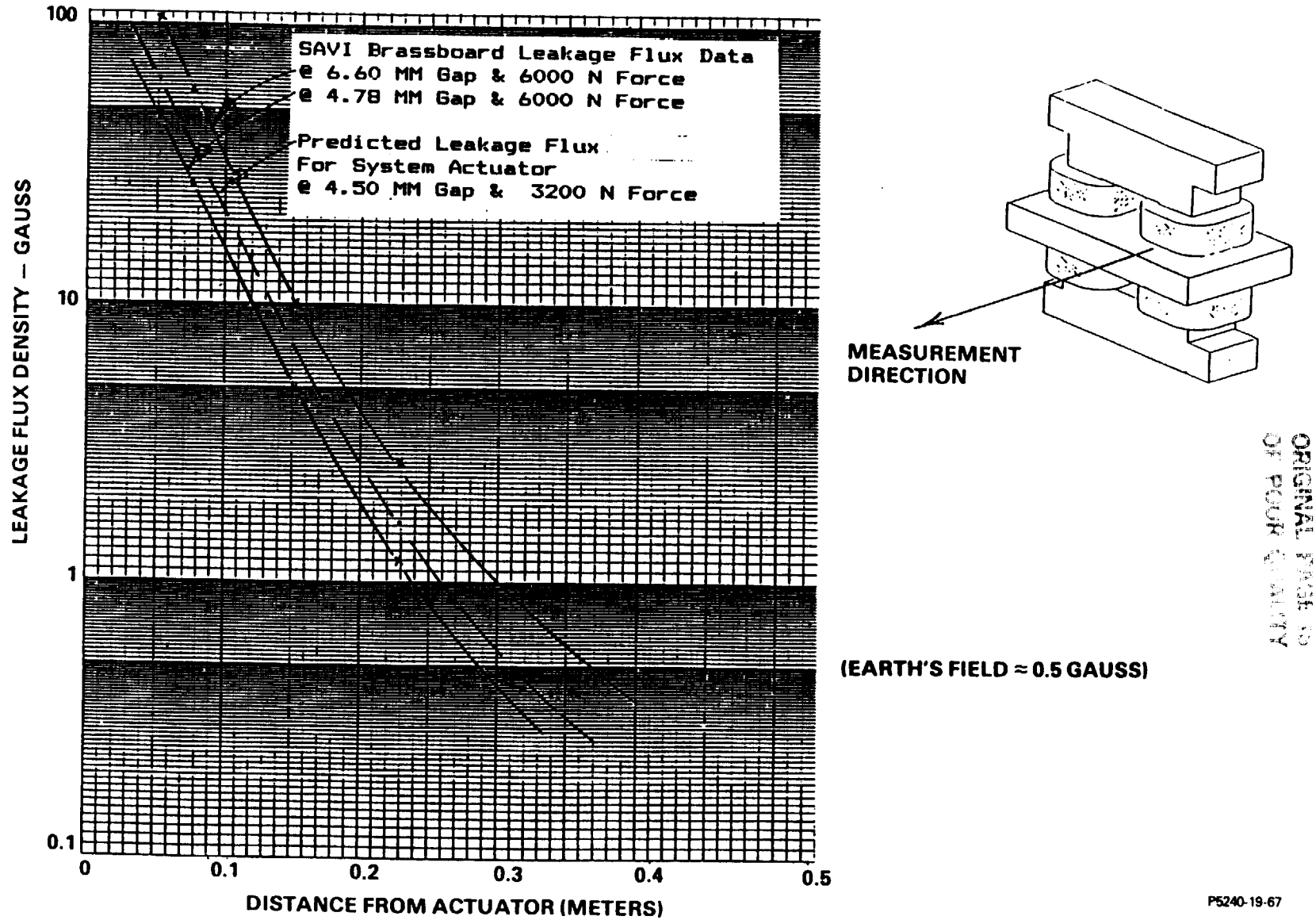

Figure A-1
Magnetic Actuator Leakage Flux

NASA
National Aeronautics and Space Administration

Report Documentation Page

1. Report No.	2. Government Accession No.	3. Recipient's Catalog No.
NASA CR 177473		

4. Title and Subtitle	5. Report Date
ATF Isolation and Pointing Study	January 1988
	6. Performing Organization Code

7. Author(s)	8. Performing Organization Report No.
William Hibble, Terry Allen, Louis Jackson, James Medbery, and Richard Self	
	10. Work Unit No. 480-36-05 & 480-52-05

9. Performing Organization Name and Address	11. Contract or Grant No.
Honeywell Satellite Systems Div., 19019 North 59th Ave Glendale, AZ 85308	NAS2-32815
	13. Type of Report and Period Covered
12. Sponsoring Agency Name and Address	Contract Report - final
National Aeronautics & Space Administration Washington, DC 20546	14. Sponsoring Agency Code

15. Supplementary Notes

Point of contact: Nasa Ames Research Center
Attn: 244-14/M. A. Smith
Moffett Field, CA 94035
(415)694-4833 or (FTS)464-4833

16. Abstract

The Astrometric Telescope Facility (ATF), an optical telescope designed to detect extrasolar planetary systems, is scheduled to be a major user of the Space Station's Payload Pointing System (PPS). However, because the ATF has such a stringent pointing stability specification (0.01 arcsec from 5 to 200 Hz) and requires +/- 180 degree roll about its line of sight, mechanisms to enhance the basic PPS capability are required. This study investigates the ATF pointing performance achievable by the addition of a magnetic isolation and pointing system (MIPS) between the PPS upper gimbal and the ATF, and separately, by the addition of a passive isolation system between the Space Station and the PPS base. The candidate MIPS can meet the ATF requirements in the presence of a 0.01g disturbance. It fits within the available annular region between the PPS and the ATF while meeting power and weight limitations and providing the required roll motion, payload data and power services. By contrast, the passive base isolator system must have an unrealistically low isolation bandwidth on all axes to meet ATF pointing requirements and does not provide roll about line of sight.

17. Key Words (Suggested by Author(s))	18. Distribution Statement
Vibration Isolation Magnetic Suspension Telescope Space Station Attached Payloads	[redacted] Subject category: 18

19. Security Classif. (of this report)	20. Security Classif. (of this page)	21. No. of pages	22. Price
Unclassified	Unclassified	98	

NASA FORM 1626 OCT 86